



A 160-Day Simulation of Space Station Debris Avoidance Operations with the United States Space Command (USSPACECOM)

Alfred Lunde (deceased)
NASA Lyndon B. Johnson Space Center
Houston, Texas

James Lee Foster, Jr.
Barrios Technology, Inc.
Houston, Texas

THE NASA STI PROGRAM OFFICE . . . IN PROFILE

Since its founding, NASA has been dedicated to the advancement of aeronautics and space science. The NASA Scientific and Technical Information (STI) Program Office plays a key part in helping NASA maintain this important role.

The NASA STI Program Office is operated by Langley Research Center, the lead center for NASA's scientific and technical information. The NASA STI Program Office provides access to the NASA STI Database, the largest collection of aeronautical and space science STI in the world. The Program Office is also NASA's institutional mechanism for disseminating the results of its research and development activities. These results are published by NASA in the NASA STI Report Series, which includes the following report types:

- **TECHNICAL PUBLICATION.** Reports of completed research or a major significant phase of research that present the results of NASA programs and include extensive data or theoretical analysis. Includes compilations of significant scientific and technical data and information deemed to be of continuing reference value. NASA's counterpart of peer-reviewed formal professional papers but has less stringent limitations on manuscript length and extent of graphic presentations.
- **TECHNICAL MEMORANDUM.** Scientific and technical findings that are preliminary or of specialized interest, e.g., quick release reports, working papers, and bibliographies that contain minimal annotation. Does not contain extensive analysis.
- **CONTRACTOR REPORT.** Scientific and technical findings by NASA-sponsored contractors and grantees.
- **CONFERENCE PUBLICATION.** Collected papers from scientific and technical conferences, symposia, seminars, or other meetings sponsored or cosponsored by NASA.
- **SPECIAL PUBLICATION.** Scientific, technical, or historical information from NASA programs, projects, and mission, often concerned with subjects having substantial public interest.
- **TECHNICAL TRANSLATION.** English-language translations of foreign scientific and technical material pertinent to NASA's mission.

Specialized services that complement the STI Program Office's diverse offerings include creating custom thesauri, building customized databases, organizing and publishing research results . . . even providing videos.

For more information about the NASA STI Program Office, see the following:

- Access the NASA STI Program Home Page at <http://www.sti.nasa.gov>
- E-mail your question via the Internet to help@sti.nasa.gov
- Fax your question to the NASA Access Help Desk at (301) 621-0134
- Telephone the NASA Access Help Desk at (301) 621-0390
- Write to:
NASA Access Help Desk
NASA Center for AeroSpace
Information
7121 Standard
Hanover, MD 21076-1320



A 160-Day Simulation of Space Station Debris Avoidance Operations with the United States Space Command (USSPACECOM)

Alfred Lunde (deceased)
NASA Lyndon B. Johnson Space Center
Houston, Texas

James Lee Foster, Jr.
Barrios Technology, Inc.
Houston, Texas

Acknowledgments

Sherry Benson, of Hernandez Engineering, did an outstanding job of organizing, scanning, and doing initial verification of much of the teletype data from USSPACECOM. Capt. Max Clayton of USSPACECOM organized and managed the daily COMBO runs, and provided help through the course of the project. Herb Estes and Rocky Duncan were major participants in the initial analysis.

Available from:

NASA Center for AeroSpace Information
7121 Standard Drive
Hanover, MD 21076-1320
301-621-0390

National Technical Information Service
5285 Port Royal Road
Springfield, VA 22161
703-605-6000

This report is also available in electronic form at <http://ston.jsc.nasa.gov/collections/TRS/>

Contents

1.	Abstract.....	1
2.	Introduction.....	1
3.	Background and Purpose.....	1
4.	Discussion of Experiment	3
4.1	Object Characteristics	4
4.1.1	Official catalog.....	4
4.1.2	Analysts’ catalog.....	4
4.2	Element Set Update Frequency	4
4.3	“Clusters”.....	4
5.	Analysis.....	5
5.1	State Vector Uncertainty	5
5.1.1	Position differences for conjunctions with COMBOs on successive days	6
5.1.2	Debris state vector uncertainty	6
5.1.3	Clusters – observation	7
5.1.4	Invariant semimajor axis	7
5.1.5	Derived epoch state vector	8
5.2	Engineering Flux Model Description	9
5.2.1	Tracked flux estimate.....	9
5.2.2	Origin of uncertainty	9
5.3	Measured Flux	9
5.4	Statistical Flux Model	10
5.4.1	Statistical flux model description	11
5.4.2	Details of statistical flux model calculation.....	11
5.4.3	Statistical flux contributions by altitude and object.....	11
5.5	Flux Discussion – Measured Flux, Statistical Model, and Engineering Model.....	12
5.5.1	Measured flux contributions by altitude and object	13
5.5.2	Object reentry.....	13
5.6	Debris Directional Distribution	14
5.7	Radial Velocity Distribution	15
5.8	Alerts and Maneuvers	16
5.8.1	Alerts and maneuvers observed for GRO.....	16
5.8.2	Alert and maneuver rate as a function of altitude.....	17
5.8.3	Alerts as a function of altitude	17
5.8.4	Maneuvers as a function of altitude.....	18
5.9	Eccentricities.....	18
6.	Operational Implications	19
6.1	Proposed Debris Avoidance Method.....	19
6.2	Example Using Current Measured Flux and Eccentricity Distribution	20
6.3	Analysis of the Single Penetration of the GRO Maneuver Box	21
6.4	Debris Flux Estimate for the Space Station Era	21
6.4.1	Space station altitude profile	21
6.4.2	Comparison of space station and International Space Station Alpha altitude profiles	22

6.4.3	Debris flux for space station.....	23
6.5	Alert Rate and Maneuver Rate from Years 2000 to 2010	23
6.5.1	Best estimate flux	25
6.5.2	Debris avoidance system capacity	25
7.	Conclusions.....	25
8.	References.....	26
Appendix A: Message Format		27
Appendix B: Verification, Flux, Alerts, and Maneuvers.....		28
	Verification	28
	Flux and Flux Detection Area.....	29
	Alerts and Maneuvers	30
Appendix C: Computer Codes		32
Appendix D: Objects		34
Appendix E: Clusters		41
Appendix F: Flux Contribution by Object		43
Appendix G: Derivation and Implementation of the Statistical Model.....		50
	Radial Dependence	50
	Latitude Dependence	51
	Flux.....	52
	Relative Velocity.....	53
	Implementation	54
	Relative Angular Distribution	56
Appendix H: Precession of Arguments of Perigee and Ascending Node		57
Appendix I: State Vector Uncertainty Analysis		59
	Time-Overlapped Data Analysis.....	59
	State Vector Uncertainty at Epoch.....	59

Tables

1	Number of conjunctions predicted on two successive days, within specified time difference	6
2	Average and RMS dispersion first- and second-day conjunction predictions	6
3	The largest contributors to measured flux taken from table 3D at indicated altitudes.....	13
4	Normalized angular coefficients for 15° angles; measured and engineering model.....	15
5	Number of penetrations of GRO alert and maneuver boxes, and annual alert and maneuver box violation rates	17
6	Distribution of eccentricities	18
7	Collision probability for the GRO conjunction with object 12630 as a function of debris state vector uncertainty.....	21
8	Projected alert and maneuver rates.....	24
D1	Cataloged objects having conjunctions with the GRO within a 100-km distance, over the time period covered by the simulation.....	34
D2	Objects from the USSPACECOM analysts' data set having conjunctions with the GRO within a 100-km distance, over the time period covered by the simulation.....	38
D3	Contribution to the measured flux by individual objects from 300 to 470 km over 10-km intervals.....	40
E1	Objects having conjunctions with the GRO within 5 sec of one another	41
F1	Contribution to the statistical flux by individual objects from 300 to 450 km averaged over a 10-km altitude band.....	43
F2	Objects making a large contribution to the statistical flux model calculation	48
G1	Normalized angular coefficients generated from catalog data.....	56

Figures

1	GRO altitude profile over time of simulation.....	3
2	Invariant semimajor axis over time of simulation	8
3	Measured, smoothed measured, and engineering model debris flux	10
4	Statistical flux at approximately one-month intervals	12
5	Comparison of measured and statistical flux.....	12
6	Comparison with statistical flux calculated from simulation catalog	14
7	A graphical comparison between the engineering model and measured angular direction distributions.....	15
8	Radial velocity distribution	16
9	Annual Space Shuttle alert rate as a function of altitude.....	17
10	Annual Space Shuttle maneuver rate as a function of altitude	18
11	Fractional residual risk vs. relative maneuver rate as a function of P_m	19
12	Predicted altitude profile for assembly complete space station and nominal MSFC solar radiation flux.....	21
13	Space station debris flux for several debris population growth assumptions.....	22
B1	Time-averaged available area for flux	30
G1	Angle between orbit path and line of constant latitude	52
G2	Velocity vector relationships	53

Acronyms

COMBO	Computation of Misses Between Orbits
CPA	closest point of approach
GP	general perturbation
GRO	Gamma Ray Observatory
ISSA	International Space Station Alpha
JSC	Johnson Space Center
LEO	low Earth orbit
MSFC	Marshall Space Flight Center
RMS	root mean square
SP	special perturbation
UVW	quasi-inertial, right-handed Cartesian coordinate system
USSPACECOM	United States Space Command

1. Abstract

A joint simulation was performed by the NASA Johnson Space Center (JSC) and United States Space Command (USSPACECOM) from September 1992 to March 1993 to obtain information concerning the space debris population for debris avoidance operations. Simulation results, which were extrapolated for use in space station operations, indicated that a probabilistic debris avoidance process was feasible.

The simulation used the Gamma Ray Observatory (GRO) as a “target” vehicle. As the simulation was carried out, USSPACECOM used the database maintained by its tracking network to search for conjunctions between the GRO and the tracked debris, and then transmitted results of the simulation to JSC for analysis.

Over the entire altitude band studied, the debris flux and frequency of penetration of Space Shuttle orbiter “alert” and “maneuver” boxes were found to be much lower than the predictions of current models. However, if a maneuver box similar to that used for the Space Shuttle was used for the space station, the number of maneuvers to avoid orbital debris would be prohibitive.

Results of the study, which are being published to document an early analysis that led to current debris avoidance operations, showed a very dynamic debris environment over the time period and altitudes covered.

2. Introduction

This paper documents an experiment, consisting of a simulation of space station debris avoidance operations, carried out by USSPACECOM over a 160-day period using the GRO, orbiting at an orbital inclination of 28.5° , as a substitute for a space station orbital inclination. The simulation, covering the first phase of the USSPACECOM debris avoidance procedures, provides a critical look at debris avoidance operational capabilities.

The actual alert rate, maneuver rate, and residual risk that would result from implementing the proposed space station debris avoidance operations procedure were examined, in 10-km steps, over an altitude band from 300 to 470 km. Comparison was made with model predictions and Space Shuttle values.

Of interest was the number of penetrations of Space Shuttle-sized alert and maneuver boxes of $\pm(5 \times 25 \times 5)$ km and $\pm(2 \times 5 \times 2)$ km about the GRO. During the simulation, there were 15 violations of the Space Shuttle rule alert box and one violation of the Space Shuttle rule maneuver box. Extrapolating to annual rates, in one year there would be 41 alerts and three maneuver box violations about the GRO. Alert and maneuver rates increased with increasing altitude. More violations occurred at space station operating altitudes that were well above the GRO altitude for the time period of the simulation.

The orbital inclination of the GRO is 28.5° while that of the planned space station is 51.6° . The debris flux model adopted by NASA predicts a slightly higher debris flux at 51.6° than for an orbital inclination of 28.5° by about 10 percent.

3. Background and Purpose

Debris avoidance is currently performed for the Space Shuttle orbiter by JSC in cooperation with USSPACECOM. JSC, working in concert with USSPACECOM, will also perform debris avoidance for the planned space station.

In support of debris avoidance for the orbiter, USSPACECOM takes note of objects that are predicted to be in near conjunction with the Space Shuttle orbiter, and updates the position and velocity estimate (state vector) of those objects. These updates are performed using standard tracking and general perturbation (GP) orbit trajectory processing. For objects with an updated state vector predicting a passage within an alert box that is $\pm(5 \times 25 \times 5)$ km, UVW (quasi-inertial, right-handed Cartesian coordinate system), about the orbiter, USSPACECOM informs JSC, performs high-intensity tracking, and employs special perturbation (SP) orbit trajectory processing. A debris avoidance maneuver is considered by the flight director if an object is predicted to pass within a maneuver box that is $\pm(2 \times 5 \times 2)$ km, UVW, about the orbiter.

Standard tracking consists of the minimum tracking needed to establish a state vector, while high-intensity tracking produces the most accurate state vector possible. The standard GP orbit trajectory processing uses invariant elements of a low-order geopotential. SP orbit trajectory processing uses a high-fidelity geopotential and integrates the state vector over time.

Most regularly tracked objects of known origin are included in an official catalog of orbiting objects. In addition, USSPACECOM maintains a working data set—called the analysts' catalog—that contains all tracked objects not appearing in the official catalog. These objects, consisting mainly of uncorrelated tracks, are not officially identified.

An alternate debris avoidance operations procedure was proposed by Foster and Estes in “A Parametric Analysis of Orbital Debris Collision Probability and Maneuver Rate for Space Vehicles.”^[1] This proposed procedure, which requires a position uncertainty for the space station and the debris object propagated to time of conjunction, appears to offer a greatly reduced maneuver rate and also quantifies the amount of risk reduction obtained for a given number of maneuvers.

The purpose of this study was to examine the consequences of implementing the proposed debris avoidance operations procedure; i.e. the resulting alert rate, maneuver rate, and residual risk. Specifically, to do this, we need to obtain:

- 1) An overall description of the interaction of the low Earth orbit (LEO) tracked debris population that has conjunctions with an orbiting space vehicle while providing insight into the different types of debris that pose a danger to an operational space station.
- 2) A direct measurement of the tracked debris flux as a function of altitude from which we may estimate alert and maneuver rates for any debris avoidance strategy.
- 3) A direct measurement of Space Shuttle criteria alert and maneuver rates as a function of altitude. The number of Space Shuttle criteria alerts and maneuvers is an excellent measure of the tasking and computational load on USSPACECOM.
- 4) A determination of the horizontal directionality distribution of the debris flux relative to the velocity vector of our simulated space station. From this, using the vehicle cross section and the total debris flux, a collision probability can be calculated as a function of horizontal angle.
- 5) The distribution of the observed debris orbit oblateness (eccentricity). An eccentricity of zero indicates a circular orbit. An eccentricity greater than 0.2 indicates an orbit that is sufficiently oblate to limit ground tracking opportunities. Eccentricity gives insight into the portion of the LEO debris population for which we may not be able to perform effective debris avoidance.
- 6) The distribution of the radial component of the debris velocity. This quantity enters into maneuver vs. risk estimates in planning for the proposed debris avoidance procedure.
- 7) An estimate of the 24-hour spatial dispersion of the state vectors for both the GRO and the debris that gives an indication of the uncertainties associated with USSPACECOM's standard tracking and GP processing. These uncertainties represent a least upper bound to those associated with USSPACECOM's high-intensity tracking and SP processing.

- 8) A comparison of debris flux and orbiter criteria alert and maneuver rates with the Kessler orbital debris flux engineering model, which has been adopted as the debris environment model for space station design.^[2]
- 9) A projection of debris flux to the time of an operational space station and the operational implications of the debris flux projections.

There was concern about the statistical validity of the data obtained from conjunctions with only a single orbiting object for a relatively short period of time. A statistical debris flux model—also developed by Kessler—that transforms orbital elements into spatial densities dependent on altitude and latitude was then used for comparison with the measured flux. The statistical model provided an additional comparison for the measured alert and maneuver rates, the horizontal angular directionality, and the eccentricities. In addition to supplying important information, the analysis of the statistical model identified the need for several operations planning tools.

4. Discussion of Experiment

Each day of the simulation, USSPACECOM searched for conjunctions, or closest point of approach, between the GRO and all other tracked objects out to a distance of 100 km from the GRO for 36 hours. All predicted conjunctions were recorded and transmitted from the USSPACECOM Space Control Center to the NASA JSC Mission Control Center.

Figure 1 shows the altitude of the GRO from September 23, 1992, until March 2, 1993. Gaps in the data are a result of not receiving messages from USSPACECOM. The simulation data covered a total of 134.4 days during a 160-day period. During the simulation, the average altitude of the GRO decreased from 383 to 359 km. The 100-km radius conjunction sphere gave access to conjunctions at altitudes from 490 to 254 km. The altitude used is geocentric, taken from the Earth's equatorial radius. The oscillations in eccentricity and their significance to the statistical flux computations are discussed in section 5.4.

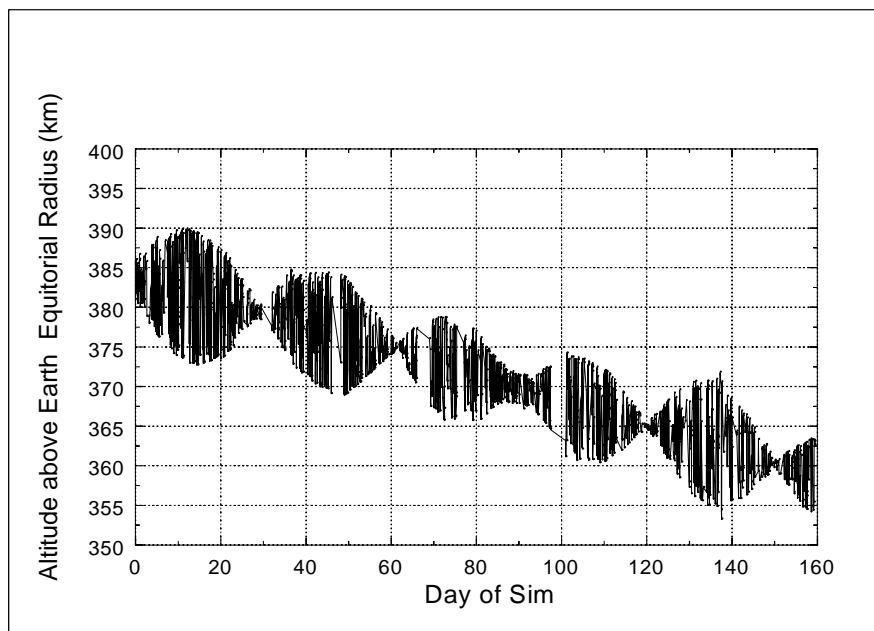


Figure 1. GRO altitude profile over time of simulation.

Each day's search, using the USSPACECOM Computation of Misses between Orbits (COMBO) program, provided 12 hours of conjunction data covering the same time period as that of the previous day's search. The root mean square (RMS) differences in the predictions of the same conjunctions on two consecutive days are an estimate of the uncertainty associated with standard USSPACECOM tracking and GP processing. Objects that appear either day, both from the official catalog or from the analysts' data set, are included in the compilation even if this is the only observation of the object in the simulation.

During the simulation, 1948 separate conjunctions were observed. Of these conjunctions, 1492 were with officially cataloged objects while 456 were with objects from the USSPACECOM analysts' catalog. Five hundred and forty separate objects were observed; of these, 296 were officially cataloged while the remaining 244 were objects from the USSPACECOM analysts' data set. Few of the analysts' catalog objects were seen in more than one conjunction with the GRO.

4.1 Object Characteristics

4.1.1 Official catalog

Table D1 (appendix D) contains a list of objects from the official catalog observed in the simulation. For each officially cataloged object, this table contains the international designation number, USSPACECOM catalog identifier, semimajor axis, eccentricity, orbital inclination, apogee, perigee, number of times the object was observed, average period between state vector updates, description of the object and its country of origin, launch date, and reentry date of the object.

Among the cataloged objects observed were 63 payloads or payload platforms, two orbiters (STS-53 and STS-54), 87 rocket bodies, and 140 pieces designated as debris by USSPACECOM.

4.1.2 Analysts' catalog

Table D2 (appendix D) contains a list of objects from the USSPACECOM analysts' catalog observed in the simulation. These objects from the analysts' catalog were renumbered from 1 to 244. For a given identifier, some of the orbital elements of objects in the analysts' catalog changed sufficiently that it was apparent an analysts' identifier, which was no longer in use, had been assigned to another object. There are also indications that single objects have different identifiers for different observations.

4.2 Element Set Update Frequency

A change in element set number (appendix A) for an object means a state vector update has occurred. For the GRO and the officially cataloged objects, the average time between state vector update was 1.14 days. On average, at the time of each day's COMBO run, about 14 percent of the debris state vectors had not been updated for more than 24 hours.

4.3 "Clusters"

A large number of objects were observed to have conjunctions with the GRO within a second or so of other objects. Appendix E contains a list of these observed "clusters." Most of the observed clusters were associated with the Russian space station *Mir*. Since it was considered highly improbable that any set of objects could remain in a cluster for 5 months, an inquiry to USSPACECOM revealed that objects docked to one another have separate identifiers although they are part of a single object. This will provide an identifier for these objects when they separate at some future time.

To ensure that the flux, alert, and maneuver rate results were not influenced, objects having conjunctions with the GRO within 5 sec of a first object were excluded in the calculations.

5. Analysis

Position uncertainty for standard USSPACECOM tracking, measured debris flux as a function of altitude, eccentricity, and relative velocity distributions and Space Shuttle alert and maneuver rates were extracted from the data. Comparisons were made with engineering flux model and statistical flux model calculations. The appendices support the analyses described in this section of the paper.

5.1 State Vector Uncertainty

The simulation provides information on uncertainties associated with USSPACECOM GP tracking in a number of ways. Analyses were carried out that considered:

- 1) Changes in state vector position for the same conjunction predicted on two successive days. Since a 36-hour time span is scanned for conjunctions every 24 hours, about half of the predicted conjunctions were predicted on two successive days.
- 2) Any variation in state vector among objects “clustered” together.
- 3) Changes in the GRO state vector for a state vector update.

The primary importance of these data is they provide an indication of the likelihood of initially not observing a conjunction in a first COMBO run, and having an object suddenly appear in close conjunction in a subsequent COMBO run—too near to time of conjunction for USSPACECOM to establish an accurate state vector and for JSC to plan a debris avoidance maneuver. To determine risk and maneuver rate as in Foster,^[1] the uncertainties to be considered are those associated with high-intensity tracking and SP high-fidelity propagation, while nominal tracking frequency and standard-fidelity processing were employed by USSPACECOM in this work. Tracking uncertainty information determined in this study represents the least upper bound on what can be obtained with high-intensity tracking and SP processing. Nevertheless, inferences can be drawn concerning the accuracies of which USSPACECOM might be capable. A detailed study of high-accuracy tracking will be the subject of a subsequent study.

Of the 1948 observed conjunctions, 751 conjunctions were predicted on two successive days. One hundred and fifteen objects were predicted to pass within 100 km of the GRO on the day before the conjunction, but were no longer predicted to do so on the following day. A further 108 objects, which passed within the 100-km sphere on the day of conjunction, were not predicted to do so on the previous day. Most of these objects were on the edge of the 100-km radius “observation sphere.” Only one object that passed within 25 km of the GRO was not predicted to pass within the 100-km radius “observation” sphere on the previous day.

Of the 751 conjunctions predicted on two successive days, the difference between the conjunction time predictions was within 20 sec for all but one conjunction. Table 1 shows the distribution of difference between predicted time of conjunction on two successive days for all objects and all conjunctions. Both debris and GRO state vectors updated for only 118 of the 751 conjunctions were predicted on two successive days. There was not necessarily any state vector updates for either the GRO or the debris object on successive days.

Table 1. Number of conjunctions predicted on two successive days, within specified time difference.

Time difference (sec)	0.2	0.5	1.0	2	5	10	20	40
No. of conjunctions (all objects)	228	415	590	683	731	747	750	751
No. of conjunctions (cataloged objects)	142	282	432	511	555	569	572	573

5.1.1 Position differences for conjunctions with COMBOs on successive days

The change in predicted conjunction geometry over a 24-hour period when a state vector update has occurred provides a measure of uncertainty in 1-day predictions. Table 2 shows average changes and the 1° dispersion in radial, downtrack, and cross-track coordinates between first- and second-day predictions for the GRO, the debris object, and the relative coordinates between the GRO and the debris. Distances are in second-day UVW, GRO coordinates. Only conjunctions with officially cataloged debris, occurring within 5 sec of the previous day’s prediction, were included. Objects in the analysts’ data set were excluded from analysis because of problems described in section 4. Also, only cases involving a state vector update were considered: there were 366 update samples for the GRO, 208 update samples for debris, and 114 samples where both the GRO and the debris state vectors were updated. In addition, cases where the downtrack dispersion exceeded 3° were omitted from the analysis. The first-day state vector coordinates are propagated to the time of the second-day conjunction prediction for comparison.

Appendix I contains an additional description of the procedure.

Table 2. Average and RMS dispersion first- and second- day conjunction predictions.

Coord.	Average 24-hour displacement (km)			24-hour σ (km)		
	GRO	debris	rel. UVW	GRO	debris	rel UVW
U	0.025	-0.01	-0.024	0.29	0.52	0.69
V	1.53	-2.07	-1.55	6.4	9.04	9.2
W	0.024	0.01	-0.56	0.19	0.44	6.36

5.1.2 Debris state vector uncertainty

The debris state vector uncertainty is the primary parameter in the proposed debris avoidance procedure. As shown below, an estimate of debris state vector uncertainty can be made based on the 24-hour debris state vector dispersion and the “nominal” Space Shuttle orbiter position at-epoch uncertainty.^[3]

For nominal operating conditions for the orbiter, NASA is able to obtain an at-epoch UVW position uncertainty of $\pm(0.04 \times 0.275 \times 0.12)$ km with an associated 80-ft (or 24-m) semimajor axis uncertainty. Averaging the position uncertainty around an orbit—i.e., over the periodic perturbations—results in an average radial position uncertainty of about 0.12 km. Assuming that USSPACECOM, using high-intensity

tracking SPs processing, is capable of comparable at-epoch uncertainty for the debris and can parameterize the UVW debris position uncertainty as $\sigma_{UVW} = (\alpha_0 + \alpha_1 t^{1/2}, \beta_0 + \beta_1 t + \beta_2 t^{3/2}, 0.12)$ km, we obtain

$$\sigma_{UVW} = \left((0.12 + 0.05t^{1/2})_{RMS}, (0.275 + 0.16t + 0.07t^{3/2})_{RMS}, 0.12 \right) \text{ km,}$$

with t in hours. This parameterization assumes that uncorrelated atmospheric density variations over relatively short time periods dominate the radial and downtrack uncertainty. The terms are added rather than being calculated as an RMS.

5.1.3 Clusters – observation

The Russian space station *Mir*, catalog object 16609, was observed 22 times; for each occurrence, from four to seven objects were in conjunction with the GRO within 5 sec of the *Mir* conjunction. As discussed in section 4.3, these objects are attached to *Mir*. The UVW RMS position dispersion of these objects, propagated to the same time, is, over the 22 conjunctions, $0.08 \times 2.94 \times 0.18$ km, after dropping one conjunction set.

5.1.4 Invariant semimajor axis

The Keplerian semimajor axis, discussed in section 4.1 and shown in appendix D, is a direct measurement of the energy of an orbit about a spherical planet. Because of the oblateness of the Earth, the Keplerian semimajor axis of an Earth-orbiting object osculates. A constant, or invariant, semimajor axis, which is a nonvarying measure of orbital energy, can be calculated using Lineberry's method.^[4] Drag from residual atmosphere causes the semimajor axis to decrease. Fluctuations in density of the residual atmosphere produce a variation in the rate of semimajor axis decrease. Over time, these fluctuations result in an uncertainty in semimajor axis, σ_{sma} , if no new state vector measurements are taken. Downtrack position uncertainty increases over an orbit by an amount $3\pi\sigma_{sma} \approx 10\sigma_a$.

Figure 2 shows the GRO invariant semimajor axis calculated for each of the 1948 observed conjunctions. There were 141 element set updates performed over the 160 days spanned by the simulation. Over the period of the simulation, the semimajor axis dropped from 6761.4 to 6736.5 km, an amount of 156 m/day.

By comparing the semimajor axis estimate for the GRO before and after an element set update, the accuracy with which USSPACECOM determines the atmosphere and drag area over 1 day can be estimated. Throughout the 141 GRO state vector updates during the span of the simulation, the average semimajor axis change was $+14.7 \pm 53$ m 1σ , meaning the semimajor axis had to be raised an average of 14.7 m at each update. The average semimajor update correction was 8.3 percent of the total change per update.

From October 1992 through March 1993, the mean monthly $F_{10.7}$ solar flux (in units of 10^{-22} Watts m^{-2} Hz^{-1}) and geomagnetic index A_p were nearly constant with monthly values of: 130.8, 15; 145.2, 14; 139.1, 13; 121.0, 17; and 142.6, 16.^[5]

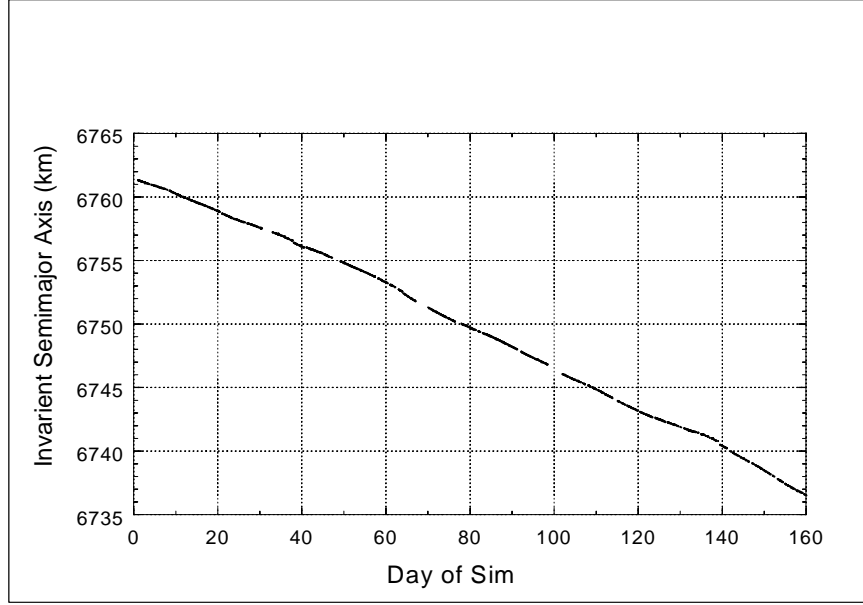


Figure 2. Invariant semimajor axis over time of simulation.

5.1.5 Derived epoch state vector

From the 24-hour UVW RMS position uncertainties for the GRO in section 5.1.1 $\pm(0.29 \times 6.4 \times 1.9)$ km and the ± 53 semimajor axis uncertainty for GRO from section 5.1.4, we infer a standard tracking UVW, GP processing state vector position uncertainty at epoch of $\pm(0.2 \times 1.6 \times 0.12)$ km. Per orbit growth in down-track position uncertainty is approximately equal to $10\sigma_{sma}$, where σ_{sma} is the semimajor axis uncertainty over the orbit. With 16 orbits per day, the daily semimajor growth is about $160\sigma_{sma}$. The 53-m semimajor axis uncertainty is due to uncertainties in measurement at each epoch and in atmospheric drag. Taking a combined contribution, σ_{sma} , from $2\sigma_{sma}^2 = 53^2 \Rightarrow \sigma_{sma} = 37.5 \text{ m} = 0.0375 \text{ km}$, we obtain down-track uncertainty, v , from

$$v^2 + (16\sigma_{sma})^2 = (6.4 \text{ km})^2 \Rightarrow v = 1.6 \text{ km}.$$

For the radial and cross track uncertainty at epoch U and W , we associate

$$2\sigma^U = 0.29^2 \Rightarrow \sigma_U = 0.2 \text{ km, and}$$

$$2\sigma^W = 0.19^2 \Rightarrow \sigma_W = 0.13 \text{ km.}$$

Note that our simulation was not carried out with the high-intensity tracking and SP processing we expect to use for space station debris avoidance. The down-track uncertainty of 1.6 km is reasonable in view of the small amount of tracking data USSPACECOM is believed to take on each standard tracking pass. The semimajor axis is well determined with the radial uncertainty, σ_U , due primarily to imprecise knowledge of perigee and eccentricity.

5.2 Engineering Flux Model Description

The Kessler engineering debris flux model predicts debris flux and debris objects per unit area per unit time as a function of debris object size, altitude, orbital inclination, solar flux, and time. The formulation of the model is described in Kessler.^[2] The engineering model is the basis of comparison for the flux measurements presented in section 5.3.

5.2.1 Tracked flux estimate

The engineering model was derived from the USSPACECOM catalog and micro impact measurements (0.1 mm and smaller) on surfaces retrieved from space after exposure to the debris environment. For initial model formulation, no data in the debris size region were between 0.1 mm and 10 cm. In formulating the model, it was assumed that USSPACECOM tracked all debris down to 10 cm in size and none below 10 cm; the model was extrapolated in this debris size region by matching flux values and derivatives between the micro region (0.1 mm and smaller) and the 10-cm tracked region.

Subsequent optical telescopic measurements by Karl Henize^[6] indicated a much higher flux than the model values in the 10-cm region and a multiplicative correction factor, so the Henize or H Factor, was added to the model to augment model flux in the 1-mm to 1-m size region. Engineering model calculations made for size ≥ 10 cm with the Henize factor set to one should closely approximate the tracked debris flux.

5.2.2 Origin of uncertainty

Debris flux dependence on time results from expansion and contraction of the Earth's atmosphere caused by variations in solar radiation output, the launch rates of objects into space, explosions of spent boosters, and collisions between orbiting objects. Solar radiation output varies in 9- to 11-year cycles, which can be predicted only approximately; launch rates vary widely. The occurrence of in-orbit explosions depends on vehicle design and the effort expended to limit them. Assuming a known number of orbiting objects, collision rates between orbiting objects can be calculated. However, even with objects of known mass, the consequences of a collision, in terms of the number and size distribution of collision products, depends on the structure of the colliding objects as well as on the collision geometry—all of which is difficult to predict, even statistically.

Any current projection of the debris population into the future involves considerable uncertainty. The model assumes a linear 5-percent growth rate of mass in orbit from 1988, a compounded 2-percent growth rate of fragments, and a direct dependence on the 13-month smoothed $F_{10.7}$ solar flux value *1 year prior* to the date for model calculation.^[2]

5.3 Measured Flux

The number of conjunctions through 1-km-wide bands was tabulated as a function of altitude. The area available for “detection” of an object at a given altitude changed continuously as the GRO descended over the period of the simulation; this area was calculated as a function of altitude for 1-km bands at ± 100 km for each conjunction. The average flux at a given altitude is calculated as the number of conjunctions over the period of the simulation and divided by the detection area averaged over the simulation at that altitude. This is then multiplied by 365/134.4 to give the annual flux. Flux depends on the relative velocity between the “target” and debris objects (equation, section 5.4.1). The relative velocity errors resulting from the GRO not actually being at the altitude of the debris were about 1 percent at the extremities of the ± 100 -km altitude range.

Figure 3 shows, over an altitude region from 300 to 470 km, the measured debris flux and a smoothed debris flux determined by averaging the measured flux over a ± 5 -km high-altitude region. Also shown in

the figure are the flux model predictions for 10-cm tracked debris. The debris flux model calculation used an $F_{10.7}$ -cm solar flux parameter of $188.1 (\times 10^{-22} \text{ Watts m}^{-2} \text{ Hz}^{-1})$, which is the 13-month smoothed solar flux averaged over October, November, and December 1991 and January and February 1992. These months cover the simulation period, 1 year before the actual simulation, as required for the solar flux input to the engineering flux model. The 10-cm debris flux model computation was made with the H factor off so as to approximate a tracked debris flux.

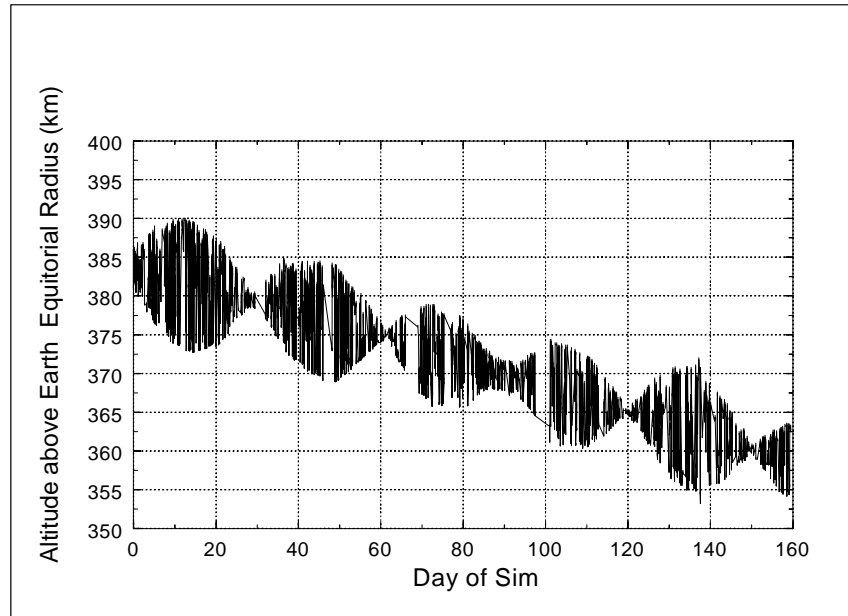


Figure 3. Measured, smoothed measured, and engineering model debris flux.

The average $F_{10.7}$ solar flux for the time period of the simulation was 135.7 with an average geomagnetic index, A_p , of 15. For a space station ballistic number of 10 lbs mass/ft², the operating altitude would vary between 435 and 411 km^[7] for an altitude strategy that requires that the station always has at least 180 days of decay time to an altitude of 150 n. mi., thereby minimizing the number of reboost maneuvers. The measured flux in this altitude region is about 0.2 objects/km²-year, while the engineering model prediction is on the order of 0.4 objects/km²-year.

There are sufficient data to conclude that the measured flux should closely approximate the average flux over the time period studied: The GRO covered about three periods in argument of ascending node (appendix H) during the 160 days of the simulation. Also over the time period of the simulation, the COMBO sphere about the GRO swept out a volume over 100 times the volume of a shell about the Earth covering the studied altitude range.

5.4 Statistical Flux Model

The simulation represents a sampling of the debris flux encountered by a single orbiting object. It was thought necessary to compare the measured flux with a flux determined from another source. Rather than consider the flux seen by another orbiting object, a comparison was made with a statistical flux generated from catalogs of orbital elements.

Two calculations were carried out. Statistical model flux calculations were performed from (1) the catalog of objects generated by the simulation, and (2) a series of USSPACECOM catalogs spanning the period of the simulation.

5.4.1 Statistical flux model description

In the development of his engineering model, Kessler developed a statistical model^[8] upon which the engineering model is partially based. This statistical model determines an average flux over time generated by an orbiting object as observed by another orbiting object. The model is applied, for each object in the USSPACECOM catalog, against an imaginary target at a specified orbital inclination and altitude. The individual fluxes from each object are summed to obtain an average statistical flux at the altitude and inclination of the imaginary target. Then the average flux seen by an orbiting object is given by

$$Flux = \sum_i \int_r \int_\beta \int_\lambda S_0(r, \beta, \lambda) S_i(r, \beta, \lambda) V_i^{rel}(r, \lambda) \cos \beta dr d\beta d\lambda ,$$

where $S_0(r, \beta, \lambda)$ and $S_i(r, \beta, \lambda)$ are the spatial densities of the target and the i th orbiting object, $V_i^{rel}(r, \beta, \lambda)$ is the relative velocity between these two objects, and the integrals are over the volume covered by the target object with r the radius, β the latitude, and λ the longitude of the volume under consideration. The spatial densities and relative velocities are calculated from the orbital elements of the objects. The sums are over all orbiting objects that cross the orbit of the target.

Insight into the appropriate radial integration limits in the calculation of the statistical debris flux at a given altitude may be obtained from figure 1. Oscillations in the GRO orbital radius caused by J2 and J3 perturbations are about 7 km, at maximum. The debris experiences similar altitude oscillations. Integrals at a given altitude were calculated over a ± 10 -km-wide strip at each altitude.

Appendix G contains a detailed derivation and discussion of the statistical model.

5.4.2 Details of statistical model flux calculation

For six different time periods, USSPACECOM catalogs—both official and analysts’—were obtained for the days 275, 305, 335, and 365 of 1992 and days 32 and 60 of 1993. These times correspond roughly to the start of the simulation, to dates 1, 2, 3, and 4 months after the start, and to the end of the simulation. Figure 4 shows the flux calculated as a function of altitude for each of the six time periods. The GRO and objects attached to *Mir* were excluded from the statistical flux computations.

5.4.3 Statistical flux contributions by altitude and object

Appendix F contains a compilation of contributions to the flux by an individual object as a function of altitude and time for those objects making the largest contribution to the statistical flux. The objects listed make up 50 percent or more of the flux in the altitude band and for the given time. We see that, at altitudes near 400 km, about 10 objects contribute half of the statistical flux. Calculations such as these can alert us to objects requiring the closest scrutiny.

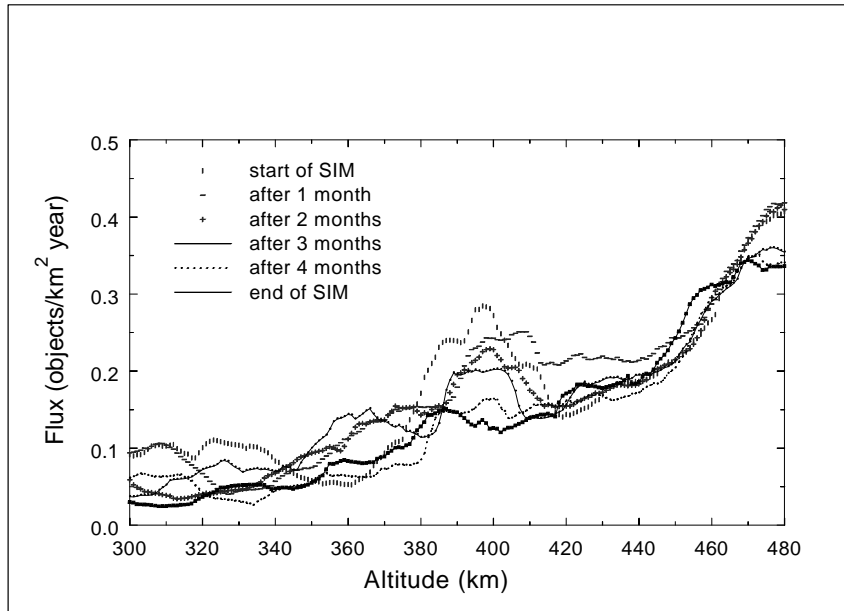


Figure 4. Statistical flux at approximately one-month intervals.

5.5 Flux Discussion – Measured Flux, Statistical Model, and Engineering Model

Figure 5 shows a compendium of flux data. Shown in the figure are:

- a) The smoothed measured flux taken from figure 3 (large open circles).

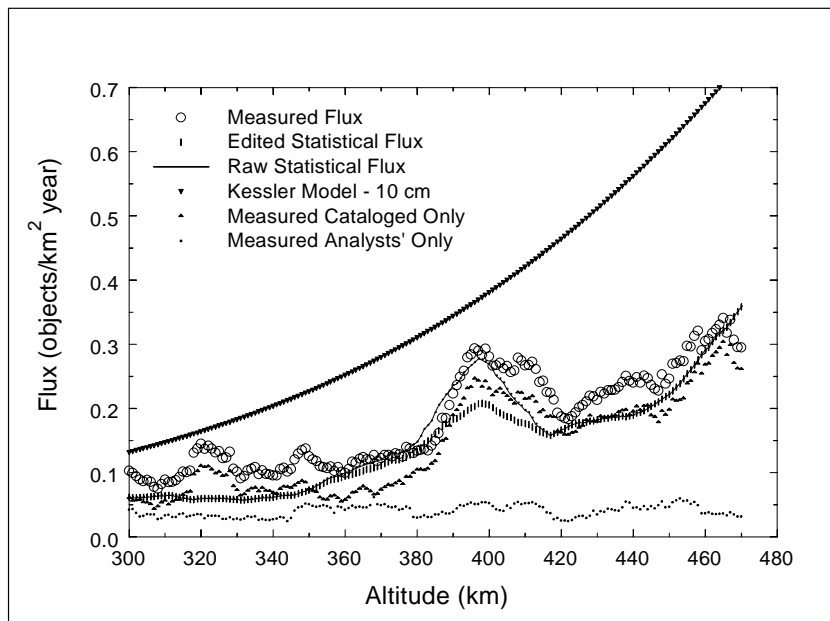


Figure 5. Comparison of measured and statistical flux.

- b) The 10-cm engineering model flux (small open circles).
- c) An *edited* statistical flux, which excludes the GRO and objects attached to *Mir*, obtained by averaging the curves in figure 4 (vertical line points).
- d) A statistical flux, which is an average of the monthly statistical fluxes excluding no objects from the flux computation (tiny points connected by line).
- e) The measured flux of cataloged objects (triangles).
- f) The measured flux of objects from the analysts' data set (small solid points).

We note that the edited statistical flux is close to the “Measured-Cataloged-Only” flux. The “Measured-Analysts’-Only” flux is a background of about 0.05 objects $\text{k}^{-2} \text{year}^{-1}$, comprising about one-quarter of the overall flux.

5.5.1 Measured flux contributions by altitude and object

Table D3 (appendix D) lists the largest contributors to the measured flux by object and altitude.

Comparing the edited statistical flux (vertical line points) with the measured flux (large open circles), broad peaks are observed in the measured flux at 320, 350, 400, 410, and 440 km. Table 3 shows the largest contributors to the measured flux at these altitudes.

Table 3. The largest contributors to measured flux taken from table 3D at indicated altitudes.

	320 km	350 km	400 km	410 km	440 km
Major flux contributors	22229 U.S. Misti	22045 <i>Mir</i> deb	22121 <i>Mir</i> deb 22190 Cosmos 2217 RB 22123 <i>Mir</i> deb 22128 <i>Mir</i> deb	22229 U.S. Misti	20389 Cosmos 2053 16308 Solwind deb

All of these objects were observed in multiple conjunctions at the altitudes shown in table 3. With the exception of object number 22229, these object numbers appear in table F1 (statistical flux contributions) at the altitude seen in table 3. Object 22229 has an elliptical orbit with a semimajor axis about that of the GRO, and the multiple conjunctions were a result of the two objects coming within 100 km of one another at apogee and perigee and very slowly moving closer together and then farther apart. This illustrates the primary problem with our method of measuring flux. To average out this effect, the simulation would need to last long enough for the two objects to again approach within 100 km of each other.

The unedited statistical flux (line and tiny points), shown in figure 5, more closely matches the measured flux than the edited statistical flux (vertical line points) that underestimates the flux in the *Mir* altitude region (390 to 410 km). Multiple conjunctions with the objects, shown as large contributors at 400 km, cause the measured flux to have a larger value at 400 km than would the result from a statistical average.

5.5.2 Object reentry

Figure 6 shows a statistical flux calculated from the catalog of objects (tables D1 and D2) produced from the simulation (crosses). This calculation overestimates the actual flux (open circles) from a factor of 3.5 in the 300-km region to a factor of 2 in the 420-km region. Table F2 identifies the objects in table F1 and shows reentry dates. By the end of the simulation, 34 of the 146 objects in the table had *not* reentered. A factor of 3.5 overestimation of flux indicates a factor of 3.5 turnover in objects at that altitude over the

simulation. A picture of the debris environment as slowly changing over a period of months is inaccurate. The debris environment at space station altitudes is very dynamic, with objects entering the atmosphere as other objects take their place in the altitude range studied.

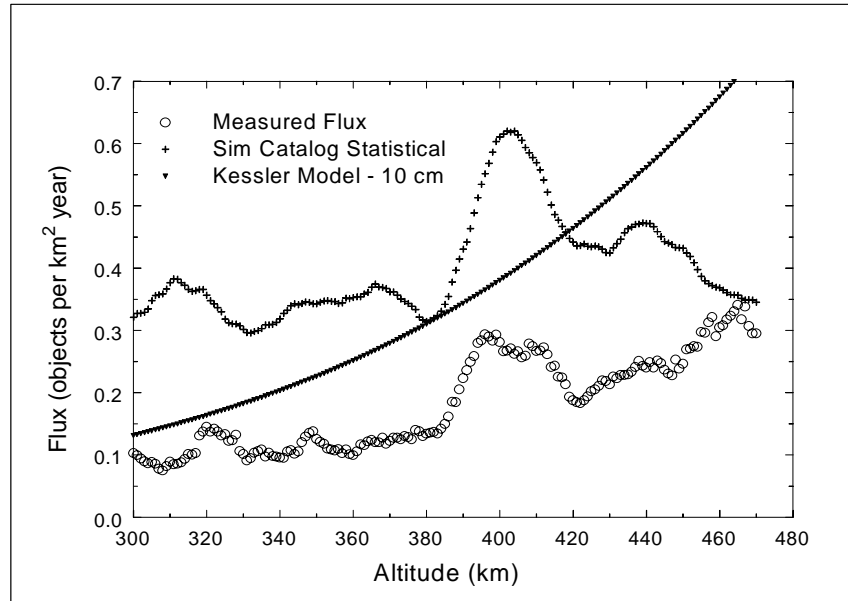


Figure 6. Comparison with statistical flux calculated from simulation catalog.

5.6 Debris Directional Distribution

The directional distribution of debris as seen from an orbiting target object is an intrinsic part of any flux model. The Kessler engineering flux model assumes that the debris flux travels horizontally, and predicts the angular direction of that flux in the horizontal plane relative to the horizontal component of the velocity vector of an orbiting object^[1] (appendix A). A direct measurement is taken from our flux measurements on a per conjunction basis and from the statistical model on a per object basis, as explained in appendix G.

In figure 7, we see that the high-altitude flux is fairly constant, and the low-altitude flux varies randomly and quickly.

Table 4 shows a comparison of the observed angular direction distribution of the debris flux together with that predicted by the Kessler engineering flux model as well as that taken from statistical model calculations. The statistical model result is averaged over the six catalogs spanning the simulation (section 5.4.2). The normalized coefficients are shown for $15^\circ (\pm 7.5)$ intervals about a given incident direction, taken from the target object velocity vector. The flux model predicts a maximum flux near 45° from the velocity direction, while the measured result maximum is near 53° and the statistical model result peaks at about 51° . A correction to the engineering model result toward larger angle might be expected, since the debris in eccentric orbits will have a higher velocity, thereby pushing the incident direction away from the GRO velocity vector.

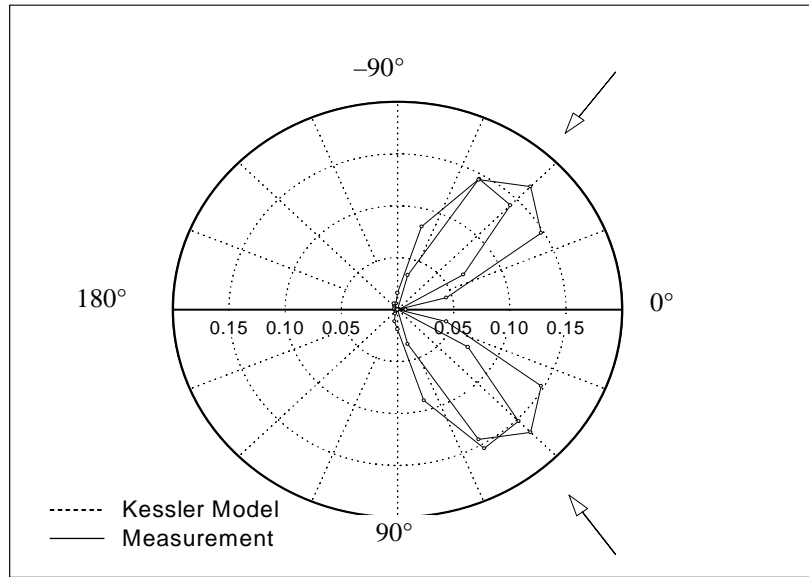


Figure 7. A graphical comparison between the engineering model and measured angular direction distributions.

Table 4. Normalized angular coefficients for 15° intervals; measured and engineering model.

Rel. angle	0°	15°	30°	45°	60°	75°	90°	105°	120°	135°	150°	165°	180°	°
Meas.	0.007	0.001	0.139	0.296	0.300	0.172	0.035	0.018	0.009	0.007	0.004	0.005	0.003	0.996
Eng. model	0.000	0.009	0.295	0.335	0.289	0.069	-	-	-	-	-	-	-	0.997
Stat. model	0.003	0.004	0.176	0.318	0.294	0.148	0.028	0.014	0.006	0.004	0.004	0.001	0.000	1.000

5.7 Radial Velocity Distribution

The flux model assumes the vertical velocity is zero. In Foster,^[1] the actual radial velocity distribution was needed to accurately assess the debris collision probability for a space vehicle. Figure 8 shows the vertical velocity distribution of the observed conjunctions relative to the GRO.

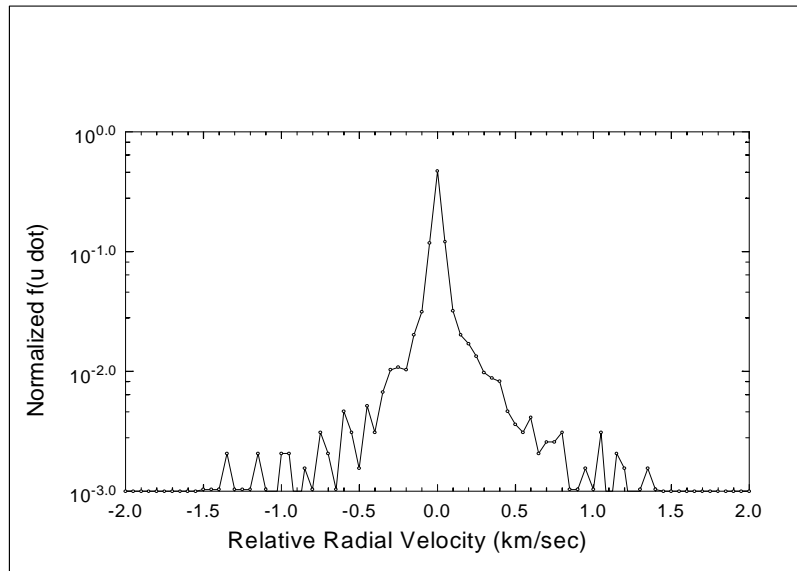


Figure 8. Radial velocity distribution.

5.8 Alerts and Maneuvers

If an object is projected to come within a box about the Space Shuttle ± 5 km radially, ± 25 km downtrack, and ± 5 km cross track, USSPACECOM declares an alert and begins high-intensity tracking and SPs processing. The $\pm(5 \times 25 \times 5)$ -km box is referred to as the Space Shuttle, or orbiter, criteria alert box. If the object is then predicted to pass within a box ± 2 km radially, ± 5 km downtrack, and ± 2 km cross track, the Space Shuttle Flight Rule Handbook^[9] states that the Flight Analysis Integration Team is to inform the flight director, who can order a debris avoidance maneuver if the primary mission objective is not impacted. The $\pm(2 \times 5 \times 2)$ -km box is referred to as the Space Shuttle criteria or orbiter criteria maneuver box.

All violations about the GRO over the period of the simulation, of the $\pm(5 \times 25 \times 5)$ -km orbiter alert box, and of the $\pm(2 \times 5 \times 2)$ -km orbiter maneuver box were recorded. These quantities were calculated for 1-km bands over the altitude range accessed by the simulation, not just immediately about the GRO, that was well below the space station altitude band. The procedure is described in more detail in appendix B.

An alert requires USSPACECOM to employ high-intensity tracking and SP processing, which produces USSPACECOM's most accurate short-term state vector, until it is verified that the risk of collision does not exceed the maneuver threshold. A projected violation of the Space Shuttle maneuver box will require high-intensity tracking and SP processing for an extended period of time. The alert and maneuver rates are indicators of the tracking and computation load borne by USSPACECOM.

5.8.1 Alerts and maneuvers observed for GRO

Using the Space Shuttle criteria, there were 15 violations of the Space Shuttle rule alert box and one violation of the Space Shuttle rule maneuver box about the GRO. Table 5 shows this information and the resulting annual alert and maneuver rate about the GRO.

Table 5. Number of penetrations of GRO alert and maneuver boxes, and annual alert and maneuver box violation rates.

No. of alerts during simulation	Annual alert rate	No. of maneuvers during simulation	Annual maneuver rate
15 ± 4	41 ± 11	1 ± 1	3 ± 3

5.8.2 Alert and maneuver rate as a function of altitude

The altitude range of the GRO was well below the operating altitude range of the space station. Further, the 15 alerts and single violation of the GRO maneuver box represent a very small portion of the total data. Alert and maneuver rates were determined for 1-km altitude bands from 300 to 470 km, assuming the target satellite to be at the center of the altitude band within the 100-km “detection” sphere. Because of the varying altitude of the GRO, access to conjunctions at altitudes above 450 km is reduced by a few percent and corrections were applied.

Comparisons for both alert rate and maneuver rate are made with engineering model and statistical results using the coefficients in table 4 and performing the numeric integrations indicated in Foster^[1] (appendix A).

5.8.3 Alerts as a function of altitude

Figure 9 shows the number of times that the alert box would have been penetrated as a function of altitude, the Kessler engineering model prediction for the number of tracked debris alerts, and the number of alerts expected from the statistical flux calculation. As expected from the flux measurements, the number of alerts predicted by the engineering model is about a factor of two too large, while the statistical model accurately predicts the number of maneuvers.

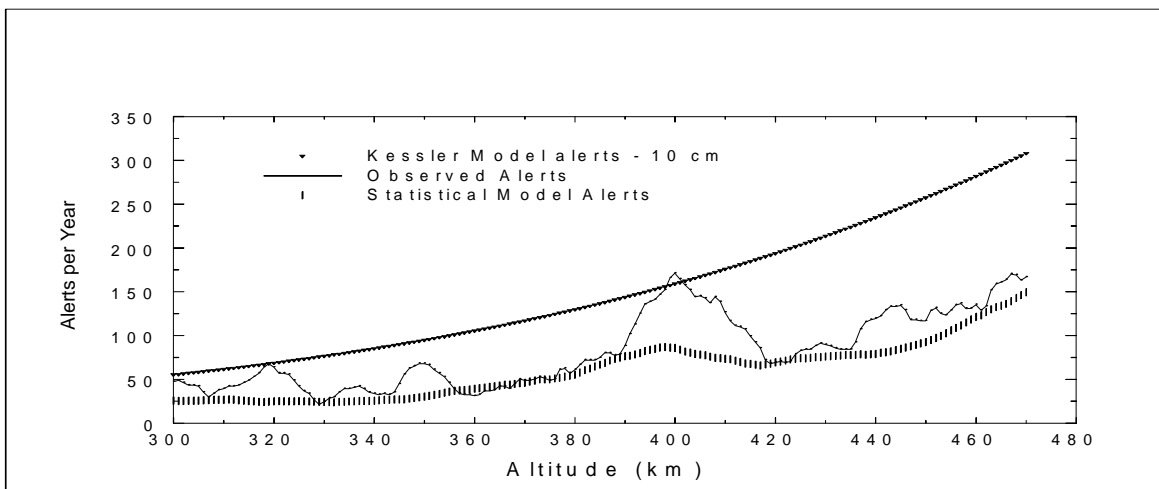


Figure 9. Annual Space Shuttle alert rate as a function of altitude.

5.8.4 Maneuvers as a function of altitude

Figure 10 shows the number of times per year the maneuver box would be have been penetrated as a function of altitude, the engineering model prediction for tracked debris, and the number of maneuvers anticipated from statistical model. Again the engineering model prediction is too high while the statistical model closely predicts, on average, the number of times the maneuver criteria was met. There are altitudes where few or no maneuvers would be performed.

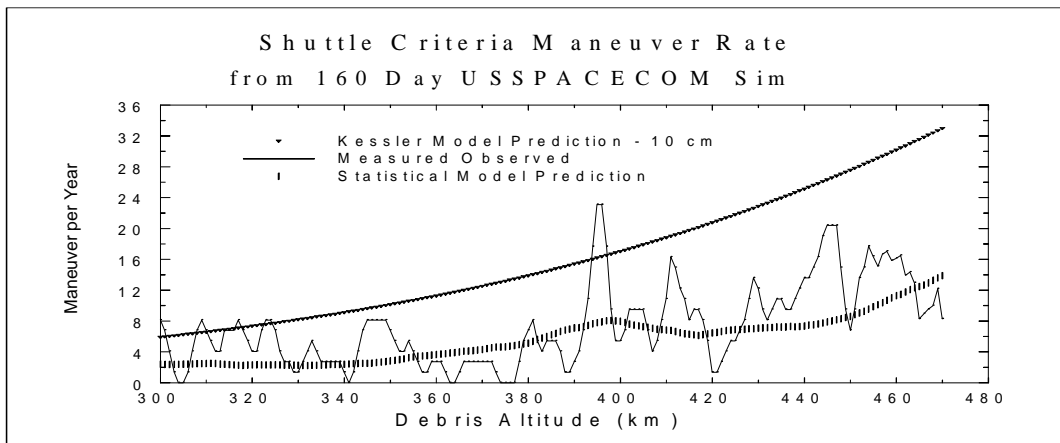


Figure 10. Annual Space Shuttle maneuver rate as a function of altitude.

5.9 Eccentricities

The distribution of eccentricities observed in the conjunctions provides information on the fraction of the tracked debris population for which effective debris avoidance can be performed: $Eccentricity = \frac{\delta_{ap}}{2 * perigee + \delta_{ap}}$ where δ_{ap} is the difference between apogee and perigee. Given a perigee of 6700 km and the Earth equatorial radius of 6378 km, an eccentricity of 0.1 corresponds to an altitude of 1800 km at perigee while an eccentricity of 0.2 corresponds to an altitude at perigee of 3300 km. The magnitude of the return radar pulse is proportional to R^{-4} . For smaller debris objects, an eccentricity of 0.1 will result in some loss of tracking opportunities, and an eccentricity of 0.2 will result in a more severe loss.

Table 6 shows the normalized eccentricity distribution coefficients from the catalog of objects collected from the simulation conjunctions, the eccentricity distribution of the individual simulation conjunctions, and the normalized eccentricity distribution coefficients predicted by the statistical model for conjunctions at altitudes from 300 to 450 km by the December 1992 catalog. The statistical model coefficients for $0 \leq e < 0.1$ varied by 15 percent, depending on the altitude band chosen. The other statistical model coefficients varied by a factor of two.

Table 6. Distribution of eccentricities.

\ e	0 to .1	.1 to .2	.2 to .3	.3 to .4	.4 to .5	.5 to .6	.6 to .7	.7 to .8	.8 to .9	.9 to 1
Sim cat.	0.640	0.094	0.034	0.026	0.023	0.066	0.072	0.045	0.0	0.0
Observed	0.835	0.075	0.014	0.011	0.007	0.023	0.023	0.013	0.0	0.0
St. model	0.922	0.043	0.011	0.002	0.002	0.012	0.012	0.005	0.0	0.0

6. Operational Implications

This section presents examples that apply the results of the previous sections and show implications of this study for an operating space station. This section also serves to illustrate ideas. Any strategy presented and any numeric values chosen for parameters are for illustration only.

6.1 Proposed Debris Avoidance Method

In JSC-25898,^[1] another debris avoidance method was proposed in which a maneuver was performed based upon a collision probability rather than a maneuver box. When, based on the last useful sensor data before a conjunction, the collision probability for the conjunction is determined to exceed a threshold P_m , a debris avoidance maneuver is performed; otherwise, it is not. For given position uncertainties for station and debris and a given P_m , there is an associated relative maneuver rate and a fractional residual risk. The actual number of maneuvers is given by the relative maneuver rate multiplied by debris flux. The fractional residual risk is that fraction of the no-maneuver risk that remains if the strategy is followed.

JSC-25898^[1] consisted of a parametric study with four levels of debris state vector uncertainty and four levels of station debris uncertainty, including “perfect.” In the parametric study, the best quality state vector for the debris was derived from the “average” quality Space Shuttle state vector propagated for one orbit.^[3] The geometry of the other levels of debris uncertainty implies a propagation of about one orbit. Figure 11 is generated from the data of JSC-25898.

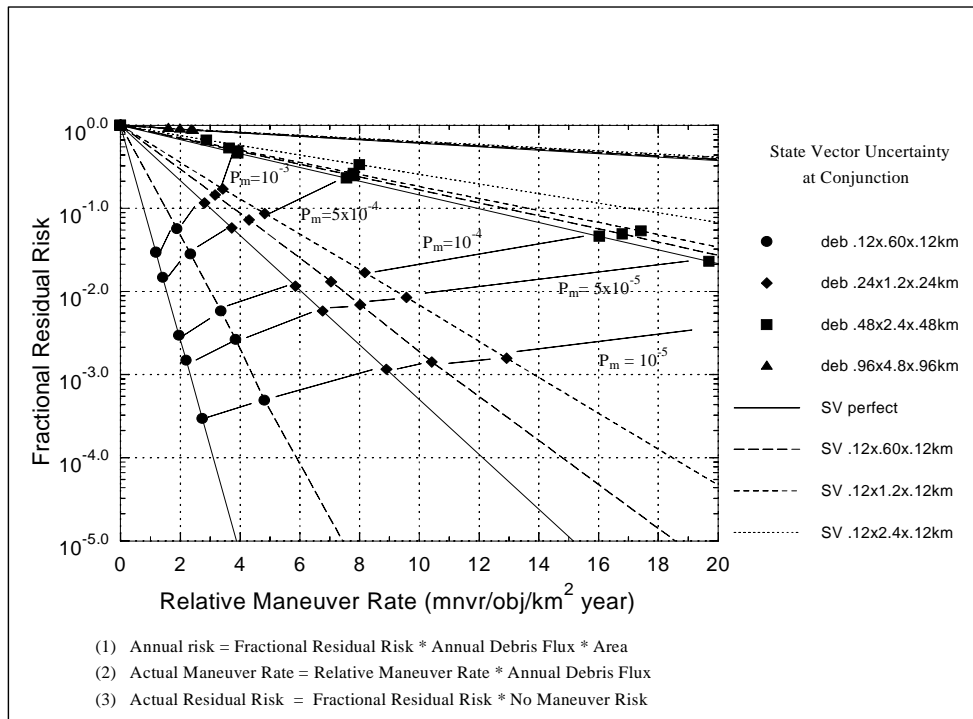


Figure 11. Fractional residual risk vs. relative maneuver rate as a function of P_m .

6.2 Example Using Current Measured Flux and Eccentricity Distribution

Applying the proposed debris avoidance strategy based on a P_m , assume that the station is perfectly tracked with a global positioning satellite, and that the state vector of debris objects with eccentricity less than 0.1 can be propagated to conjunction with an uncertainty $\pm 0.12 \times \pm 0.6 \times \pm 0.12$ km, or $\pm(0.12 \times 0.6 \times 0.12)$ km, (UVW).

As eccentricity increases, objects become harder to track at apogee and tracking opportunities are lost at some tracking sites. Assume that objects with eccentricities of between 0.1 and 0.2 can be propagated to conjunction with an uncertainty of $\pm(0.24 \times 1.2 \times 0.24)$ km and that objects with larger eccentricities cannot be tracked with sufficient precision to justify a maneuver. Assume that a P_m of 10^{-4} has been chosen. (We recall that P_m is the probability of penetration of a 60-m radius sphere about the station. A P_m of 10^{-4} then corresponds to a collision probability of less than 2×10^{-5} for a 2000-m² space station, or about the maximum collision probability associated with the orbiter maneuver box.)

For the period of time covered by the simulation, the space station would have had an altitude of between 234 and 209 km. The debris flux at this altitude over the period of the simulation was about 0.2 objects/km² year.

From table 6, 83.5 percent of the conjunctions are with objects that have an eccentricity less than 0.1 and 7.5 percent are with objects that have an eccentricity between 0.1 and 0.2. The remaining objects will be difficult to track over a short period of time. Therefore, we can assume that:

- 1) For a P_m of 10^{-4} , figure 11 shows relative maneuver rates of two and six maneuvers per year for uncertainties of $\pm(0.12 \times 0.6 \times 0.12)$ km and $\pm(0.24 \times 1.2 \times 0.24)$ km.
- 2) For a P_m of 10^{-4} , figure 11 shows fractional residual risks of 3×10^{-3} and 1.05×10^{-2} for uncertainties of $\pm(0.12 \times 0.6 \times 0.12)$ km and $\pm(0.24 \times 1.2 \times 0.24)$ km.
- 3) Fluxes of 0.2×0.835 and 0.2×0.075 are associated with uncertainties of $\pm(0.12 \times 0.6 \times 0.12)$ km and $\pm(0.24 \times 1.2 \times 0.24)$ km.
- 4) The fraction of the tracked debris population for which no maneuver is considered is $-0.835 - 0.075 = 0.09$.
- 5) For the 1992/1993 time frame:
 - Annual number of maneuvers = $2.0 \times (0.28 \times 0.835) + 6.0 \times (0.2 \times 0.075) = 0.42$.
 - Fractional residual risk = $(1 - 0.835 - 0.075) + 3 \times 10^{-3} \times 0.835 + 1.05 \times 10^{-2} \times 0.075 = 0.093$.

Under the stated assumptions:

- 1) The strategy eliminates $100\% - 9.3\% = 91.7\%$ of whatever debris risk there was with an anticipated maneuver rate of 0.42 maneuvers per year. The fractional residual risk is almost entirely due to that portion of the debris population for which objects cannot be tracked with sufficient precision to justify a maneuver. The choice of P_m has little effect on fractional residual risk because most of the residual risk comes from that fraction of the debris population that we hypothesize to be so poorly tracked that the collision probability never exceeds P_m . However, the choice of P_m strongly influences the maneuver rate.
- 2) The engineering model predicts twice this flux and twice this maneuver rate. Note that, for twice the debris flux, the absolute value of the risk doubles but the fractional residual risk is unchanged.

6.3 Analysis of the Single Penetration of the GRO Maneuver Box

It is helpful to examine the single penetration of the maneuver box about the GRO.

This conjunction with object 12630 occurred on October 29, 1992, at an altitude of 382 km. At the predicted time of conjunction, object 12630 was at a position $(-1.062, 1.8962, -0.6728)$ km, UVW, with respect to the GRO. Table 7 shows the collision probability between the GRO and object 12630 calculated using the integral method in Foster^[1] assuming perfect tracking on the GRO and six 3-hour propagation debris uncertainty bins, four of which are from figure 11.

For a P_m of 10^{-4} , a maneuver would not have been performed unless the state vector uncertainty had been between $\pm(0.5 \times 2.4 \times 0.5)$ km and $\pm(1.8 \times 9 \times 1.8)$ km.

Table 7. Collision probability for the GRO conjunction with object 12630 as a function of debris state vector uncertainty.

Pos. uncertainty of debris object	0.12×0.6×0.12 km	0.24×1.2×0.24 km	0.48×2.4×0.48 km	0.74×3.6×0.74 km	0.96×4.8×0.96 km	1.8×9.0×1.8 km
Collision prob.	2.5×10^{-21}	8.5×10^{-8}	9.6×10^{-5}	2.1×10^{-4}	2.0×10^{-4}	9.6×10^{-5}

6.4 Debris Flux Estimate for the Space Station Era

To plan for space station operations, an estimate of debris flux as a function of time over the lifetime of the station is necessary. The debris avoidance system must have sufficient capacity to handle the highest debris flux anticipated over the life of the station.

6.4.1 Space station altitude profile

The minimum operating altitude for the space station was specified to be that for which 180 days was needed for the station to decay to a 150 n. mi. altitude (figure 12). Assuming a 90-day period between reboots, this strategy implies a reboost altitude corresponding to 270 days for decay to 150 n. mi., and an average altitude over an increment corresponding to 225 days for decay to 150 n. mi.

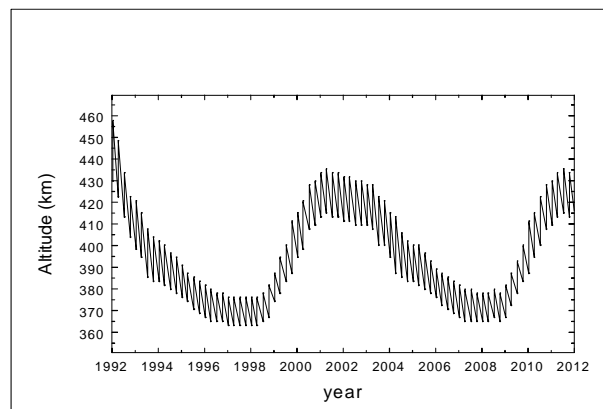


Figure 12. Predicted altitude profile for assembly complete space station and nominal MSFC solar radiation flux.

The actual altitudes at any given time depend on atmospheric density, which is determined by solar flux. Solar flux varies in cycles that are roughly 11 years in length, with a minimum value $F_{10.7}$ -cm solar flux value of about 70 and a maximum value of from 90 (-2σ) to more than 200 ($+2\sigma$) over a solar cycle.

Figure 12 shows the altitude profile predicted for a completed space station and a nominal Marshall Space Flight Center (MSFC) atmosphere and atmospheric prediction from January 1992 to the year 2012.^[5] The altitudes were derived from Carley^[7] using a ballistic coefficient B_n for the completed space station of $10 \text{ lbs ft}^{-1} \text{ sec}^{-2}$.

For minima in the $F_{10.7}$ -cm solar flux cycle, the corresponding space station altitude range will be approximately constant because of the very small variation, from solar cycle to solar cycle, observed in minimum solar flux. As solar flux increases, the debris flux at LEO altitudes decreases; however the operational altitude of the space station becomes higher, placing the station in a region of increased debris flux. The effect of solar flux uncertainty on long-term debris flux predictions is negligible compared with the uncertainty inherent in the debris flux model.

Rather than rely on solar cycle predictions, the space station shielding requirement specified a design to accommodate the debris flux at an operating altitude of 215 n. mi. (398 km) produced by a constant $F_{10.7}$ -cm solar flux of 70. This overestimates the debris flux, integrated over a solar cycle, by about 30 percent (figure 13).

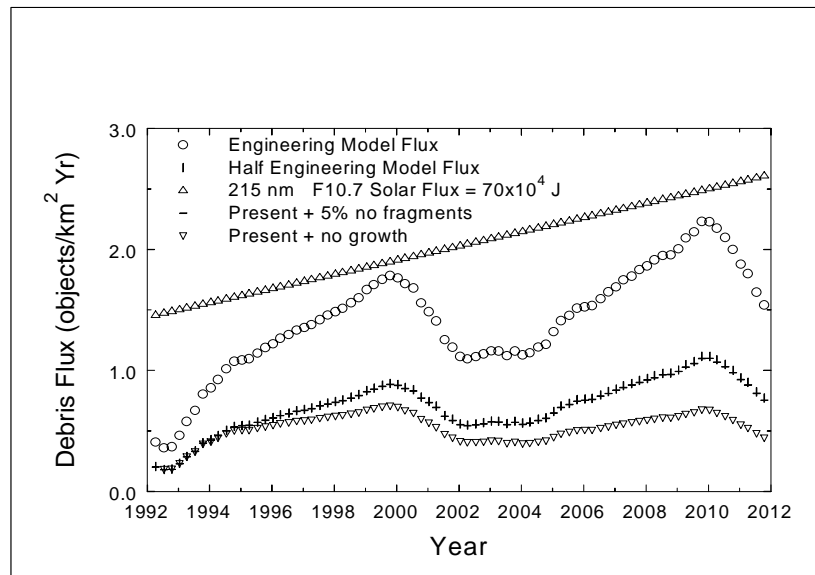


Figure 13. Space station debris flux for several debris population growth assumptions.

6.4.2 Comparison of space station and International Space Station Alpha altitude profiles

The ballistic coefficient for the completed International Space Station Alpha (ISSA) is $14.1 \text{ lbs ft}^{-1} \text{ sec}^{-2}$. Because of its larger ballistic coefficient, ISSA will orbit at a slightly lower altitude than space station for an altitude strategy dependent on number of days for decay to a reference altitude. However, because of the difference in orbital inclination between the stations, the ISSA orbit ($i=51.6^\circ$) will experience a somewhat

higher debris flux than the space station orbit ($i=28.5^\circ$) at the same altitude. These effects largely cancel out each other, and the debris flux observed by ISSA will be close to that for space station.

6.4.3 Debris flux for space station

For the period 1992 to 2012, Figure 13 shows the debris flux for:

- a) The space station shielding design requirement flux (215 n. mi. and solar flux = 70, represented by plus signs (+)).
- b) The engineering model flux, using the altitude profile of figure 12 and the MSFC solar flux, represented by large open circles (O).
- c) The engineering model half-value flux for the figure 12 altitude profile and the MSFC solar flux estimate, estimated by vertical lines (|).
- d) Present flux with 5-percent growth but no fragmentation, again for the altitude profile of figure 12 and the nominal MSFC solar flux estimate, represented by small open circles (o).
- e) The present flux with no growth or fragmentation, represented by inverted triangles (∇).

The present flux with no growth or fragmentation should represent a lower limit on the debris flux than we might expect, while the space station shielding design requirement represents an upper limit on the debris flux than we might expect, on average, over the period of ISSA operation.

6.5 Alert Rate and Maneuver Rate from Years 2000 to 2010

The average debris flux projection and the associated alert and maneuver rates for the years 2000 to 2010, when the space station will be in operation, are of concern. Debris flux will depend on the station altitude over time. Figure 12 shows the assembly-complete space station altitude profile as it would be for the years 1992 through 2012, assuming the 50th-percentile MSFC solar flux projection^[5] and using the altitude table of Carley^[7] for a ballistic number of 10.

Using this altitude profile, the debris flux as a function of time, at space station altitude, was calculated for four different situations and for an altitude of 215 n. mi. and a solar flux of 70, which corresponds to an upper-limit envelope of the debris flux adopted for shielding calculations. The result of these calculations is shown in figure 13.

Table 8 shows average debris flux from figure 13 together with the Space Shuttle criteria alert, the Space Shuttle criteria maneuver rate, the maneuver rate and fractional residual risk associated with a UVW debris position uncertainty of $0.12 \times 0.6 \times 0.12$ km and a P_m of 10^{-4} , and the maneuver rate and fractional residual risk associated with a UVW position uncertainty of $0.24 \times 1.5 \times 0.24$ km and a P_m of 10^{-4} . The fractional residual risk values were taken from figure 11.

Also shown in table 8, for space station altitude, are:

- 1) The present (1992/1993) space station altitude debris flux of 0.2 objects/km²-year. From this, we observe an annual rate of about 80 alerts and about eight penetrations of the Space Shuttle maneuver box, at space station altitude. From figure 11, for a P_m of 10^{-4} , the annual maneuver rate would be 0.4 maneuvers/year for the 0.6-km downtrack uncertainty ellipsoid, and 1.2 maneuvers/year for the 1.2-km downtrack uncertainty.

Table 8. Projected alert and maneuver rates.

	Present debris flux (1)	No-growth debris flux with solar variation (2)	Eng. Model debris flux (3)	Half eng. model debris flux prediction (4)	Shielding design debris flux (5)
Year(s)	1993	2000–2010	2000–2010	2000–2010	2010
Tracked debris flux (km ² y ⁻¹)	0.2	0.5	1.6	0.8	2.5
Space Shuttle criteria alerts	80	200	640	320	1000
Space Shuttle crit. maneuvers	8	20	64	32	100
Maneuvers/ fract. res. risk 0.12×0.6×12 P _m =10 ⁻⁴	0.4 0.003	1 0.003	3.2 0.003	1.6 0.003	5 0.003
Maneuvers/ fract. res. risk 0.24×1.2×0.24 P _m =10 ⁻⁴	1.2 0.01	3 0.01	9 0.01	4.8 0.01	15 0.01

- 2) The present debris population, without growth, projected using the engineering debris flux model parameterization that considers solar variations. The flux, averaged over the years 2000 to 2010, is 0.5 objects/km² year. This results in an annual alert rate of about 200 and about 20 passages per year through the Space Shuttle maneuver box, at space station altitude. For a P_m of 10⁻⁴, the annual maneuver rate would be one maneuver per year for the 0.6-km downtrack uncertainty ellipsoid, and three maneuvers per year for the 1.2-km downtrack uncertainty.
- 3) The engineering flux model prediction averaged over the years 2000 to 2010. Projecting the unmodified engineering flux model prediction results in an average flux of 1.6 objects/km² year. The resulting annual alert rate is about 320 with about 32 penetrations of the Space Shuttle maneuver box. The annual P_m=10⁻⁴ maneuver rate would be 3.2 maneuvers per year for the 0.6-km downtrack uncertainty ellipsoid, and nine maneuvers per year for the 1.2 km downtrack uncertainty.
- 4) One half the engineering flux model prediction averaged over the years 2000 to 2010. Taking one half of the engineering model, averaged over the years 2000 to 2010, we obtain an average flux of 0.8 objects/km² year, with an annual alert rate of 160 and 80 penetrations per year of the Space Shuttle maneuver box. The annual maneuver rates are 1.6 for the 0.6-km downtrack uncertainty ellipsoid, and 4.8 for the 1.2-km downtrack uncertainty.
- 5) The year 2010 value of the space station environment shielding design flux in figure 13 of 2.5 objects/km². For that flux, annual Space Shuttle alert and potential maneuver rates of 1000 and 100 result. The annual maneuver rates are 5 for the 0.6-km downtrack uncertainty ellipsoid, and 15 for the 1.2-km downtrack uncertainty.

6.5.1 Best estimate flux

Historically, debris flux has been at a minimum following a maximum in the solar cycle, at which time the flux has increased, eventually surpassing its pre-solar maximum value. This increase has not been smooth, however. The LEO flux has increased in *steps* of 50 percent or more as explosions and collisions occur before dramatically decreasing at the next solar cycle maximum. The engineering model approximates a discontinuous process with a continuous function. Typically, the engineering model prediction in the space station altitude range has been considerably higher than the actual flux; but, on occasion, the flux has exceeded the engineering model prediction value.

The engineering model prediction of $1.6 \text{ objects km}^{-2} \text{ year}^{-1}$ averaged over the years 2000 to 2010 is *too high*, based on historical data as well as the present flux. With no growth of the current debris population (only replacement of reentered mass) and no further fragmentation of debris from either explosion or collision, we project, from the engineering flux model, a debris flux of $0.5 \text{ objects km}^{-2} \text{ year}^{-1}$, averaged over the years 2000 to 2010. This is a *lower limit* on the debris flux, which might be expected for the space station. From figure 13, an averaged space station altitude tracked debris flux, over the years 2000 to 2010 and assuming current tracking capabilities, should be roughly $1 \text{ object km}^{-2} \text{ year}^{-1}$, with 400 alerts per year; that is, there should be 40 annual penetrations of the Space Shuttle maneuver box. From figure 11 for a P_m of 10^{-4} , we expect about two maneuvers per year if all debris has the 0.6-km downtrack position uncertainty (propagated to conjunction), and about six maneuvers per year if all debris has an associated 1.2-km downtrack uncertainty.

6.5.2 Debris avoidance system capacity

The year 2010 value of the space station environment design flux in figure 12 predicts 1000 annual Space Shuttle criteria alerts and 100 annual Space Shuttle criteria maneuvers. The alert rate is the frequency at which USSPACECOM must undertake high-intensity tracking and SP processing. The Space Shuttle criteria maneuver rate approximates the frequency at which USSPACECOM must carry out high-intensity tracking and SP processing on an object over a sustained period of time. With the variations inherent in the debris flux, we might expect to encounter this level of debris flux for a brief period over the life of the ISSA.

7. Conclusions

The simulation provides some insight into the debris flux that can be expected for an operating space station. Data provide a comparison between the actually observed debris flux and the engineering model. The observed flux is approximately half of that expected from the engineering model.

The observed 24-hour position dispersion is as expected for GPs processing and indicates that USSPACECOM will be able to produce the quality state vector information with high-intensity tracking and SPs processing that will be needed to successfully implement a debris avoidance procedure based on a collision probability.

The demand on USSPACECOM resources for NASA support during space station assembly and operations will increase considerably over that for current Space Shuttle operations. At times over the life of the space station, the debris flux is expected to be considerably higher than the current value.

During this simulation, a small number of objects contributed a majority of the debris flux. Certain objects were seen repeatedly during the simulation.

The collision probability selected for a maneuver threshold will determine the fractional residual risk and the maneuver rate resulting from the proposed debris avoidance strategy. About 10 percent of the conjunctions seem to be with objects that have sufficiently large eccentricities to limit tracking opportunities. The state vector uncertainties may be sufficiently large that the space station will seldom perform a debris avoidance maneuver for these objects. It is possible for the maneuver rate to be strongly dependent on the maneuver threshold value, while the fractional residual risk is relatively insensitive to the chosen threshold.

8. References

1. Foster JL and Estes HS, JSC-25898, *A Parametric Analysis of Orbital Debris Collision Probability and Maneuver Rate for Space Vehicles*, August 1992.
2. Kessler DJ, Reynolds RC, and Anz-Meador PD, NASA TM100-471, *Orbital Debris Environment for Spacecraft Designed to Operate in Low Earth Orbit*, April 1989. SSP-30425, Rev. A, *Space Station Natural Environment Definition for Design*, June 1991.
3. Peterson DP, Memo to FB Lowes from WH Heilman, *Covariance Matrices*, August 25, 1988.
4. Lineberry EC, JSC Internal Note No. 74-FM-84, *Invariant Orbital Elements for Use in the Description of Motion about an Oblate Earth*, December 4, 1974.
5. Euler HC Jr., Marshall Space Flight Center (EL54), *Solar Activity Inputs for Upper Atmospheric Models Used In Programs to Estimate Space Craft Orbital Lifetime*, January 6, 1994.
6. Henize KG, Stanley JF, AIAA 90-1990, *Optical Observations of Space Debris*, 1990.
7. Carley KW, JSC-36099, *Space Station Freedom Orbital Decay Handbook*, August 1992.
8. Kessler DJ, ICARUS 48,39-48, *Derivation of the Collision Probability between Orbiting Objects: The Lifetimes of Jupiter's Outer Moons*, 1981.
9. *Space Shuttle Flight Rule Handbook*, Johnson Space Center Mission Control Center.

Also used in this document was the following general reference:

Abramowitz M and Stegun IA, *Handbook of Mathematical Functions*, U.S. Government Printing Office, June 1964.

Appendix A: Message Format

The COMBO messages received from USSPACECOM are in the following form:

```
SATELLITE RELATIVE MOTION PROGRAM (UNITS: KM, KM/SEC)
FROM start time TO stop time MAX SEP. COMBO range from target KM
ABSOLUTE MINIMUM or RELATIVE MINIMA
DATE      SATELLITES  AZ2 EL2  AZSUN ELSUN  SPACING
PHI1     LAMBDA1    H1     PHI2  LAMBDA2 H2
DU      DV        DW     DUDOT DVDOT  DWDOT
X1      Y1        Z1     X2    Y2     Z2
X1DOT   Y1DOT     Z1DOT  X2DOT Y2DOT  Z2DOT
DIHEDRAL EL SET NUMBERS
```

The *start time* and *stop time* are the start and stop times of the time span covered by the COMBO run written as YYDDHHMMSS.SSS.

DATE is the time of conjunction and is written as YY DD HH MM SS.SSS; that is, year, day of year, hour of day, minute of hour, and seconds of minute.

SATELLITES is three quantities: (1) the primary satellite number, (2) a letter **V**, if the secondary satellite is illuminated (else a blank), and (3) the secondary satellite number.

AZ2 and **EL2** are the azimuth and elevation of the secondary satellite as viewed from the primary satellite at conjunction in degrees.

AZSUN and **ELSUN** are the azimuth and elevation of the Sun as viewed from the primary satellite at time of conjunction.

SPACING is the separation of the two satellites at closest point of approach (CPA), in kilometers.

H1, **PHI1**, and **LAMBDA1** are geocentric altitude, latitude, and longitude of the primary satellite at CPA, in kilometers and degrees.

H2, **PH2**, and **LAMBDA2** are the same quantities for the secondary satellite.

DU, **DV**, and **DW** are the radial, downtrack, and cross-track separation of the two vehicles at CPA in kilometers.

DUDOT, **DVDOT**, and **DWDOT** are the corresponding relative velocities in kilometers per second.

X1, **Y1**, **Z1** and **X1DOT**, **Y1DOT**, **Z1DOT** are the x, y, z components of the primary satellites position and velocity at CPA in kilometers and kilometers per second; the coordinate system is Geocentric Cartesian Mean Equinox of Epoch.

X2, **Y2**, **Z2** and **X2DOT**, **Y2DOT**, **Z2DOT** are the same quantities for the secondary satellite.

DIHEDRAL is the angle between the orbital planes of the primary and secondary objects in degrees.

EL. SET NUMBERS are the element set numbers for the primary and secondary objects. A change in this parameter means that an element set update has occurred.

The parameters are interrelated; the message has been constructed so as to provide double redundancy. If a quantity is incorrectly transmitted, the error can be detected and corrected from information in the COMBO message.

Appendix B: Verification, Flux, Alerts, and Maneuvers

Verification

Interrelationships between the USSPACECOM message parameters permitted verification of the scanner data. Using the variable names from appendix A, the following relationships were used for verification. The limits are indications of the innate precision of the USSPACECOM data.

The relation

$$\left| \sqrt{DU^2 + DV^2 + DW^2} - \sqrt{(X1 - X2)^2 + (Y1 - Y2)^2 + (Z1 - Z2)^2} \right| < 0.005 \text{ km}$$

verifies the magnitude and signs of the six position components as well as the magnitudes of the three relative position components.

Similarly,

$$\left| \sqrt{DUDOT^2 + DVDOT^2 + DWDOT^2} - \sqrt{(X1DOT - X2DOT)^2 + (Y1DOT - Y2DOT)^2 + (Z1DOT - Z2DOT)^2} \right| < 0.00003 \text{ km/sec}$$

verifies the magnitude and signs of the six velocity components as well as the magnitude of the three relative velocity components.

The altitudes H1 and H2 and latitudes $\lambda_i = \text{LAMBDA1}$ or LAMBDA2 satisfied

$$\left| \sqrt{X_i^2 + Y_i^2 + Z_i^2} - \sqrt{\zeta^2 + \xi^2} \right| < 0.1 \text{ km}, \quad i = 1, 2,$$

where

$$\zeta = \frac{R_0}{\sqrt{1 + \frac{\tan \lambda_i}{1 - e^2}}}, \quad \xi = (1 - e^2)(R_0^2 - \zeta^2), \quad \text{with } R_0 = 6378.135$$

as the Earth equatorial radius and $e = 0.081395$ as the eccentricity of a cross section of the Earth containing the polar axis.

The relative position and velocity satisfied

$$\sqrt{DUDOT * DU + DVDOT * DV + DWDOT * DW} < 0.002,$$

verifying the signs and magnitudes of the relative position and velocity components. Requiring the eccentricity, e , and orbital inclination, i , of the GRO, which were calculated from position and velocity vectors, to satisfy

$$e < 0.0025 \text{ and } (i - 28.46^\circ) < 0.027,$$

provided additional verification of the signs and magnitudes of the GRO state vector components.

Angular momentum was calculated as $\vec{h}_i = \vec{r}_i \times \vec{v}_i$, where

$$\vec{r}_i = X_i \hat{i} + Y_i \hat{j} + Z_i \hat{k} \quad \wedge \quad \vec{v}_i = \dot{X}_i \hat{i} + \dot{Y}_i \hat{j} + \dot{Z}_i \hat{k}.$$

Orbital inclination is then given by $i = \frac{h_3}{|\vec{h}|}$.

Energy is $E = \frac{1}{2}v^2 - \frac{\mu_e}{r}$ and eccentricity is $e = \sqrt{1 + 2E \frac{h^2}{\mu_e^2}}$, where $\mu_e = 3.986012 \times 10^5 \text{ kg}^3/\text{sec}^{-2}$.

Times, recorded as YYDDHHSS.SSS, were required to be in sequential order, and all time differences in time overlapped data that were greater than 1 sec were verified.

Flux and Flux Detection Area

Over the period of the simulation, predicted conjunctions within a 100-km radius sphere surrounding the GRO were recorded. The analysis spanned altitudes from 290 to 490 km in 1-km bands. The effective area for debris “detection” in an altitude band depended on the altitude of the GRO. We had a choice between calculating an effective detection area for each conjunction or determining an average area for an altitude band over the period of the simulation. We chose to calculate the average area.

For the j th conjunction, the area available over a ± 0.5 -km band at altitude h_i is calculated in 1-km intervals between 290 and 490 km as

$$a_{ij} = 2 * \sqrt{100^2 - (h_{GRO} - h_i)^2} \text{ km} * 1 \text{ km}$$

where the altitudes h_{GRO} and h_i are with respect to the Earth’s equatorial radius and are given by

$$h_{GRO} = \sqrt{X1^2 + Y1^2 + Z1^2} - R_0, \quad H_i = r_i - r_0.$$

The flux at a given altitude is then

$$Flux = \frac{\text{number of debris conjunctions at } h_i \pm 0.5 \text{ km}}{\bar{A}_i \text{ km}^2} * \frac{365}{134},$$

where the effective area is given by

$$A_i = \frac{\sum_j a_{ij}}{\text{total number of conjunctions}}.$$

The conjunction altitude is

$$h_i^c = \sqrt{X^2 + Y^2 + Z^2} - R_0.$$

Figure B1 shows the available time-averaged area as a function of altitude. The use of an area averaged over the time span of the simulation extends the region for which data can be obtained and reduces fluctuations at the high and low altitudes of the simulation. However, the procedure weighs the early high-altitude data more heavily than the late data, and the late low-altitude data more heavily than the early data. The procedure is statistically valid if the flux is constant over time, or if the period of the fluctuations is small compared with the time span of the simulation. In figure 7, we see that the high-altitude flux is fairly constant and the low-altitude flux varies randomly and quickly.

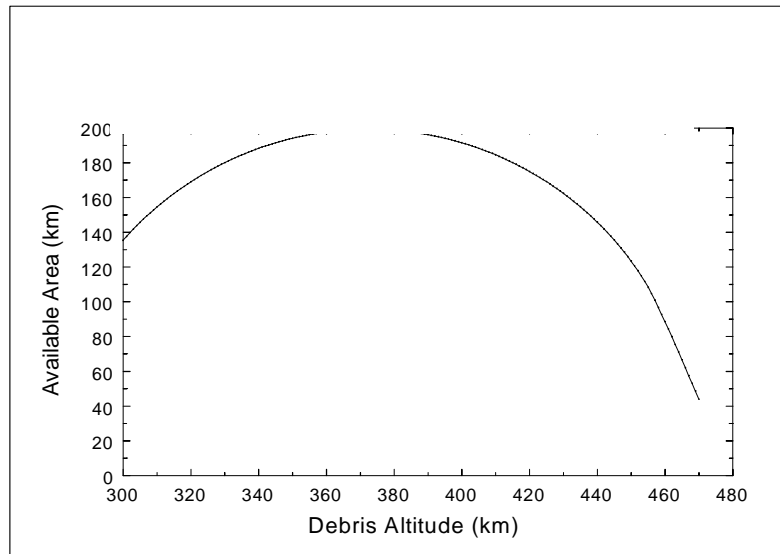


Figure B1. Time-averaged available area for flux.

Alerts and Maneuvers

The Space Shuttle alert box is $\pm(5 \times 25 \times 5)$ km, UVW. For a conjunction, the time of crossing the side boundary of the alert box is

$$t_{5\text{km}} = \frac{DW - 5}{DWDOT}.$$

The downtrack distance, D_v , at the time at which the side boundary of the alert box is crossed is

$$D_v = |t_{25\text{km}} * DVDOT + DV|.$$

If $D_v < 25$ km, the object is within the alert box at conjunction. Rather than considering ± 5 -km, or 10-km, high boxes, we consider each 1-km horizontal slice separately. The number of passages through the four boxes above and the four boxes below are added to the contribution from the central box; to this

is added the averaged contribution from the boxes 5 km above and below the central box. This is done in 1-km steps, from 300 to 470 km.

The Space Shuttle maneuver box is $\pm(2 \times 5 \times 2)$ km. The same algorithm used for alerts is used in the maneuver determination, with 2 km substituted for the 5-km cross-track distance and 5 km substituted for the 25-km downtrack distance.

For 1-km-high bins, the half contribution point is at 99.2 km from the GRO for alerts and 99.7 km for maneuvers. At 1-km intervals, the *access* to alerts and maneuvers as a function of altitude is determined (in the manner of figure B1), and a time-averaged correction is made to the number of passages through each 1-km-high alert and maneuver region before combining the vertical regions to calculate numbers of alerts and maneuvers.

Appendix C: Computer Codes

The large quantity of data required the development of computer codes to aid in the analysis. The following codes accordingly were written:

DVERIFY – A data verification program that uses some of the redundancies in the COMBO message to identify errors from the scanning process for the parameters of interest in this analysis. This program reads a control file that lists the data files to be read. When a FORTRAN read error is encountered, sufficient information is available on the computer screen to immediately find and correct the error. Once the data is read, the program identifies errors from the message redundancies and generates a list of errors in a file. All of the data can then be dealt with efficiently.

FILLIN – Because the data contained dropped columns as well as scanner errors, it was sometimes necessary to iteratively guess a missing digit and observe the resulting digit pattern. Use of this program provides an efficient means of dealing with entire missing columns.

SEPARATE – Generates non-time-overlapped data sets using the control file used for DVERIFY. The control file gives filenames and start and stop times for the COMBO runs.

DURATION – Computes time length of non-time-overlapped data (134.378 days).

OBJINDX – Generates a file with the number of conjunctions for each object.

OBJECTS – Using the OBJINDX file, this program groups objects and computes eccentricity, semi-major axis, and orbital inclination for each observation of each object. The average value of these parameters is compared with the individual values. Using this program, a number of small remaining errors, not detected in the verification process, are corrected and several objects with very different orbital parameters for the same identification number are assigned different identification numbers for each separate set of parameters.

XCLUSTRS – This program finds objects with GRO conjunctions less than 5 sec apart and that have the same eccentricity, semimajor axis, orbital inclination, and argument of ascending node.

XOVERLAP – Analysis of duplicate/non-duplicate events in the same time period using the basic data file. This program generates the data on timing accuracy presented in table 1. The program uses the control file and the COMBO files.

DOUBLES – Analysis of duplicate events in the OBJECTS file.

ANALYZE – Calculates debris flux, alert and maneuver rate, the angular distribution of the velocity of the secondary object with respect to the velocity vector of the primary, and the radial velocity distribution.

KESSLER – Engineering model flux computation as a function of altitude, orbital inclination, and solar flux.

VEL&DIR – Calculates relative velocity as a function of relative conjunction angle, and determines the distribution as a function of angle (table 4 and figure 7).

CATFLUX – Computes a statistical flux from a catalog of orbiting objects as a function of altitude and orbital inclination.

ALTFLUX1 – Determines those objects that make the largest contribution to the debris flux as a function of altitude.

Appendix D: Objects

Table D1. Cataloged objects having conjunctions with the GRO within a 100-km distance, over the time period covered by the simulation. Shown are the international designator (intl des.), the USSPACECOM object number (obj), eccentricity (e), orbital inclination (i), altitude above mean equatorial radius at perigee and apogee, number of observations over the simulation, mean time between state vector updates in days, description of the object, country of origin, launch date, and reentry date for those objects that have reentered.

intl des.	obj	a (km)	e	i (deg)	perigee (km)	apogee (km)	# obs	days/ updt	description	country	launch	reentry
1960-014A	60	7263.2	0.0674	49.93	395.4	1374.8	3	0.64	EXPLORER 8	US	3 NOV 60	
1963-014U	2373	8949.4	0.2473	84.29	357.9	4784.6	1	na	WESTFORD NEEDLES	US	9 MAY 63	22 JUN 93
1963-024A	604	6793.1	0.0020	58.22	401.1	428.7	25	0.90	TIROS 7	US	19 JUN 63	
1963-025B	614	7829.7	0.1433	82.08	329.2	2573.8	2	2.08	HITCH HIKER 1	US	27 JUN 63	
1963-047A	694	7354.5	0.0701	30.34	461.0	1491.6	1	na	ATLAS CENTAUR 2	US	27 NOV 63	
1964-006A	746	9887.5	0.3129	60.86	415.1	6603.6	1	na	ELEKTRON 1	USSR	30 JAN 64	
1964-006C	750	8935.5	0.2406	60.85	407.3	4707.5	2	1.39	ELEKTRON 1 DEB	USSR	30 JAN 64	
1964-006S	19173	7523.8	0.1034	60.73	367.5	1923.8	5	1.38	ELEKTRON 1 DEB	USSR	30 JAN 64	
1964-006T	19990	8410.2	0.1939	60.77	401.3	3662.7	4	1.58	ELEKTRON 1 DEB	USSR	30 JAN 64	
1964-006U	19991	8379.0	0.1911	60.74	399.9	3601.9	5	1.46	ELEKTRON 1 DEB	USSR	30 JAN 64	
1964-006W	19993	8283.1	0.1819	60.78	398.2	3411.7	6	1.36	ELEKTRON 1 DEB	USSR	30 JAN 64	
1964-006X	19994	7989.2	0.1532	60.75	384.4	2837.8	4	0.83	ELEKTRON 1 DEB	USSR	30 JAN 64	
1964-006Y	19995	7612.7	0.1076	60.51	415.1	2054.1	7	na	ELEKTRON 1 DEB	USSR	30 JAN 64	
1964-006Z	19996	8258.2	0.1795	60.80	397.6	3362.5	2	1.79	ELEKTRON 1 DEB	USSR	30 JAN 64	
1964-006AA	19997	8366.0	0.1913	60.81	387.5	3588.3	1	na	ELEKTRON 1 DEB	USSR	30 JAN 64	
1964-006AC	20101	7611.0	0.1271	60.73	265.7	2200.0	3	na	ELEKTRON 1 DEB	USSR	30 JAN 64	
1964-038A	829	9818.3	0.3093	60.83	403.8	6476.5	1	na	ELEKTRON 3	USSR	10 JUL 64	
1964-038C	831	8861.2	0.2351	60.77	399.4	4566.8	3	1.80	ELEKTRON 3 DEB	USSR	10 JUL 64	
1965-038B	1378	6851.9	0.0068	97.87	427.2	520.2	10	0.99	OPS 8386 R/B (ALTAIR)	US	20 MAY 65	
1965-051C	1440	6848.8	0.0043	98.55	441.0	500.3	13	0.92	TIROS 10 DEB	US	2 JUL 65	
1965-078A	1613	7959.5	0.1480	144.24	403.1	2759.6	6	1.64	OV1 2	US	5 OCT 65	
1965-078B	1616	7897.9	0.1412	144.26	404.5	2634.9	7	0.34	OV1 2 R/B	US	5 OCT 65	
1965-082BW	1715	6775.8	0.0011	31.86	390.3	405.0	16	0.55	OV 2 1/LCS 2 DEB	US	15 OCT 65	5 FEB 93
1965-082EB	1836	6777.9	0.0012	32.19	391.7	407.8	24	0.73	OV 2 1/LCS 2 DEB	US	15 OCT 65	17 APR 93
1965-082GY	1963	6853.8	0.0014	32.05	466.0	485.2	2	1.17	OV 2 1/LCS 2 DEB	US	15 OCT 65	
1965-082LS	3355	6736.8	0.0024	31.65	342.5	374.8	3	na	OV 2 1/LCS 2 DEB	US	15 OCT 65	3 NOV 92
1965-112Q	1937	6857.4	0.0017	55.94	467.8	490.7	3	1.79	COSMOS 103 DEB	USSR	28 DEC 65	
1966-026F	2179	6796.2	0.0025	98.00	400.9	435.3	29	0.74	OPS 0340 DEB	US	31 MAR 66	20 APR 93
1966-034A	2150	8626.8	0.2204	82.39	347.3	4149.9	2	1.87	OPS 1527 (OV-3 1)	US	22 APR 66	
1966-034B	2167	7639.2	0.1224	82.36	326.0	2196.0	3	1.00	OPS 1527 DEB	US	22 APR 66	
1966-070A	2389	8149.3	0.1735	81.43	357.3	3185.0	1	na	OV3 3	US	4 AUG 66	
1966-070D	2800	8342.4	0.1858	81.46	414.4	3514.2	1	na	OV3 3 DEB	US	4 AUG 66	
1967-001D	2643	18640.6	0.6416	26.76	302.7	24222.2	2	1.46	INTELSAT 2 F-2 R/B(2)	US	11 JAN 67	
1967-001T	5988	7035.7	0.0713	26.58	149.3	1165.8	4	0.43	INTELSAT 2 F-2 DEB	US	11 JAN 67	29 JAN 93
1967-001V	5990	6901.0	0.0440	26.65	219.5	826.1	1	na	INTELSAT 2 F-2 DEB	US	11 JAN 67	14 OCT 92
1967-001AB	13907	15969.5	0.5812	24.39	309.7	18873.1	1	na	INTELSAT 2 F-2 DEB	US	11 JAN 67	
1967-001AL	13958	19286.6	0.6517	27.09	338.6	25478.3	1	na	INTELSAT 2 F-2 DEB	US	11 JAN 67	
1967-001AM	14756	16281.5	0.5944	26.56	225.9	19580.9	3	1.07	INTELSAT 2 F-2 DEB	US	11 JAN 67	
1967-001AJ	21692	18982.0	0.6440	26.91	379.3	24828.4	1	na	INTELSAT 2 F-2 DEB	US	11 JAN 67	
1967-043B	2780	6726.7	0.0028	84.92	330.0	367.2	22	0.67	OPS 1967	US	9 MAY 67	14 MAR 93
1967-048D	19222	6795.1	0.0022	89.52	402.1	431.8	1	na	OPS 7218 DEB	US	18 MAY 67	9 JAN 93
1967-104B	3019	6927.6	0.0151	64.07	444.8	654.0	7	2.79	COSMOS 185 R/B	USSR	27 OCT 67	
1968-019B	3151	6668.9	0.0023	81.17	275.6	306.0	1	na	COSMOS 206 R/B	USSR	14 MAR 68	5 NOV 92
1968-091CB	5714	7087.3	0.0416	62.35	414.2	1004.1	6	0.83	COSMOS 249 DEB	USSR	20 OCT 68	
1968-091CQ	14414	6901.5	0.0116	62.26	443.2	603.5	1	na	COSMOS 249 DEB	USSR	20 OCT 68	15 OCT 93
1968-097EG	15536	6899.7	0.0125	62.31	435.4	607.8	10	0.99	COSMOS 252 DEB	USSR	1 NOV 68	4 JUL 93
1969-064C	4053	8183.4	0.1888	30.34	259.9	3350.7	14	1.08	INTELSAT 3 F-5 DEB	US	26 JUL 69	
1969-082AT	4175	6808.8	0.0009	69.99	424.5	436.9	7	0.75	OPS 7613 DEB	US	30 SEP 69	14 DEC 92
1969-082FV	4518	6844.6	0.0026	69.80	448.8	484.2	5	0.67	OPS 7613 DEB	US	30 SEP 69	5 JUN 93
1969-084B	4120	6859.2	0.0061	81.24	439.4	522.7	7	1.17	METEOR 1-2 R/B	USSR	6 OCT 69	
1969-097A	4221	7652.0	0.1170	102.76	378.7	2169.1	4	1.71	AZUR (GRS-A)	FRG	8 NOV 69	
1969-097B	4222	7188.8	0.0631	102.84	356.7	1264.6	9	0.88	AZUR R/B	US	8 NOV 69	
1970-003B	4298	21466.3	0.6889	27.63	299.5	29876.8	3	2.59	INTELSAT 3 F-6 R/B(2)	US	15 JAN 70	
1970-011A	4330	7819.8	0.1432	31.07	321.9	2561.4	5	0.88	OHSUMI (LAMBDA-4S 5)	JPN	11 FEB 70	
1970-021B	4354	21421.6	0.6871	25.31	325.5	29761.4	1	na	NATO 1 R/B	US	20 MAR 70	
1970-021C	5975	21894.4	0.6930	25.81	343.4	30689.2	1	na	NATO 1 DEB	US	20 MAR 70	
1970-034A	4382	7684.1	0.1135	68.43	434.1	2177.9	1	na	MAO 1	PRC	24 APR 70	
1970-034B	4392	7170.7	0.0531	68.38	411.4	1173.7	4	1.62	MAO 1 R/B	PRC	24 APR 70	
1970-085A	4583	6852.0	0.0012	81.17	465.5	482.3	5	1.74	METEOR 1-6	USSR	15 OCT 70	
1970-085B	4584	6885.9	0.0065	81.20	463.3	552.2	1	na	METEOR 1-6 R/B	USSR	15 OCT 70	
1970-089BG	5242	6766.0	0.0089	62.69	327.4	448.3	5	0.49	COSMOS 374 DEB	USSR	23 OCT 70	17 NOV 92

intl des.	obj	a (km)	e	i (deg)	perigee (km)	apogee (km)	# obs	days/ update	description	country	launch	reentry
1971-003C	18277	6844.1	0.0043	81.19	436.7	495.2	12	1.02	METEOR 1-7 DEB	USSR	20 JAN 71	
1971-015C	5009	6926.4	0.0154	65.58	441.7	654.8	9	0.58	COSMOS 397 DEB	USSR	25 FEB 71	11 APR 93
1971-015AN	5191	6783.6	0.0063	65.76	362.4	448.6	7	1.20	COSMOS 397 DEB	USSR	25 FEB 71	28 JAN 93
1971-015AZ	5244	6964.8	0.0202	65.93	446.3	727.1	1	na	COSMOS 397 DEB	USSR	25 FEB 71	
1971-015CD	5761	7127.6	0.0456	65.84	424.3	1074.6	4	0.57	COSMOS 397 DEB	USSR	25 FEB 71	
1971-015CT	15342	6823.7	0.0077	66.54	392.7	498.3	8	0.70	COSMOS 397 DEB	USSR	25 FEB 71	23 DEC 92
1971-016A	4966	7761.5	0.1536	51.49	190.7	2575.9	3	0.42	COSMOS 398	USSR	26 FEB 71	
1971-052A	5281	7132.1	0.0556	73.98	357.5	1150.5	3	1.18	COSMOS 426	USSR	4 JUN 71	
1971-052B	5282	7189.1	0.0625	73.98	361.7	1260.2	3	1.26	COSMOS 426 R/B	USSR	4 JUN 71	
1971-119A	5729	7565.1	0.1049	73.99	393.6	1980.3	4	1.43	AUREOLE 1	FR	27 DEC 71	
1971-119B	5730	7532.4	0.1014	73.91	390.3	1918.1	9	0.49	AUREOLE 1 R/B	USSR	27 DEC 71	
1972-011B	5853	6818.4	0.0028	81.19	421.3	459.2	19	1.69	COSMOS 476 R/B	USSR	1 MAR 72	
1972-058BF	7889	6694.5	0.0019	98.59	303.7	329.1	2	0.51	LANDSAT 1 DEB	US	23 JUL 72	10 OCT 92
1972-058CH	7942	6819.7	0.0030	98.22	421.0	462.0	20	0.68	LANDSAT 1 DEB	US	23 JUL 72	16 APR 93
1972-058FC	8386	6857.8	0.0022	96.65	464.6	494.7	5	1.10	LANDSAT 1 DEB	US	23 JUL 72	8 DEC 93
1973-078C	6895	6976.9	0.0400	28.82	319.9	877.7	5	0.84	EXPLORER 50 R/B(1)	US	26 OCT 73	
1973-107A	7003	7308.4	0.0741	73.99	389.0	1471.6	3	2.47	AUREOLE 2	FR	26 DEC 73	
1973-107B	7004	7278.5	0.0710	73.98	383.8	1416.9	5	1.18	AUREOLE 2 R/B	USSR	26 DEC 73	
1974-044A	7337	7355.1	0.0799	82.96	389.4	1564.5	2	2.51	COSMOS 660	USSR	18 JUN 74	
1974-044B	7338	7223.3	0.0639	82.97	383.9	1306.5	1	na	COSMOS 660 R/B	USSR	18 JUN 74	
1974-066B	7418	6849.4	0.0030	81.23	451.0	491.6	9	1.04	COSMOS 673 R/B	USSR	16 AUG 74	
1974-075C	7468	9643.8	0.3186	24.30	189.2	6342.2	2	0.43	WESTAR 2 R/B(2)	US	10 OCT 74	
1974-089G	8138	6808.8	0.0024	101.50	414.6	446.8	2	na	NOAA 4 DEB	US	15 NOV 74	14 NOV 92
1975-056B	7969	6866.0	0.0032	81.25	466.2	509.6	3	1.68	COSMOS 744 R/B	USSR	20 JUN 75	
1975-072B	8063	8085.9	0.1708	89.18	327.1	3088.4	1	na	COS B R/B	US	9 AUG 75	
1975-076A	8127	6690.2	0.0017	81.21	300.4	323.7	2	1.30	COSMOS 756	USSR	22 AUG 75	
1975-077B	8133	7261.6	0.0677	25.32	392.0	1374.8	2	1.31	SYMPHONIE 2 R/B(1)	US	27 AUG 75	
1975-100C	8368	8885.6	0.2544	23.37	247.1	4767.7	2	0.40	GOES 1 R/B(2)	US	16 OCT 75	
1976-022A	8744	7369.5	0.0819	82.94	387.7	1595.0	12	1.44	COSMOS 807	USSR	12 MAR 76	
1976-022B	8745	7204.6	0.0628	82.94	374.3	1278.5	6	1.76	COSMOS 807 R/B	USSR	12 MAR 76	
1976-024A	8754	6783.8	0.0012	81.23	397.7	413.6	24	1.52	COSMOS 808	USSR	16 MAR 76	20 NOV 93
1976-024B	8755	6845.2	0.0029	81.25	447.1	486.9	6	1.07	COSMOS 808 R/B	USSR	16 MAR 76	
1976-039D	14514	7137.0	0.0689	109.93	266.9	1250.8	4	1.50	LAGEOS DEB	US	4 MAY 76	8 DEC 93
1976-066C	9017	15155.6	0.5635	24.49	237.8	17317.1	2	0.83	PALAPA 1 R/B(2)	US	8 JUL 76	
1976-120AY	11221	6880.3	0.0051	65.85	467.3	537.0	1	na	COSMOS 880 DEB	USSR	9 DEC 76	
1976-126W	9725	6824.9	0.0124	65.73	361.8	531.8	10	0.65	COSMOS 886 DEB	USSR	27 DEC 76	21 DEC 92
1977-015B	9854	6863.9	0.0044	81.17	455.3	516.2	8	0.95	COSMOS 895 R/B	USSR	26 FEB 77	
1977-057A	10113	6765.8	0.0014	97.37	378.0	397.4	28	0.78	METEOR 1-28	USSR	29 JUN 77	28 AUG 93
1977-061A	10134	6741.5	0.0010	81.19	356.4	370.3	24	0.90	COSMOS 925	USSR	7 JUL 77	29 APR 93
1977-065CW	10269	7161.1	0.0558	29.10	383.4	1182.5	3	1.76	HIMAWARI DEB	US	14 JUL 77	
1977-065DK	10313	6945.0	0.0204	28.91	424.9	708.8	4	0.67	HIMAWARI DEB	US	14 JUL 77	31 MAY 93
1977-065FD	10634	7271.7	0.0624	28.90	439.7	1347.5	2	1.83	HIMAWARI DEB	US	14 JUL 77	
1977-121BY	20327	7454.2	0.0832	65.86	455.6	1696.5	2	1.97	COSMOS 970 DEB	USSR	21 DEC 77	
1978-012C	10723	21918.7	0.6993	29.19	213.6	30867.6	2	1.31	IUE R/B(2)	US	26 JAN 78	
1978-016C	12908	11105.4	0.4037	26.34	244.4	9210.1	2	0.43	OPS 6391 DEB	US	9 FEB 78	
1978-026AD	12188	6811.3	0.0004	98.76	430.7	435.7	1	na	LANDSAT 3 DEB	US	5 MAR 78	13 MAR 93
1978-026BR	12224	6826.7	0.0012	98.80	440.4	456.7	1	na	LANDSAT 3 DEB	US	5 MAR 78	31 DEC 92
1978-026BY	12231	6806.8	0.0027	98.73	410.6	446.8	16	1.07	LANDSAT 3 DEB	US	5 MAR 78	19 MAR 93
1978-039C	10794	10053.8	0.3441	26.91	215.8	7135.6	1	na	YURI R/B(2)	US	7 APR 78	
1978-094A	11055	6841.2	0.0012	81.18	454.9	471.2	11	1.25	COSMOS 1043	USSR	10 OCT 78	
1978-094C	22536	6812.3	0.0010	81.17	427.3	441.0	1	na	COSMOS 1043	USSR	10 OCT 78	11 MAR 93
1978-100AS	20307	7501.2	0.0930	82.65	425.3	1820.8	2	2.41	COSMOS 1045 DEB	USSR	26 OCT 78	
1979-017AM	16084	6843.6	0.0021	97.88	451.4	479.5	10	0.85	SOLWIND DEB	US	24 FEB 79	
1979-017BX	16308	6812.4	0.0017	97.78	422.6	445.9	22	1.05	SOLWIND DEB	US	24 FEB 79	
1979-017CA	16311	6841.8	0.0020	97.83	450.2	477.1	8	1.13	SOLWIND DEB	US	24 FEB 79	
1979-017FE	16480	6841.6	0.0019	97.83	450.8	476.1	10	1.18	SOLWIND DEB	US	24 FEB 79	
1979-017GJ	16551	6808.6	0.0020	97.85	416.5	444.4	29	1.50	SOLWIND DEB	US	24 FEB 79	
1979-017HD	16570	6680.4	0.0017	97.78	291.2	313.4	8	0.32	SOLWIND DEB	US	24 FEB 79	6 DEC 92
1979-017JF	16878	6852.3	0.0018	97.87	461.6	486.6	4	3.17	SOLWIND DEB	US	24 FEB 79	
1979-017JH	17094	6853.6	0.0030	97.84	455.1	495.8	11	1.56	SOLWIND DEB	US	24 FEB 79	
1979-020A	11285	6979.2	0.0200	73.98	461.2	740.8	1	na	INTERCOSMOS 19	USSR	27 FEB 79	
1979-067A	11457	6721.2	0.0015	81.17	333.2	352.9	25	0.85	COSMOS 1116	USSR	20 JUL 79	11 MAR 93
1980-030A	11765	7284.8	0.0724	66.12	379.2	1434.0	4	na	COSMOS 1174	USSR	18 APR 80	
1980-030N	11781	7160.6	0.0533	66.23	400.5	1164.3	4	1.62	COSMOS 1174 DEB	USSR	18 APR 80	
1980-030V	12347	6966.4	0.0262	66.05	405.4	771.0	9	0.49	COSMOS 1174 DEB	USSR	18 APR 80	
1980-030Y	12354	7266.7	0.0659	66.12	410.0	1367.1	7	1.44	COSMOS 1174 DEB	USSR	18 APR 80	
1980-030AE	12360	6892.6	0.0199	66.03	377.0	651.9	6	0.82	COSMOS 1174 DEB	USSR	18 APR 80	16 FEB 94
1980-030AQ	13932	6978.0	0.0202	65.66	459.0	740.7	1	na	COSMOS 1174 DEB	USSR	18 APR 80	9 SEP 93
1980-098B	12445	12354.7	0.4533	23.66	376.5	11576.6	1	na	INTELSAT 5 F-2 R/B	US	6 DEC 80	
1981-003A	12138	7439.5	0.0889	82.98	399.7	1723.0	1	na	COSMOS 1238	USSR	16 JAN 81	
1981-012A	12295	17315.3	0.6167	28.37	259.0	21615.4	1	na	KIKU 3 (ETS-4)	JPN	11 FEB 81	
1981-033A	12388	7428.9	0.0889	82.97	390.4	1711.1	3	1.33	COSMOS 1263	USSR	9 APR 81	
1981-033B	12389	7322.3	0.0773	82.95	378.1	1510.2	6	1.52	COSMOS 1263 R/B	USSR	9 APR 81	
1981-094A	12848	7430.2	0.0880	82.49	398.1	1705.9	3	0.22	AUREOLE 3	FR	21 SEP 81	
1981-094B	12849	7524.2	0.0985	82.50	405.1	1887.0	5	1.61	AUREOLE 3 R/B	USSR	21 SEP 81	
1981-122B	13011	22042.9	0.6976	10.55	286.7	31042.8	1	na	MARECS 1 CAP/MOD	ESA	20 DEC 81	
1982-100F	13608	14422.8	0.5384	52.13	279.6	15809.6	2	1.70	COSMOS 1413-1415 DEB	USSR	12 OCT 82	
1982-110D	13658	24298.1	0.7232	23.26	348.6	35491.3	1	na	SBS 3 R/B (PAM)	US	11 NOV 82	

intl des.	obj	a (km)	e	i (deg)	perigee (km)	apogee (km)	# obs	days/ update	description	country	launch	reentry
1983-006B	13786	9042.2	0.2701	28.50	221.0	5107.0	3	0.36	SAKURA 2A R/B	JPN	4 FEB 83	
1983-030B	13985	7753.3	0.1399	25.35	290.6	2459.6	4	0.81	RCA/SATCOM 6 R/B(1)	US	11 APR 83	
1983-041B	14051	7856.1	0.1372	25.35	399.7	2556.2	2	2.88	GOES 6 R/B(1)	US	28 APR 83	
1983-046A	14075	6692.8	0.0122	82.83	233.2	396.1	11	2.45	COSMOS 1463	USSR	19 MAY 83	24 JAN 93
1983-065C	14168	14076.4	0.5332	23.22	193.1	15203.5	1	na	GALAXY 1 R/B(2)	US	28 JUN 83	
1983-066E	14167	9391.2	0.2995	46.49	200.7	5825.5	1	na	GORIZONT 7 DEB	USSR	1 JUL 83	
1983-084G	14277	15664.8	0.5706	51.95	347.7	18225.6	1	na	COSMOS 1490-1492 DEB	USSR	10 AUG 83	
1983-094B	14329	7550.1	0.1189	25.49	274.1	2069.9	7	0.98	SATCOM 7 R/B(1)	US	8 SEP 83	
1983-111A	14483	7473.8	0.0930	82.92	400.2	1791.1	2	3.09	COSMOS 1508	USSR	11 NOV 83	
1983-111B	14484	7369.7	0.0841	82.91	372.0	1611.1	2	1.52	COSMOS 1508 R/B	USSR	11 NOV 83	
1984-011E	14693	6926.1	0.0413	28.16	262.2	833.7	5	2.30	PALAPA B2 R/B (PAM)	US	3 FEB 84	
1984-011F	14694	7038.0	0.0518	27.67	295.2	1024.6	5	1.73	WESTAR 6 R/B (PAM)	US	3 FEB 84	
1984-047G	15053	15897.0	0.5734	52.05	404.1	18633.6	1	na	COSMOS 1554-1556 DEB	USSR	19 MAY 84	
1984-047H	15054	15260.1	0.5594	51.99	345.7	17418.2	3	0.66	COSMOS 1554-1556 DEB	USSR	19 MAY 84	
1984-068A	15080	6717.1	0.0152	50.63	237.1	440.8	8	0.75	COSMOS 1578	USSR	28 JUN 84	10 JAN 93
1984-093E	15244	13462.7	0.5018	27.22	329.2	13839.9	2	1.53	LEASAT 2 R/B	US	30 AUG 84	
1984-093G	15246	24585.7	0.7250	25.24	382.3	36032.8	1	na	TELESTAR 3C R/B	US	30 AUG 84	
1984-095H	15266	15850.7	0.5765	52.06	334.3	18610.8	1	na	COSMOS 1593-1595 DEB	USSR	4 SEP 84	
1984-106U	22151	6949.7	0.0289	66.99	370.5	772.6	1	na	COSMOS 1603 DEB	USSR	28 SEP 84	14 OCT 92
1984-106AD	22160	6886.9	0.0287	66.98	311.0	706.4	1	na	COSMOS 1603 DEB	USSR	28 SEP 84	13 OCT 92
1984-113E	15390	13471.6	0.5028	27.07	319.9	13866.9	1	na	LEASAT 1 R/B	US	8 NOV 84	
1984-123C	15441	6824.8	0.0006	98.97	442.7	450.6	7	0.45	NOAA 9 DEB	US	12 DEC 84	11 NOV 92
1985-015C	15562	22982.4	0.7091	6.81	308.4	32900.2	1	na	ARABSAT 1/SBTS 1 R/B	ESA	8 FEB 85	
1985-025B	15631	15310.9	0.5719	22.91	176.7	17688.9	1	na	INTELSAT 5A F-10 R/B	US	22 MAR 85	
1985-028D	15644	23325.3	0.7126	22.83	325.9	33568.3	1	na	ANIK C1 R/B	US	12 APR 85	
1985-028E	16229	13971.6	0.5198	26.94	331.4	14855.5	1	na	LEASAT 3 R/B	US	12 APR 85	
1985-037H	15715	15848.2	0.5730	52.08	389.0	18551.0	1	na	COSMOS 1650-1652 DEB	USSR	17 MAY 85	
1985-056B	15876	20755.9	0.6742	12.54	383.4	28372.1	1	na	GIOTTO R/B	ESA	2 JUL 85	
1985-076E	15996	24320.8	0.7232	26.10	354.0	35531.3	2	1.39	AUSSAT 1 R/B	US	27 AUG 85	
1986-016C	16600	17510.9	0.6228	28.02	227.4	22038.1	3	1.22	BS 2B R/B(2)	JPN	12 FEB 86	
1986-017A	16609	6779.4	0.0010	51.63	394.4	408.1	22	0.47	MIR	USSR	19 FEB 86	
1986-017FU	21882	6689.5	0.0014	51.60	302.0	320.8	10	0.47	MIR DEB	USSR	19 FEB 86	21 JAN 93
1986-017FW	21884	6688.4	0.0013	51.61	301.4	319.2	9	1.37	MIR DEB	USSR	19 FEB 86	19 JAN 93
1986-017GE	22023	6722.8	0.0013	51.60	335.8	353.4	9	0.60	MIR DEB	USSR	19 FEB 86	12 DEC 92
1986-017GF	22024	6743.8	0.0015	51.60	355.4	375.9	15	0.95	MIR DEB	USSR	19 FEB 86	4 MAY 93
1986-017GG	22045	6740.6	0.0011	51.60	355.3	369.6	21	1.16	MIR DEB	USSR	19 FEB 86	4 MAY 93
1986-017GH	22046	6698.1	0.0010	51.59	313.1	326.9	4	0.85	MIR DEB	USSR	19 FEB 86	19 OCT 92
1986-017GJ	22106	6722.2	0.0009	51.62	337.8	350.3	14	0.77	MIR DEB	USSR	19 FEB 86	26 FEB 93
1986-017GK	22107	6731.5	0.0012	51.64	345.1	361.5	9	0.59	MIR DEB	USSR	19 FEB 86	10 DEC 92
1986-017GM	22121	6770.7	0.0011	51.63	385.3	399.8	22	0.89	MIR DEB	USSR	19 FEB 86	28 OCT 93
1986-017GN	22122	6745.5	0.0012	51.65	359.0	375.7	10	0.74	MIR DEB	USSR	19 FEB 86	2 DEC 92
1986-017GP	22123	6780.3	0.0011	51.64	394.7	409.7	25	1.00	MIR DEB	USSR	19 FEB 86	
1986-017GQ	22124	6731.2	0.0021	51.65	338.7	367.4	1	na	MIR DEB	USSR	19 FEB 86	3 NOV 92
1986-017GR	22127	6781.5	0.0011	51.63	396.0	410.7	18	0.95	MIR DEB	USSR	19 FEB 86	
1986-017GS	22128	6781.4	0.0012	51.64	394.9	411.6	20	0.99	MIR DEB	USSR	19 FEB 86	
1986-017GT	22129	6730.0	0.0023	51.63	336.7	367.1	1	na	MIR DEB	USSR	19 FEB 86	17 NOV 92
1986-017GU	22130	6745.9	0.0011	51.64	360.0	375.5	7	0.42	MIR DEB	USSR	19 FEB 86	1 NOV 92
1986-017GV	22131	6732.9	0.0019	51.61	341.7	367.8	4	1.02	MIR DEB	USSR	19 FEB 86	12 NOV 92
1986-017GW	22209	6750.2	0.0012	51.64	363.7	380.5	11	1.08	MIR DEB	USSR	19 FEB 86	9 APR 93
1986-017GX	22225	6754.0	0.0013	51.64	367.1	384.6	10	1.05	MAK 2	USSR	19 FEB 86	1 APR 93
1986-017GY	22228	6718.3	0.0009	51.65	334.3	346.0	1	na	MIR DEB	USSR	19 FEB 86	8 DEC 92
1986-019JK	17555	6812.0	0.0022	97.95	418.7	449.1	2	4.45	SPOT 1 VIKING DEB	ESA	22 FEB 86	19 NOV 92
1986-071G	16984	9317.5	0.2797	64.24	129.7	5749.1	2	0.42	COSMOS 1778-1780 DEB	USSR	16 SEP 86	29 JAN 93
1986-071H	16985	7387.3	0.1204	64.08	119.6	1898.7	1	na	COSMOS 1778-1780 DEB	USSR	16 SEP 86	26 NOV 92
1987-012B	17481	6852.6	0.0068	31.10	428.1	520.8	4	0.77	ASTRO C R/B	JPN	5 FEB 87	
1987-012K	18927	6777.6	0.0034	30.82	376.5	422.4	17	0.62	ASTRO C DEB	JPN	5 FEB 87	13 APR 93
1987-030A	17845	6779.6	0.0010	51.64	394.7	408.2	22	na	KVANT 1	USSR	31 MAR 87	
1987-073E	18332	19832.6	0.6595	46.97	375.7	26533.2	1	na	EKRAN 16 DEB	USSR	3 SEP 87	
1988-006B	18845	6785.3	0.0025	98.66	390.2	424.1	9	0.36	USA 29 DEB	US	3 FEB 88	29 OCT 92
1988-051F	19220	19050.5	0.6500	9.86	289.7	25054.9	1	na	METEOSAT P2 DEB	ESA	15 JUN 88	
1988-063C	19332	19397.5	0.6560	7.49	294.0	25744.8	2	na	INSAT/EUTELSAT R/B	ESA	21 JUL 88	
1988-063F	20488	15104.5	0.5534	7.44	368.0	17084.7	1	na	INSAT/EUTELSAT DEB	ESA	21 JUL 88	
1988-066E	19348	18672.4	0.6432	46.83	284.0	24304.5	1	na	COSMOS 1961 DEB	USSR	1 AUG 88	
1988-091C	19549	23668.5	0.7181	26.34	294.4	34286.3	1	na	TDRS 3 R/B(1) (IUS-1)	US	29 SEP 88	
1988-109D	19690	15779.8	0.5832	7.04	188.5	18614.7	2	0.56	SKYNET/ASTRA DEB	ESA	11 DEC 88	22 OCT 93
1989-016C	19824	10348.0	0.3576	75.06	269.4	7670.4	1	na	EXOS D R/B(2)	JPN	21 FEB 89	
1989-016K	19952	9052.7	0.2668	75.61	259.3	5089.8	3	1.19	EXOS D DEB	JPN	21 FEB 89	
1989-016M	19963	10009.4	0.3352	75.16	275.8	6986.7	4	1.56	EXOS D DEB	JPN	21 FEB 89	
1989-016N	20021	9502.3	0.3011	74.38	263.2	5985.1	1	na	EXOS D DEB	JPN	21 FEB 89	
1989-021C	19884	22043.1	0.7001	26.78	232.6	31097.2	1	na	TDRS 4 R/B(1) (IUS-1)	US	13 MAR 89	
1989-033C	19970	18758.5	0.6446	27.99	289.3	24471.4	1	na	MAGELLAN R/B(1)	US	4 MAY 89	
1989-052F	20116	21918.8	0.6966	46.90	272.2	30809.1	2	1.03	GORIZONT 18 DEB	USSR	5 JUL 89	
1989-067C	20195	22690.0	0.7086	23.57	233.2	32390.4	1	na	BSB R-1 R/B(2)	US	27 AUG 89	
1989-093A	20335	6779.8	0.0010	51.64	394.9	408.3	21	na	KVANT 2	USSR	26 NOV 89	
1989-094B	20339	6822.4	0.0018	73.53	432.2	456.2	1	na	MOLNIYA 3-36 R/B(2)	USSR	28 NOV 89	
1989-100A	20389	6818.2	0.0011	73.53	432.5	447.7	20	0.68	COSMOS 2053	USSR	27 DEC 89	
1990-001F	20406	15778.1	0.5762	26.56	308.2	18491.7	1	na	JCSAT 2 R/B	US	1 JAN 90	
1990-008B	20453	7215.2	0.0547	35.66	442.1	1232.0	1	na	USA 50 R/B(1)	US	24 JAN 90	
1990-025C	20535	9297.7	0.2947	37.40	180.0	5659.1	1	na	USA 54 R/B(2)	US	26 MAR 90	18 JAN 94

intl des.	obj	a (km)	e	i (deg)	perigee (km)	apogee (km)	# obs	days/ updt	description	country	launch	reentry
1990-028A	20546	6864.9	0.0100	94.12	417.8	555.6	10	0.75	PEGSAT	US	5 APR 90	
1990-048A	20635	6779.8	0.0010	51.64	394.9	408.4	21	na	KRISTALL	USSR	31 MAY 90	
1990-061F	20698	21342.3	0.6850	47.09	345.6	29582.7	1	na	COSMOS 2085 DEB	USSR	18 JUL 90	
1990-065C	20811	23137.6	0.7099	17.96	332.9	33186.0	1	na	CRRES DEB	US	25 JUL 90	
1990-065R	21778	23748.5	0.7154	17.86	380.4	34360.4	1	na	CRRES DEB	US	25 JUL 90	
1990-074B	20763	7243.2	0.0541	24.75	472.9	1257.2	1	na	BSB R-2 R/B(1)	US	18 AUG 90	
1990-078B	20775	7499.1	0.0988	82.97	379.8	1862.1	2	1.76	COSMOS 2098 R/B	USSR	28 AUG 90	
1990-079C	20778	15113.5	0.5681	7.47	149.0	17321.7	1	na	SKYNET/EUTELSAT R/B	ESA	30 AUG 90	28 AUG 93
1990-081BH	20897	6781.4	0.0021	98.85	389.3	417.3	5	0.95	FENGYUN 1-2 DEB	PRC	3 SEP 90	21 JAN 93
1990-093B	20919	7040.6	0.0423	24.76	364.6	960.3	8	1.01	INMARSAT 2 F-1 R/B	US	30 OCT 90	
1990-094E	20927	13140.3	0.5035	46.57	145.3	13379.0	2	0.48	GORIZONT 21 DEB	USSR	3 NOV 90	
1990-100C	20947	23736.0	0.7170	7.42	339.9	34375.7	1	na	SATCOM/GSTAR R/B	ESA	20 NOV 90	
1990-104A	20966	6863.1	0.0014	82.51	475.1	494.9	2	0.59	COSMOS 2106	USSR	28 NOV 90	
1990-104AA	21994	6761.9	0.0006	82.51	380.0	387.5	5	1.42	COSMOS 2106 DEB	USSR	28 NOV 90	11 OCT 92
1990-104AD	22001	6722.0	0.0007	82.49	338.9	348.7	2	na	COSMOS 2106 DEB	USSR	28 NOV 90	2 OCT 92
1990-104AE	22002	6701.8	0.0007	82.42	319.1	328.3	1	na	COSMOS 2106 DEB	USSR	28 NOV 90	6 OCT 92
1990-104AF	22003	6692.4	0.0007	82.55	309.3	319.1	1	na	COSMOS 2106 DEB	USSR	28 NOV 90	6 OCT 92
1990-116G	21961	16352.6	0.5989	46.56	181.2	19767.8	1	na	RADUGA 1-2 DEB	USSR	27 DEC 90	
1991-005A	21065	6793.3	0.0005	64.99	411.5	418.9	27	0.53	COSMOS 2122	USSR	18 JAN 91	28 MAR 93
1991-010D	21114	18323.1	0.6380	46.79	254.4	23635.5	1	na	COSMOS 2133 DEB	USSR	14 FEB 91	
1991-015D	21142	17632.1	0.6236	6.75	259.4	22248.4	1	na	ASTRA/MOP DEB	ESA	2 MAR 91	
1991-018B	21150	7116.1	0.0474	24.96	400.7	1075.2	5	1.71	INMARSAT 2 R/B(1)	US	8 MAR 91	
1991-021A	21190	6784.4	0.0020	65.85	392.4	420.1	25	0.92	COSMOS 2137	USSR	19 MAR 91	
1991-024A	21213	6695.6	0.0005	72.66	314.3	320.6	5	0.65	ALMAZ 1	USSR	31 MAR 91	17 OCT 92
1991-037B	21393	7724.0	0.1227	25.01	397.8	2293.9	2	1.69	AURORA II R/B(1)	US	29 MAY 91	
1991-062C	21696	6884.9	0.0084	31.35	448.6	565.0	2	0.85	SOLAR-A DEB	JPN	30 AUG 91	27 JUN 93
1991-062D	21697	6887.0	0.0087	31.33	448.7	569.0	5	0.82	SOLAR-A DEB	JPN	30 AUG 91	4 AUG 93
1991-062E	21698	6850.1	0.0069	31.35	424.8	519.0	2	na	SOLAR-A DEB	JPN	30 AUG 91	11 MAY 93
1991-062F	21699	6901.2	0.0094	31.36	458.1	588.0	1	na	SOLAR-A DEB	JPN	30 AUG 91	23 FEB 94
1991-062G	21786	6865.0	0.0124	31.21	401.5	572.2	9	0.94	SOLAR-A DEB	JPN	30 AUG 91	9 JUN 93
1991-072A	21743	6687.5	0.0095	73.98	245.5	373.2	4	0.42	COSMOS 2164	USSR	10 OCT 91	12 DEC 92
1991-075B	21766	23864.5	0.7204	7.66	295.5	34677.3	1	na	INTELSAT VI-F1 R/B	ESA	29 OCT 91	
1991-086A	21819	8131.6	0.1618	82.57	437.7	3069.3	3	2.04	INTERCOSMOS 25	USSR	18 DEC 91	
1991-086B	21820	8132.3	0.1620	82.57	436.6	3071.7	2	3.38	INTERCOSMOS 25 R/B	USSR	18 DEC 91	
1991-086F	21905	8124.1	0.1602	82.58	444.8	3047.0	2	1.73	INTERCOSMOS 25 DEB	USSR	18 DEC 91	
1991-088B	21834	7117.5	0.0752	31.03	201.9	1276.9	6	0.62	PRC 34 R/B	PRC	28 DEC 91	12 APR 93
1992-007B	21868	6850.5	0.0067	97.68	426.1	518.6	7	0.62	JERS R/B	JPN	11 FEB 92	
1992-010C	21895	20166.9	0.6745	6.55	187.1	27390.5	1	na	SUPERBIRD/ARABSAT PLAT	FR	26 FEB 92	
1992-018A	21928	6639.0	0.0032	64.83	239.8	281.8	3	0.49	COSMOS 2183	USSR	8 APR 92	16 FEB 93
1992-031B	21988	6686.1	0.0098	30.22	242.2	373.7	1	na	EUVE R/B	US	7 JUN 92	16 OCT 92
1992-032B	21990	23545.5	0.7215	26.76	178.3	34156.5	1	na	INTELSAT K R/B	US	10 JUN 92	
1992-039C	22016	15616.1	0.5803	34.77	176.6	18299.3	1	na	USA 83 R/B(2)	US	7 JUL 92	
1992-043E	22047	22183.7	0.7067	46.50	127.6	31483.5	1	na	GORIZONT 26 DEB	USSR	14 JUL 92	18 JUN 93
1992-044B	22050	6965.8	0.0548	27.44	203.7	971.7	4	0.51	GEOTAIL R/B(1)	US	24 JUL 92	16 MAR 93
1992-046A	22054	6780.7	0.0009	51.63	396.2	409.0	18	0.76	SOYUZ TM-15	USSR	27 JUL 92	1 FEB 93
1992-054B	22088	6819.5	0.0361	27.98	193.6	689.2	5	0.45	AUSSAT B1 R/B(1)	PRC	13 AUG 92	12 DEC 92
1992-055A	22090	6783.8	0.0007	51.63	400.9	410.5	4	na	PROGRESS M-14	USSR	15 AUG 92	21 OCT 92
1992-060C	22118	24562.6	0.7312	6.98	223.6	36145.3	1	na	HISPASAT/SATCOM R/B	ESA	10 SEP 92	20 OCT 93
1992-065F	22202	6668.7	0.0048	62.84	258.8	322.3	1	na	FOTON 5 DEB	USSR	8 OCT 92	3 NOV 92
1992-069B	22190	6729.3	0.0214	62.83	206.9	495.3	1	na	COSMOS 2217 R/B(1)	USSR	21 OCT 92	25 NOV 92
1992-071A	22203	6772.4	0.0014	51.64	384.6	404.0	16	1.26	PROGRESS M-15	USSR	27 OCT 92	7 FEB 93
1992-075A	22217	6623.5	0.0082	82.58	190.8	300.0	1	na	RESURS 500	USSR	15 NOV 92	22 NOV 92
1992-077A	22226	6630.6	0.0117	67.13	175.0	329.9	2	0.40	COSMOS 2220	USSR	20 NOV 92	18 JAN 93
1992-078A	22229	6746.8	0.0070	96.75	321.2	416.0	73	2.85	MSTI	US	21 NOV 92	18 JUL 93
1992-078B	22230	6758.1	0.0091	96.75	318.6	441.3	8	0.71	SCOUT G-1 R/B	US	21 NOV 92	9 FEB 93
1992-081B	22239	6682.3	0.0161	62.79	196.5	411.8	1	na	COSMOS 2222 R/B(1)	USSR	25 NOV 92	28 DEC 92
1992-081G	22244	6685.7	0.0202	62.80	172.9	442.3	1	na	COSMOS 2222 DEB	USSR	25 NOV 92	9 DEC 92
1992-085B	22256	6659.6	0.0118	62.80	203.0	359.9	2	0.44	MOLNIYA 3-43 R/B(1)	USSR	2 DEC 92	14 DEC 92
1992-086A	22259	6699.4	0.0011	57.01	314.1	328.4	1	na	STS-53	US	2 DEC 92	9 DEC 92
1992-087A	22260	6643.5	0.0043	64.67	236.8	293.9	1	na	COSMOS 2223	USSR	9 DEC 92	16 DEC 93
1992-090A	22278	6994.8	0.0583	28.16	209.2	1024.2	5	0.65	AUSSAT B2	AUS	21 DEC 92	
1992-090B	22279	6953.0	0.0535	28.15	202.8	946.8	2	0.73	AUSSAT B2 R/B(1)	PRC	21 DEC 92	19 JUN 93
1992-093FY	22483	6804.3	0.0145	71.09	327.3	525.0	3	0.87	COSMOS 2227 DEB	USSR	25 DEC 92	22 FEB 93
1992-093HG	22546	6861.1	0.0084	94.11	425.5	540.4	1	na	COSMOS 2227 DEB	USSR	25 DEC 92	
1992-095B	22301	6634.6	0.0080	62.80	203.7	309.2	1	na	COSMOS 2229 R/B	USSR	29 DEC 92	16 JAN 93
1992-095C	22302	6649.2	0.0094	62.81	208.7	333.4	2	0.43	COSMOS 2229 DEB	USSR	29 DEC 92	11 FEB 93
1992-095E	22304	6681.7	0.0061	62.80	263.0	344.2	1	na	COSMOS 2229 DEB	USSR	29 DEC 92	29 JAN 93
1992-095F	22305	6753.2	0.0102	62.78	306.4	443.8	4	na	COSMOS 2229 DEB	USSR	29 DEC 92	18 JAN 93
1993-002B	22310	6723.1	0.0209	62.84	204.1	485.8	3	0.56	MOLNIYA 1-85 R/B(1)	USSR	13 JAN 93	4 MAR 93
1993-002C	22311	6744.3	0.0283	62.82	175.5	556.8	4	0.55	MOLNIYA 1-85 PLAT	USSR	13 JAN 93	5 FEB 93
1993-003A	22313	6688.1	0.0008	28.49	304.5	315.5	1	na	STS 54	US	13 JAN 93	19 JAN 93
1993-004A	22317	6636.4	0.0132	67.14	170.5	346.0	5	0.53	COSMOS 2231	USSR	19 JAN 93	25 MAR 93
1993-005A	22319	6774.2	0.0011	51.64	388.5	403.7	4	na	SOYUZ TM-16	USSR	24 JAN 93	22 JUL 93
1993-006B	22322	6719.8	0.0201	62.81	206.2	477.1	4	0.56	COSMOS 2232 R/B(1)	USSR	26 JAN 93	9 MAR 93
1993-006C	22323	6703.7	0.0230	62.84	171.4	479.8	2	na	COSMOS 2232 PLAT	USSR	26 JAN 93	14 FEB 93
1993-006E	22325	6709.8	0.0198	62.85	198.1	465.3	4	0.78	COSMOS 2232 DEB	USSR	26 JAN 93	28 FEB 93

Table D2. Objects from the USSPACECOM analysts' data set having conjunctions with the GRO within a 100-km distance, over the time period covered by the simulation. The objects have been renumbered starting from the number 1. Shown are the object number (obj), eccentricity (e), orbital inclination (i), altitude above mean equatorial radius at perigee and apogee, number of observations over the simulation, and mean time between state vector updates in days.

obj	a (km)	e	i (deg)	perigee (km)	apogee (km)	# obs	days/ updt	obj	a (km)	e	i (deg)	perigee (km)	apogee (km)	# updt	days/ updt
1	6689.9	0.0016	28.49	301.3	322.2	1	na	65	9532.8	0.2937	26.44	355.2	5954.0	1	na
2	6842.5	0.0403	33.97	188.5	740.1	1	na	66	14459.4	0.5420	24.04	244.5	15918.1	2	na
3	6840.6	0.0407	33.95	184.1	740.9	1	na	67	19858.1	0.6625	29.57	324.1	26635.7	1	na
4	7008.3	0.0606	28.01	205.7	1054.6	1	na	68	6773.7	0.0004	51.63	392.8	398.4	3	na
5	6900.2	0.0147	67.09	420.4	623.8	1	na	69	6682.4	0.0168	62.84	192.0	416.6	1	na
6	7031.6	0.0286	71.14	452.3	854.7	2	na	70	7319.4	0.0683	71.44	441.6	1440.9	1	na
7	6974.1	0.0322	71.13	371.3	820.6	2	na	71	6805.9	0.0031	82.53	406.5	449.0	11	na
8	6949.9	0.0293	71.13	367.8	775.6	1	na	72	7106.3	0.0755	65.46	191.9	1264.5	1	na
9	6879.3	0.0231	71.11	342.4	659.8	1	na	73	7047.2	0.0699	65.44	176.7	1161.4	3	na
10	6879.3	0.0229	71.11	343.8	658.4	1	na	74	7897.3	0.1441	60.78	380.8	2657.5	1	na
11	6861.2	0.0195	71.10	349.0	617.1	1	na	75	6631.3	0.0127	62.84	168.6	337.6	1	na
12	6757.2	0.0349	82.96	143.0	615.1	10	na	76	6870.1	0.0447	63.19	185.0	798.9	1	na
13	6809.8	0.0019	65.04	418.7	444.7	1	na	77	6821.5	0.0347	64.75	206.5	680.2	1	na
14	6879.3	0.0320	74.02	280.9	721.4	1	na	78	6707.2	0.0179	64.48	208.7	449.4	1	na
15	6800.0	0.0339	62.90	191.2	652.5	1	na	79	7566.0	0.1384	72.07	23.4	2352.3	2	na
16	6877.5	0.0322	74.01	277.9	720.9	1	na	80	6681.5	0.0167	62.80	191.6	415.1	1	na
17	6816.3	0.0010	65.04	431.0	445.2	1	na	81	8360.9	0.1997	61.58	313.2	3652.2	1	na
18	6663.5	0.0131	72.87	198.0	372.7	1	na	82	6809.8	0.0009	81.17	425.6	437.6	1	na
19	6650.8	0.0109	67.93	199.9	345.4	2	na	83	23162.9	0.7119	29.97	293.9	33275.6	1	na
20	6808.2	0.0027	65.04	411.5	448.5	1	na	84	8874.8	0.2438	84.38	333.4	4659.8	1	na
21	6664.1	0.0134	72.86	197.0	375.0	1	na	85	6828.6	0.0027	97.95	432.2	468.6	1	na
22	6789.6	0.0290	62.84	214.7	608.2	3	na	86	12978.6	0.4762	52.15	420.4	12780.5	1	na
23	6701.1	0.0176	62.85	205.3	440.7	1	na	87	24056.7	0.7239	26.72	264.4	35092.7	1	na
24	6828.6	0.0164	50.68	338.7	562.3	1	na	88	23162.9	0.7119	29.97	293.9	33275.6	1	na
25	6624.3	0.0078	64.80	194.8	297.5	1	na	89	6941.8	0.0450	66.73	251.0	876.4	1	na
26	6634.8	0.0213	65.01	115.6	397.7	3	na	90	6728.7	0.0038	66.77	324.9	376.3	3	na
27	6665.7	0.0008	65.12	281.9	293.1	1	na	91	6822.0	0.0323	69.86	220.0	667.8	2	na
28	6639.3	0.0223	65.01	112.9	409.3	3	na	92	7077.5	0.0654	142.90	236.3	1162.4	2	na
29	7758.7	0.1543	64.90	183.8	2577.4	1	na	93	6774.2	0.0009	51.63	390.1	402.0	2	na
30	6634.7	0.0225	73.41	107.0	406.0	2	na	94	6789.5	0.0011	51.64	403.8	418.8	6	na
31	6635.7	0.0113	62.81	182.7	332.5	1	na	95	6774.6	0.0012	51.63	388.2	404.7	1	na
32	6719.1	0.0190	62.85	213.0	469.0	1	na	96	7162.4	0.0563	62.66	380.8	1187.8	1	na
33	6794.9	0.0336	62.90	188.5	644.9	1	na	97	6941.5	0.0516	99.43	205.1	921.6	1	na
34	6664.8	0.0134	72.86	197.7	375.7	2	na	98	6708.3	0.0160	71.09	223.0	437.3	1	na
35	7145.3	0.0870	74.00	145.4	1388.8	1	na	99	6778.0	0.0010	51.63	393.3	406.4	2	na
36	7145.2	0.0870	74.00	145.4	1388.8	1	na	100	6813.8	0.0017	73.53	424.3	447.1	4	na
37	6907.1	0.0617	82.52	102.5	955.5	2	na	101	6652.4	0.0115	67.14	198.0	350.4	1	na
38	7046.8	0.0772	82.97	124.8	1212.5	1	na	102	6703.7	0.0061	59.38	285.0	366.0	2	na
39	6660.7	0.0166	63.31	172.0	393.2	1	na	103	6788.0	0.0338	62.82	180.4	639.3	1	na
40	6661.4	0.0165	56.97	173.4	393.0	1	na	104	6789.5	0.0290	62.84	214.2	608.5	3	na
41	6634.3	0.0081	63.00	202.1	310.1	2	na	105	6774.8	0.0052	56.85	361.4	431.9	15	na
42	7085.5	0.0653	142.88	244.5	1170.3	1	na	106	6632.5	0.0114	67.14	179.0	329.8	5	na
43	6793.3	0.0003	65.02	412.8	417.5	2	na	107	6726.6	0.0037	70.68	323.5	373.4	5	na
44	6705.0	0.0154	73.37	223.7	430.0	2	na	108	6740.9	0.0019	72.65	350.1	375.5	4	na
45	6775.7	0.0012	97.02	389.5	405.5	6	na	109	6780.5	0.0012	51.64	394.6	410.2	2	na
46	6875.2	0.0314	74.01	281.5	712.6	1	na	110	6663.1	0.0029	138.66	265.7	304.3	1	na
47	6717.1	0.0022	51.64	323.9	354.0	1	na	111	6784.6	0.0007	51.63	402.0	410.9	2	na
48	7962.6	0.1503	64.56	387.4	2781.6	1	na	112	6822.3	0.0217	72.65	296.0	592.3	1	na
49	6605.3	0.0220	63.74	81.8	372.5	1	na	113	6648.5	0.0085	63.00	213.8	327.0	2	na
50	6942.1	0.0685	63.66	88.1	1039.8	1	na	114	6648.3	0.0077	63.01	218.8	321.4	1	na
51	6834.5	0.0087	66.90	396.6	516.1	1	na	115	7588.5	0.1375	29.24	166.9	2253.7	1	na
52	10466.0	0.3629	3.87	289.3	7886.4	1	na	116	7564.5	0.1349	31.39	166.0	2206.7	1	na
53	6776.0	0.0026	70.40	380.2	415.6	4	na	117	6684.4	0.0006	57.01	302.2	310.3	4	na
54	7132.9	0.0481	66.34	411.4	1098.2	4	na	118	6624.3	0.0078	64.80	194.8	297.5	1	na
55	6683.8	0.0014	51.59	296.5	314.8	1	na	119	6713.8	0.0280	28.59	147.8	523.4	1	na
56	6851.0	0.0243	66.51	306.3	639.4	1	na	120	6712.6	0.0282	29.02	145.4	523.4	1	na
57	7191.8	0.0977	69.23	111.3	1515.9	1	na	121	6795.2	0.0005	65.03	413.4	420.7	2	na
58	6671.1	0.0132	62.81	204.9	381.0	1	na	122	6711.6	0.0276	30.60	147.9	519.0	1	na
59	11285.6	0.4145	7.65	230.0	9584.8	1	na	123	6684.7	0.0258	42.81	133.6	479.5	3	na
60	6793.6	0.0105	66.50	344.4	486.5	2	na	124	6704.2	0.0286	32.98	134.3	517.8	1	na
61	6965.7	0.0321	65.98	364.3	810.8	1	na	125	6785.7	0.0011	51.62	400.0	415.2	1	na
62	22923.3	0.7186	63.60	72.2	33018.1	1	na	126	6685.2	0.0011	57.01	299.6	314.5	2	na
63	11268.4	0.4258	46.98	92.6	9688.0	1	na	127	6692.8	0.0020	28.48	301.4	327.8	6	na
64	7498.9	0.1095	61.53	299.9	1941.7	1	na	128	6784.0	0.0011	51.64	398.3	413.4	4	na

obj	a	e	i	perigee	apogee	#	days/	obj	a	e	i	perigee	apogee	#	days/
	(km)		(deg)	(km)	(km)	updt	updt		(km)		(deg)	(km)	(km)	updt	updt
129	6624.5	0.0118	57.01	169.4	323.3	2	na	206	7852.3	0.1404	60.75	371.4	2576.9	3	na
130	25209.1	0.7369	26.48	254.9	37407.1	1	na	207	6727.1	0.0191	62.88	220.7	477.3	1	na
131	23466.9	0.7145	27.85	322.8	33854.7	3	na	208	15284.7	0.5721	34.71	162.8	17650.4	1	na
132	16618.8	0.6050	34.59	186.7	20294.5	1	na	209	13355.6	0.5031	17.72	257.7	13697.3	1	na
133	18852.4	0.6459	26.61	298.4	24650.2	1	na	210	13595.8	0.5031	26.70	377.5	14057.8	1	na
134	20511.1	0.6738	29.85	313.5	27952.4	1	na	211	21022.7	0.6809	7.81	330.3	28958.8	1	na
135	19357.5	0.6530	6.36	338.7	25620.0	1	na	212	13873.0	0.5087	17.92	437.7	14552.0	1	na
136	7194.4	0.0961	62.44	124.6	1507.9	1	na	213	13629.1	0.5069	26.28	342.1	14159.9	1	na
137	6659.2	0.0014	0.00	271.7	290.3	1	na	214	13936.9	0.5257	23.89	232.6	14884.8	1	na
138	6829.4	0.0015	61.01	441.1	461.3	14	na	215	14641.8	0.5492	27.05	222.1	16305.2	1	na
139	6828.8	0.0015	61.01	440.5	460.8	9	na	216	16557.9	0.5912	7.79	389.9	19969.5	1	na
140	6964.3	0.0479	97.71	252.4	920.0	1	na	217	21014.2	0.6808	6.54	329.7	28942.4	2	na
141	6753.3	0.0004	57.02	372.3	378.0	12	na	218	13102.8	0.4958	24.18	228.5	13220.9	1	na
142	7003.9	0.0510	97.70	268.5	983.1	1	na	219	14506.8	0.5329	7.86	397.3	15860.0	2	na
143	7011.7	0.0501	97.95	282.5	984.6	7	na	220	26755.9	0.7507	27.47	291.2	40464.3	1	na
144	7017.5	0.0548	97.71	254.9	1023.8	1	na	221	12667.5	0.4668	26.51	376.7	12201.9	1	na
145	6868.4	0.0128	68.00	402.4	578.1	4	na	222	13653.2	0.5143	7.45	252.5	14297.5	1	na
146	6933.7	0.0373	62.48	296.8	814.2	1	na	223	5763.6	0.2165	66.22	-1862.2	633.2	1	na
147	6863.6	0.0127	67.99	398.5	572.4	2	na	224	19518.7	0.6544	46.94	368.3	25912.8	1	na
148	6763.0	0.0029	51.67	365.0	404.7	14	na	225	25681.5	0.7437	63.39	204.1	38402.7	1	na
149	6679.2	0.0166	62.84	189.8	412.2	2	na	226	13693.3	0.5091	26.66	343.5	14286.8	1	na
150	9787.4	0.3172	26.94	305.1	6513.4	1	na	227	21374.2	0.6851	7.43	352.0	29640.2	1	na
151	9913.9	0.3211	63.22	352.2	6719.3	1	na	228	18368.9	0.6370	10.84	289.4	23692.2	1	na
152	6704.7	0.0167	62.83	214.7	438.5	1	na	229	14913.7	0.5562	24.29	240.1	16831.0	1	na
153	6922.6	0.0145	31.57	444.0	645.0	2	na	230	18194.6	0.6311	7.65	334.4	23298.5	1	na
154	7892.1	0.1443	60.74	375.3	2652.7	5	na	231	15675.6	0.5741	24.55	297.5	18297.3	2	na
155	8539.9	0.2285	23.63	210.6	4112.9	1	na	232	19365.6	0.6533	8.26	336.7	25638.1	1	na
156	6492.3	0.1286	26.56	-720.8	949.1	1	na	233	22910.3	0.7037	7.85	409.2	32655.2	1	na
157	10395.5	0.3482	63.32	397.8	7637.0	3	na	234	20449.3	0.6669	46.55	433.5	27708.7	1	na
158	6676.9	0.0133	62.82	209.8	387.6	2	na	235	20378.0	0.6717	46.81	312.3	27687.4	1	na
159	10041.3	0.3375	3.93	273.4	7053.0	2	na	236	18580.0	0.6356	19.71	393.2	24010.5	1	na
160	6705.9	0.0187	62.85	202.3	453.2	1	na	237	23750.2	0.7175	30.37	332.2	34411.9	1	na
161	6720.6	0.0011	51.64	335.4	349.6	6	na	238	12568.1	0.4741	27.03	231.8	12148.1	2	na
162	6677.9	0.0016	99.13	289.0	310.6	1	na	239	16549.1	0.5991	26.53	256.1	20085.8	1	na
163	7914.4	0.1470	60.74	373.2	2699.4	4	na	240	20386.8	0.6681	46.77	389.0	27628.3	1	na
164	6632.4	0.0112	62.87	179.8	328.6	1	na	241	9542.6	0.3066	7.37	238.3	6090.6	1	na
165	6655.4	0.0102	62.87	209.4	345.1	1	na	242	12778.7	0.4800	26.55	267.2	12534.0	2	na
166	9472.4	0.2949	41.23	300.6	5888.0	1	na	243	24573.2	0.7248	6.95	384.1	36005.9	1	na
167	6738.4	0.0019	51.61	347.5	372.9	15	na	244	21648.6	0.6843	26.34	457.1	30083.8	1	na
168	6716.4	0.0196	62.84	206.4	470.1	4	na								
169	11729.9	0.4288	18.04	322.5	10381.0	1	na								
170	11911.3	0.4490	37.62	185.4	10880.9	1	na								
171	7869.2	0.1419	60.77	374.5	2607.5	4	na								
172	6713.9	0.0199	62.86	202.5	469.1	1	na								
173	6676.6	0.0165	62.80	188.5	408.4	1	na								
174	6688.2	0.0168	62.84	198.0	422.2	1	na								
175	6652.4	0.0149	62.76	174.8	373.8	2	na								
176	6691.3	0.0168	62.79	200.6	425.7	1	na								
177	9344.4	0.2854	17.90	299.2	5633.3	1	na								
178	6732.8	0.0012	51.63	346.4	362.9	3	na								
179	6877.5	0.0232	82.77	339.5	659.1	4	na								
180	8361.4	0.2128	65.68	204.3	3762.2	1	na								
181	9043.9	0.2762	26.86	167.6	5164.0	2	na								
182	6760.5	0.0055	98.56	344.9	419.8	14	na								
183	6849.5	0.0018	81.17	458.9	483.9	7	na								
184	7884.1	0.1438	60.77	372.4	2639.5	3	na								
185	6679.0	0.0124	62.86	217.8	383.8	1	na								
186	6958.3	0.0296	65.98	374.0	786.3	1	na								
187	8240.4	0.1829	60.82	355.4	3369.2	2	na								
188	8303.8	0.1850	60.81	389.9	3461.5	1	na								
189	6704.7	0.0017	51.62	315.0	338.1	3	na								
190	7387.6	0.0796	65.81	421.2	1597.7	1	na								
191	6828.7	0.0396	47.62	179.9	721.2	1	na								
192	8432.7	0.1973	60.78	391.0	3718.1	1	na								
193	7371.2	0.0707	65.38	472.0	1514.2	1	na								
194	6716.2	0.0028	51.67	319.5	356.5	1	na								
195	6800.0	0.0343	28.11	188.7	655.0	1	na								
196	6732.1	0.0224	62.82	202.8	505.1	4	na								
197	6738.8	0.0234	62.82	202.4	518.8	3	na								
198	8044.5	0.1662	82.56	329.1	3003.6	3	na								
199	7606.4	0.1249	26.44	278.3	2178.2	2	na								
200	8411.3	0.1929	64.20	410.9	3655.4	2	na								
201	6670.4	0.0008	51.58	287.1	297.5	1	na								
202	9048.4	0.2585	26.66	331.4	5009.1	2	na								
203	10936.9	0.3847	59.50	351.2	8766.4	2	na								
204	7875.2	0.1430	60.73	371.3	2622.8	1	na								
205	7218.2	0.0808	67.19	256.5	1423.7	1	na								

Table D3. Contribution to the measured flux by individual objects from 300 to 470 km over 10-km intervals. The actual number of conjunctions is shown rather than the flux. Objects from the analysts' data set are marked by an asterisk.

alt	sum										
300.	50	310.	49	320.	85	330.	70	340.	64	350.	94
-----		-----		-----		-----		-----		-----	
124*	4	16570	2	22229	19	22229	17	167*	5	22045	9
21884	3	8127	2	21882	4	22130	2	11457	4	10134	6
21882	3	126*	2	21213	4	14329	2	10134	4	182*	5
14694	2	117*	2	2780	4	4330	2	168*	3	22024	4
117*	2	41*	2	21884	3	22225	2	2780	3	18845	3
16570	2	11457	2	22305	3	47*	1	22230	3	11457	3
143*	2	20101	1	6895	2	15244	1	22024	3	174*	3
11457	2	55*	1	129*	2	19220	1	22001	2	22106	3
110*	1	21988	1	189*	2	12908	1	22131	2	184*	3
22088	1	66*	1	9 obj	50.6%	15390	1	105*	2	22209	3
21213	1	21834	1			13608	1	22045	2	15054	2
113*	1	158*	1			15644	1	11 obj	51.6%	22107	2
164*	1	14075	1			22122	1			4053	2
13 obj	50.0%	21884	1			89*	1			13 obj	51.1%
		21743	1			19970	1				
		162*	1			15 obj	50.0%				
		22122	1								
		22023	1								
		242*	1								
		19 obj	51.0%								
alt	sum										
360.	77	370.	93	380.	95	390.	159	400.	201	410.	185
-----		-----		-----		-----		-----		-----	
2780	6	141*	12	10134	10	10113	13	22128	13	22229	33
11457	6	167*	5	2179	5	22123	8	22123	13	21065	22
108*	4	11457	4	1715	4	22121	6	21190	11	604	9
107*	4	1836	4	22225	4	22127	6	22121	9	8754	7
167*	4	148*	3	8745	4	22128	6	22127	8	100*	4
10113	4	22045	3	22045	3	5730	5	18927	8	2780	4
1836	4	22121	3	22024	3	21190	5	10113	7	12354	4
10134	3	22088	2	22121	3	18927	4	8754	7	2179	4
22023	3	9725	2	10113	3	22024	4	148*	5	12347	3
21994	2	18927	2	4298	2	8754	4	8744	5	19991	3
10 obj	51.9%	4053	2	53*	2	8744	3	45*	5	10 obj	50.3%
		22311	2	4053	2	22045	3	16609	4		
		7*	2	26*	2	22130	3	604	4		
		22322	2	206*	2	1836	3	12231	4		
		14 obj	51.6%	14 obj	51.6%	16609	3	14 obj	51.2%		
						604	3				
						11765	2				
						17 obj	50.9%				
alt	sum										
420.	116	430.	129	440.	133	450.	114	460.	99	470.	54
-----		-----		-----		-----		-----		-----	
16551	9	16308	11	20389	14	5853	5	17094	6	9854	4
604	7	16551	10	16308	10	139*	4	138*	5	7418	4
21190	6	20546	6	138*	8	18277	4	1440	5	11055	3
1715	5	1378	6	5853	7	4120	4	5009	5	1440	3
21065	5	5853	5	15536	7	1440	4	16480	5	184*	3
7942	5	19995	4	16551	6	17094	4	16084	4	7969	3
1836	4	18277	4	2179	4	7942	3	7418	4	16311	3
12347	4	2179	3	139*	4	2179	3	11055	4	16878	3
8754	4	100*	3	7942	4	4222	3	7942	3	4583	2
1616	3	1715	2	3019	3	16084	3	3019	3	9 obj	51.9%
71*	3	20919	2	10 obj	50.4%	16480	3	8386	3		
22230	3	74*	2			11055	3	2179	2		
12 obj	50.0%	5761	2			15536	2	15342	2		
		15441	2			16551	2	13 obj	51.5%		
		54*	2			20389	2				
		4175	2			4175	2				
		16 obj	51.2%			12849	2				
						8755	2				
						21905	2				
						19 obj	50.0%				

**Appendix E:
Clusters**

Table E1. Objects having conjunctions with the GRO within 5 sec of one another.

obj.	year	day	second	e	a (km)	i (deg)
22203	92	312	25.296	0.001636	6784.228	51.640
20635	92	312	25.382	0.001639	6784.224	51.641
22054	92	312	26.298	0.001638	6784.348	51.640
17845	92	312	27.410	0.001640	6784.499	51.642
cg altitude = 6776.139 km						
mean rms dispersion = 0.12 15.68 3.80 km in u,v,w coordinates						
20335	92	323	5.769	0.001487	6783.885	51.642
20635	92	323	5.866	0.001486	6783.904	51.642
22203	92	323	5.970	0.001483	6783.914	51.642
22054	92	323	6.005	0.001484	6783.916	51.642
16609	92	323	6.154	0.001448	6783.922	51.643
17845	92	323	6.254	0.001452	6783.933	51.642
cg altitude = 6777.702 km						
mean rms dispersion = 0.16 2.98 0.61 km in u,v,w coordinates						
20335	92	323	10.166	0.001349	6783.893	51.642
20635	92	323	10.271	0.001346	6783.898	51.642
22203	92	323	10.380	0.001347	6783.916	51.642
22054	92	323	10.419	0.001343	6783.914	51.642
16609	92	323	10.598	0.001356	6783.934	51.644
17845	92	323	10.676	0.001374	6783.941	51.642
cg altitude = 6778.581 km						
mean rms dispersion = 0.13 3.26 0.71 km in u,v,w coordinates						
17845	92	345	15.830	0.000759	6780.492	51.638
20335	92	345	15.830	0.000759	6780.492	51.638
22203	92	345	15.830	0.000759	6780.489	51.638
20635	92	345	15.833	0.000747	6780.509	51.638
22054	92	345	15.838	0.000760	6780.496	51.638
16609	92	345	16.010	0.000749	6780.533	51.637
cg altitude = 6778.916 km						
mean rms dispersion = 0.08 6.33 1.03 km in u,v,w coordinates						
20335	92	345	19.849	0.001574	6780.447	51.638
17845	92	345	19.849	0.001574	6780.447	51.638
22203	92	345	19.850	0.001574	6780.451	51.638
22054	92	345	19.857	0.001572	6780.448	51.638
20635	92	345	19.864	0.001587	6780.464	51.638
16609	92	345	20.059	0.001570	6780.497	51.637
cg altitude = 6772.681 km						
mean rms dispersion = 0.06 6.61 1.00 km in u,v,w coordinates						
30	92	350	0.073	0.013359	6664.124	72.858
18	92	350	0.074	0.013357	6664.133	72.858
cg altitude = 6739.559 km						
mean rms dispersion = 0.00 0.00 0.00 km in u,v,w coordinates						
31	92	353	37.324	0.087011	7145.238	74.004
32	92	353	37.987	0.087011	7145.233	74.004
cg altitude = 6724.700 km						
mean rms dispersion = 0.30 5.12 1.89 km in u,v,w coordinates						
25	92	354	31.144	0.022246	6640.686	65.014
23	92	354	31.146	0.022246	6640.681	65.014
cg altitude = 6743.724 km						
mean rms dispersion = 0.00 0.00 0.01 km in u,v,w coordinates						
16609	92	312	18.067	0.000921	6784.091	51.641
20335	92	312	18.278	0.000867	6784.107	51.641
22203	92	312	18.478	0.000869	6784.142	51.640
20635	92	312	18.568	0.000862	6784.150	51.641
22054	92	312	19.438	0.000872	6784.268	51.640
17845	92	312	20.510	0.000874	6784.407	51.641
cg altitude = 6782.158 km						
mean rms dispersion = 0.16 15.02 3.53 km in u,v,w coordinates						
obj.	year	day	second	e	a (km)	i (deg)
17845	92	355	20.604	0.001477	6778.084	51.633
22054	92	355	20.635	0.001485	6778.083	51.634
22203	92	355	20.678	0.001491	6778.091	51.634
16609	92	355	20.691	0.001503	6778.097	51.634
20635	92	355	20.711	0.001490	6778.099	51.634
20335	92	355	20.714	0.001489	6778.093	51.634

cg altitude = 6770.681 km
 mean rms dispersion = 0.105 5.011 1.006 km in
 u,v,w coordinates

39 92 359 53.820 0.000371 6794.143 65.024
 116 92 359 53.820 0.000371 6794.143 65.024
 cg altitude = 6792.515 km
 mean rms dispersion = 0.00 0.00 0.00 km in u,v,w
 coordinates

22 92 360 29.386 0.007751 6624.296 64.803
 113 92 360 29.387 0.007751 6624.296 64.803
 cg altitude = 6661.463 km
 mean rms dispersion = 0.00 0.00 0.00 km in u,v,w
 coordinates

23 92 362 18.625 0.020736 6632.205 65.002
 119 92 362 18.625 0.020736 6632.204 65.002
 cg altitude = 6755.126 km
 mean rms dispersion = 0.00 0.00 0.00 km in u,v,w
 coordinates

16609 93 9 53.679 0.000355 6774.294 51.629
 20635 93 9 53.853 0.000342 6774.334 51.629
 20335 93 9 53.884 0.000356 6774.325 51.629
 17845 93 9 53.887 0.000351 6774.331 51.629
 22203 93 9 53.980 0.000366 6774.354 51.629
 22054 93 9 54.027 0.000371 6774.350 51.629
 cg altitude = 6775.858 km
 mean rms dispersion = 0.07 2.40 0.64 km in u,v,w
 coordinates

16609 93 9 55.318 0.001191 6774.187 51.629
 20635 93 9 55.525 0.001178 6774.220 51.628
 20335 93 9 55.547 0.001190 6774.227 51.629
 17845 93 9 55.555 0.001189 6774.245 51.629
 22203 93 9 55.635 0.001203 6774.256 51.629
 22054 93 9 55.679 0.001206 6774.263 51.629
 cg altitude = 6768.494 km
 mean rms dispersion = 0.04 2.35 0.43 km in u,v,w
 coordinates

17845 93 19 59.902 0.000297 6773.673 51.627
 22054 93 19 59.902 0.000298 6773.664 51.627
 20335 93 19 59.907 0.000299 6773.677 51.627
 20635 93 19 59.908 0.000298 6773.684 51.627
 22203 93 19 59.909 0.000299 6773.674 51.627
 16609 93 19 0.192 0.000394 6773.696 51.628
 cg altitude = 6774.007 km
 mean rms dispersion = 0.43 1.16 0.29 km in u,v,w
 coordinates

99 93 22 44.561 0.029073 6789.120 62.843
 19 93 22 48.128 0.029011 6789.247 62.844
 cg altitude = 6830.704 km
 mean rms dispersion = 0.38 27.91 8.01 km in u,v,w
 coordinates

99 93 22 12.925 0.028883 6789.061 62.842
 19 93 22 16.685 0.028828 6789.132 62.844
 cg altitude = 6731.447 km
 mean rms dispersion = 0.222 34.019 16.589 km in u,
 v, w coordinates

9 93 26 54.006 0.023067 6879.273 71.113
 10 93 26 55.804 0.022866 6879.294 71.107
 cg altitude = 6725.490 km
 mean rms dispersion = 0.71 15.50 6.69 km in u,v,w
 coordinates

obj.	year	day	second	e	a (km)	i (deg)
22203	93	28	10.426	0.000557	6774.107	51.630
20335	93	28	10.426	0.000557	6774.107	51.630
17845	93	28	10.426	0.000557	6774.107	51.630
22054	93	28	10.540	0.000573	6774.131	51.630
20635	93	28	10.542	0.000572	6774.131	51.630
22319	93	28	10.579	0.000580	6774.143	51.630
16609	93	28	11.484	0.000608	6774.321	51.632
cg altitude = 6772.048 km						
mean rms dispersion = 0.26 48.01 11.62 km in u,v,w						
coordinates						

88 93 28 0.097 0.001217 6774.027 51.630
 87 93 28 1.853 0.001216 6774.124 51.630
 cg altitude = 6769.049 km
 mean rms dispersion = 0.07 16.53 2.16 km in u,v,w
 coordinates

99 93 28 46.443 0.029147 6790.375 62.845

19 93 28 52.714 0.029098 6790.456 62.847
 cg altitude = 6696.724 km
 mean rms dispersion = 0.54 49.77 7.613 km in u,v,w
 coordinates

17845 93 37 54.181 0.001153 6775.884 51.640
 20335 93 37 54.290 0.001073 6775.936 51.641
 22319 93 37 54.417 0.001078 6775.955 51.641
 20635 93 37 54.596 0.001039 6775.992 51.641
 16609 93 37 54.886 0.001118 6776.006 51.639
 cg altitude = 6770.269 km
 mean rms dispersion = 0.28 5.07 1.38 km in u,v,w
 coordinates

22319 93 46 56.780 0.001607 6775.071 51.639
 20635 93 46 56.943 0.001612 6775.094 51.640
 20335 93 46 56.943 0.001609 6775.081 51.640
 17845 93 46 57.497 0.001620 6775.183 51.640
 16609 93 46 57.814 0.001596 6775.248 51.639
 cg altitude = 6766.938 km
 mean rms dispersion = 0.12 7.49 1.54 km in u,v,w
 coordinates

22319 93 46 54.014 0.000914 6775.098 51.639
 20335 93 46 54.132 0.000945 6775.115 51.640
 20635 93 46 54.132 0.000945 6775.115 51.640
 17845 93 46 54.689 0.000941 6775.207 51.640
 16609 93 46 55.030 0.000939 6775.270 51.640
 cg altitude = 6772.463 km
 mean rms dispersion = 0.07 7.74 1.51 km in u,v,w
 coordinates

22319 93 46 54.014 0.000914 6775.098 51.639
 20335 93 46 54.132 0.000945 6775.115 51.640
 20635 93 46 54.132 0.000945 6775.115 51.640
 17845 93 46 54.689 0.000941 6775.207 51.640
 16609 93 46 55.030 0.000939 6775.270 51.640
 cg altitude = 6772.463 km
 mean rms dispersion = 0.07 7.74 1.51 km in u,v,w
 coordinates

16609 93 55 53.331 0.001662 6772.151 51.631
 22319 93 55 55.523 0.001704 6772.424 51.631
 20335 93 55 55.536 0.001703 6772.422 51.631
 20635 93 55 55.550 0.001703 6772.427 51.631
 17845 93 55 55.568 0.001707 6772.430 51.630
 cg altitude = 6763.898 km
 mean rms dispersion = 0.01 16.60 4.24 km in u,v,w
 coordinates

16609 93 55 53.331 0.001662 6772.151 51.631
 22319 93 55 55.523 0.001704 6772.424 51.631
 20335 93 55 55.536 0.001703 6772.422 51.631
 20635 93 55 55.550 0.001703 6772.427 51.631
 17845 93 55 55.568 0.001707 6772.430 51.630
 cg altitude = 6763.898 km
 mean rms dispersion = 0.01 16.60 4.24 km in u,v,w
 coordinates

Appendix F: Flux Contribution by Object

Table F1. Contribution to the statistical flux by individual objects from 300 to 470 km averaged over a 10-km altitude band.

day 275 1992 275 - 1992	day 304 1992 304 - 1992	day 335 1992 335 - 1992	day 365 1992 365 - 1992	day 032 1993 032 - 1993	day 060 1993 060 - 1993
alt sum 300.0 0.0914 ----- 16570 0.0222 8127 0.0190 22120 0.0163 3obj 63.0%	alt sum 300.0 0.0587 ----- 22107 0.0159 21884 0.0064 22217 0.0042 16985 0.0035 4obj 51.1%	alt sum 300.0 0.0587 ----- 22107 0.0159 21884 0.0064 22217 0.0042 16985 0.0035 4obj 51.1%	alt sum 300.0 0.0370 ----- 15342 0.0067 22280 0.0035 22229 0.0032 14075 0.0021 22226 0.0019 22301 0.0014 6obj 50.8%	alt sum 300.0 0.0610 ----- 11457 0.0190 22313 0.0117 2obj 50.4%	alt sum 300.0 0.0300 ----- 22310 0.0028 22260 0.0021 22483 0.0020 22527 0.0019 14694 0.0013 22322 0.0012 22317 0.0012 22526 0.0011 22529 0.0009 22525 0.0009 10obj 51.7%
alt sum 310.0 0.1026 ----- 16570 0.0221 8127 0.0134 21213 0.0126 22120 0.0100 4obj 56.7%	sum alt 310.0 0.0389 ----- 8138 0.0066 22107 0.0044 16985 0.0025 22217 0.0019 22133 0.0016 14075 0.0014 22226 0.0014 7obj 51.0%	alt sum 310.0 0.0389 ----- 8138 0.0066 22107 0.0044 16985 0.0025 22217 0.0019 22133 0.0016 14075 0.0014 22226 0.0014 7obj 51.0%	alt sum 310.0 0.0519 ----- 22259 0.0109 15342 0.0091 22229 0.0057 22280 0.0039 4obj 57.1%	sum alt 310.0 0.0628 ----- 11457 0.0190 2780 0.0130 2obj 51.0%	alt sum 310.0 0.0248 ----- 22527 0.0024 22483 0.0020 22322 0.0013 22317 0.0013 22526 0.0011 14694 0.0010 22529 0.0009 22525 0.0009 14514 0.0008 22520 0.0008 10obj 50.0%
alt sum 320.0 0.1008 ----- 21213 0.0177 21882 0.0158 21884 0.0132 22046 0.0122 4obj 58.5%	alt sum 320.0 0.0404 ----- 8138 0.0102 22229 0.0025 22133 0.0018 22230 0.0017 22226 0.0016 14075 0.0014 6895 0.0013 7obj 50.9%	alt sum 320.0 0.0404 ----- 8138 0.0102 22229 0.0025 22133 0.0018 22230 0.0017 22226 0.0016 14075 0.0014 6895 0.0013 7obj 50.9%	alt sum 320.0 0.0721 ----- 22259 0.0162 11457 0.0071 15342 0.0058 2780 0.0055 22229 0.0044 5obj 54.1%	sum alt 320.0 0.0408 ----- 2780 0.0142 22313 0.0034 22317 0.0018 6895 0.0014 4obj 50.8%	alt sum 320.0 0.0366 ----- 10134 0.0075 22527 0.0038 22483 0.0021 6895 0.0014 22317 0.0013 22322 0.0013 22526 0.0011 7obj 50.9%
alt sum 330.0 0.1037 ----- 7889 0.0162 22002 0.0109 22003 0.0098 21882 0.0094 22046 0.0094 5obj 53.7%	alt sum 330.0 0.0462 ----- 8138 0.0069 22229 0.0049 22230 0.0045 9725 0.0026 22133 0.0024 22226 0.0018 6obj 50.1%	alt sum 330.0 0.0462 ----- 8138 0.0069 22229 0.0049 22230 0.0045 9725 0.0026 22133 0.0024 22226 0.0018 6obj 50.1%	alt sum 330.0 0.0728 ----- 11457 0.0188 2780 0.0104 22230 0.0059 22259 0.0053 4obj 55.6%	alt sum 330.0 0.0305 ----- 2780 0.0065 22317 0.0024 6895 0.0014 22311 0.0013 2167 0.0010 8063 0.0009 614 0.0008 4330 0.0008 22310 0.0007 9obj 51.9%	alt sum 330.0 0.0516 ----- 10134 0.0188 18927 0.0034 22527 0.0024 22483 0.0023 4obj 52.2%

alt sum 340.0 0.0832 ----- 7889 0.0145 22002 0.0143 21991 0.0136 3obj 50.9%	alt sum 340.0 0.0678 ----- 11457 0.0082 8138 0.0071 2780 0.0063 22228 0.0058 22230 0.0045 9725 0.0042 6obj 53.4%	alt sum 340.0 0.0678 ----- 11457 0.0082 8138 0.0071 2780 0.0063 22228 0.0058 22230 0.0045 9725 0.0042 6obj 53.4%	alt sum 340.0 0.0696 ----- 22106 0.0118 11457 0.0117 2780 0.0107 22024 0.0043 4obj 55.3%	alt sum 340.0 0.0440 ----- 10134 0.0187 22317 0.0033 2obj 50.1%	alt sum 340.0 0.0476 ----- 10134 0.0113 18927 0.0074 22483 0.0027 10113 0.0024 4obj 50.1%
alt sum 350.0 0.0578 ----- 21991 0.0110 22003 0.0092 22002 0.0080 7889 0.0059 4obj 59.0%	alt sum 350.0 0.0935 ----- 11457 0.0187 22228 0.0156 2780 0.0104 8138 0.0094 4obj 57.8%	alt sum 350.0 0.0935 ----- 11457 0.0187 22228 0.0156 2780 0.0104 8138 0.0094 4obj 57.8%	alt sum 350.0 0.0999 ----- 22106 0.0156 10134 0.0108 22024 0.0103 2780 0.0089 22045 0.0088 5obj 54.5%	alt sum 350.0 0.0568 ----- 10134 0.0187 18927 0.0058 14439 0.0050 3obj 52.0%	alt sum 350.0 0.0549 ----- 10113 0.0153 18927 0.0082 22483 0.0046 3obj 51.2%
alt sum 360.0 0.0530 ----- 21994 0.0085 22023 0.0080 21991 0.0053 2780 0.0051 4obj 50.6%	alt sum 360.0 0.1117 ----- 11457 0.0104 22228 0.0098 22024 0.0093 2780 0.0086 22106 0.0082 22045 0.0079 4175 0.0070 7obj 54.8%	alt sum 360.0 0.1117 ----- 11457 0.0104 22228 0.0098 22024 0.0093 2780 0.0086 22106 0.0082 22045 0.0079 4175 0.0070 7obj 54.8%	alt sum 360.0 0.1439 ----- 10134 0.0186 22045 0.0156 22209 0.0156 1715 0.0145 12224 0.0143 5obj 54.6%	alt sum 360.0 0.0632 ----- 10113 0.0216 18927 0.0091 14439 0.0057 3obj 57.6%	alt sum 360.0 0.0832 ----- 10113 0.0192 1836 0.0145 18927 0.0071 2179 0.0062 4obj 56.6%
alt sum 370.0 0.0934 ----- 11457 0.0148 21994 0.0146 22023 0.0097 2780 0.0085 4obj 51.1%	alt sum 370.0 0.1364 ----- 10134 0.0185 22106 0.0155 22045 0.0155 22024 0.0136 4175 0.0130 5obj 55.9%	alt sum 370.0 0.1364 ----- 10134 0.0185 22106 0.0155 22045 0.0155 22024 0.0136 4175 0.0130 5obj 55.9%	alt sum 370.0 0.1353 ----- 10113 0.0171 22209 0.0155 22225 0.0155 12224 0.0153 1715 0.0082 5obj 52.9%	alt sum 370.0 0.0727 ----- 10113 0.0188 18927 0.0087 1836 0.0070 14439 0.0040 4obj 53.0%	alt sum 370.0 0.0890 ----- 2179 0.0151 1836 0.0145 12231 0.0093 10113 0.0063 4obj 50.8%
alt sum 380.0 0.1713 ----- 11457 0.0185 22124 0.0123 22130 0.0117 10134 0.0114 21994 0.0102 22024 0.0096 3355 0.0093 22045 0.0084 8obj 53.3%	alt sum 380.0 0.1432 ----- 10113 0.0179 22209 0.0154 10134 0.0117 4175 0.0101 22045 0.0076 22106 0.0073 22024 0.0063 7obj 53.3%	alt sum 380.0 0.1432 ----- 10113 0.0179 22209 0.0154 10134 0.0117 4175 0.0101 22045 0.0076 22106 0.0073 22024 0.0063 7obj 53.3%	alt sum 380.0 0.1140 ----- 22225 0.0155 22121 0.0154 10113 0.0138 12224 0.0076 22299 0.0066 5obj 51.6%	alt sum 380.0 0.0845 ----- 1836 0.0144 8754 0.0097 2179 0.0079 21190 0.0064 18927 0.0053 5obj 51.8%	alt sum 380.0 0.1283 ----- 12231 0.0218 8754 0.0185 2179 0.0154 22530 0.0086 4obj 50.1%
alt sum 390.0 0.2389 ----- 10134 0.0184 22124 0.0154 22130 0.0154 22122 0.0154 22107 0.0154 22129 0.0154 22131 0.0154 10113 0.0120 8obj 51.4%	alt sum 390.0 0.1954 ----- 22209 0.0154 22225 0.0154 22121 0.0154 16609 0.0154 1715 0.0144 10113 0.0134 22123 0.0091 7obj 50.4%	alt sum 390.0 0.1954 ----- 22209 0.0154 22225 0.0154 22121 0.0154 16609 0.0154 1715 0.0144 10113 0.0134 22123 0.0091 7obj 50.4%	alt sum 390.0 0.1959 ----- 8754 0.0184 22121 0.0154 16609 0.0154 22123 0.0154 22127 0.0154 22128 0.0154 22299 0.0113 7obj 54.5%	alt sum 390.0 0.1449 ----- 8754 0.0184 16609 0.0154 22203 0.0154 22054 0.0154 2179 0.0125 5obj 53.2%	alt sum 390.0 0.1465 ----- 8754 0.0184 22530 0.0154 16609 0.0154 7942 0.0135 12231 0.0124 5obj 51.3%

alt sum 400.0 0.2721 ----- 10113 0.0209 22131 0.0153 22106 0.0153 22121 0.0153 16609 0.0153 22128 0.0153 22123 0.0153 22127 0.0153 22128 0.0153 22123 0.0153 22127 0.0153 22129 0.0111 9obj 51.2%	alt sum 400.0 0.2278 ----- 8754 0.0183 22121 0.0154 16609 0.0153 22123 0.0153 22127 0.0153 22128 0.0153 1715 0.0143 22225 0.0114 8obj 53.0%	alt sum 400.0 0.2278 ----- 8754 0.0183 22121 0.0154 16609 0.0153 22123 0.0153 22127 0.0153 22128 0.0153 1715 0.0143 22225 0.0114 8obj 53.0%	alt sum 400.0 0.2019 ----- 8754 0.0183 16609 0.0153 22123 0.0153 22127 0.0153 22128 0.0153 1836 0.0143 22299 0.0099 7obj 51.5%	alt sum 400.0 0.1636 ----- 16609 0.0154 22203 0.0154 22054 0.0154 604 0.0124 2179 0.0110 8754 0.0087 7942 0.0082 7obj 52.8%	alt sum 400.0 0.1262 ----- 604 0.0158 7942 0.0137 21065 0.0078 16609 0.0069 22530 0.0068 21190 0.0063 5853 0.0035 22526 0.0024 8obj 50.1%
alt sum 410.0 0.2072 ----- 8754 0.0183 21065 0.0164 22121 0.0153 16609 0.0153 22128 0.0153 22123 0.0153 22127 0.0153 7obj 53.6%	alt sum 410.0 0.1751 ----- 21065 0.0164 8754 0.0140 604 0.0133 1836 0.0107 22128 0.0083 22127 0.0075 2179 0.0067 22123 0.0063 21190 0.0060 9obj 50.9%	alt sum 410.0 0.1751 ----- 21065 0.0164 8754 0.0140 604 0.0133 1836 0.0107 22128 0.0083 22127 0.0075 2179 0.0067 22123 0.0063 21190 0.0060 9obj 50.9%	alt sum 410.0 0.1402 ----- 21065 0.0164 604 0.0158 21190 0.0082 16551 0.0073 2179 0.0069 1836 0.0060 7942 0.0054 5853 0.0053 8obj 50.8%	alt sum 410.0 0.1515 ----- 21065 0.0164 7942 0.0131 604 0.0111 12231 0.0098 16551 0.0096 2179 0.0089 21190 0.0074 7obj 50.4%	alt sum 410.0 0.1390 ----- 21065 0.0164 16551 0.0108 7942 0.0080 604 0.0078 12188 0.0075 5853 0.0072 21190 0.0065 16308 0.0040 5009 0.0037 9obj 51.7%
alt sum 420.0 0.1437 ----- 8754 0.0181 604 0.0157 16551 0.0092 21065 0.0088 21190 0.0084 16308 0.0064 18927 0.0064 7obj 50.8%	alt sum 420.0 0.1543 ----- 2179 0.0113 604 0.0101 16308 0.0097 21065 0.0087 1836 0.0086 5853 0.0075 21190 0.0065 22148 0.0054 7942 0.0041 20546 0.0039 21868 0.0039 11obj 51.8%	alt sum 420.0 0.1543 ----- 2179 0.0113 604 0.0101 16308 0.0097 21065 0.0087 1836 0.0086 5853 0.0075 21190 0.0065 22148 0.0054 7942 0.0041 20546 0.0039 21868 0.0039 11obj 51.8%	alt sum 420.0 0.1563 ----- 16551 0.0155 16308 0.0116 7942 0.0097 21065 0.0086 5853 0.0085 20897 0.0079 2179 0.0072 604 0.0069 21190 0.0055 9obj 52.0%	alt sum 420.0 0.1612 ----- 16551 0.0167 7942 0.0132 16308 0.0131 5853 0.0094 12231 0.0087 21065 0.0085 21868 0.0056 1378 0.0051 20546 0.0049 9obj 52.9%	alt sum 420.0 0.1708 ----- 16551 0.0191 22536 0.0182 16308 0.0147 12188 0.0089 21065 0.0086 20389 0.0084 5853 0.0067 21868 0.0061 8obj 53.0%
alt sum 430.0 0.1691 ----- 16308 0.0170 16551 0.0159 1715 0.0142 1836 0.0111 604 0.0105 5853 0.0087 2179 0.0067 21868 0.0050 8obj 52.6%	alt sum 430.0 0.1725 ----- 16308 0.0212 20389 0.0111 2179 0.0097 7942 0.0080 18734 0.0069 5853 0.0064 21868 0.0061 1378 0.0056 22229 0.0052 22230 0.0048 20546 0.0042 11obj 51.7%	alt sum 430.0 0.1725 ----- 16308 0.0212 20389 0.0111 2179 0.0097 7942 0.0080 18734 0.0069 5853 0.0064 21868 0.0061 1378 0.0056 22229 0.0052 22230 0.0048 20546 0.0042 11obj 51.7%	alt sum 430.0 0.1885 ----- 16308 0.0212 20389 0.0171 20897 0.0149 16551 0.0139 2179 0.0085 7942 0.0082 12231 0.0078 21868 0.0067 8obj 52.2%	alt sum 430.0 0.1679 ----- 16308 0.0212 20389 0.0171 12231 0.0116 16551 0.0116 7942 0.0082 5853 0.0066 18277 0.0057 1378 0.0051 8obj 51.9%	alt sum 430.0 0.1778 ----- 22536 0.0181 16308 0.0172 20389 0.0171 16551 0.0104 4518 0.0100 12188 0.0071 18277 0.0063 5853 0.0062 8obj 52.0%

alt sum 440.0 0.1866	alt sum 440.0 0.1832	alt sum 440.0 0.1832	alt sum 440.0 0.1949	alt sum 440.0 0.1717	alt sum 440.0 0.1859
20389 0.0171 16308 0.0147 1836 0.0121 16551 0.0120 1715 0.0090 18845 0.0089 2179 0.0081 5853 0.0062 1378 0.0061 9obj 50.4%	20389 0.0171 16308 0.0114 2179 0.0099 7942 0.0070 18277 0.0068 5853 0.0063 18734 0.0060 1440 0.0059 16084 0.0052 4120 0.0047 8755 0.0045 22230 0.0042 1378 0.0042 13obj 50.7%	20389 0.0171 16308 0.0114 2179 0.0099 7942 0.0070 18277 0.0068 5853 0.0063 18734 0.0060 1440 0.0059 16084 0.0052 4120 0.0047 8755 0.0045 22230 0.0042 1378 0.0042 13obj 50.7%	20389 0.0143 20897 0.0135 12231 0.0120 7942 0.0107 16308 0.0095 5853 0.0077 1440 0.0072 18277 0.0067 16551 0.0057 16084 0.0055 8755 0.0050 11obj 50.2%	20389 0.0128 5853 0.0088 1440 0.0083 16308 0.0080 4518 0.0079 12231 0.0075 16084 0.0063 18277 0.0063 8755 0.0053 4120 0.0051 16551 0.0045 16311 0.0044 11055 0.0038 13obj 51.9%	4518 0.0110 12188 0.0104 1440 0.0094 20389 0.0088 5853 0.0080 11055 0.0079 16084 0.0071 16308 0.0065 8755 0.0062 18277 0.0062 22486 0.0059 4120 0.0054 16311 0.0051 13obj 52.6%
alt sum 450.0 0.2138	alt sum 450.0 0.2148	alt sum 450.0 0.2148	alt sum 450.0 0.2129	alt sum 450.0 0.2042	alt sum 450.0 0.2431
18845 0.0212 20389 0.0128 16084 0.0091 16311 0.0087 16480 0.0085 5853 0.0079 7942 0.0071 8755 0.0067 1440 0.0065 2179 0.0060 4120 0.0058 16551 0.0053 17094 0.0052 13obj 51.8%	16480 0.0105 16084 0.0105 11055 0.0105 16311 0.0101 1440 0.0087 8755 0.0079 5853 0.0077 12231 0.0075 7418 0.0066 7942 0.0062 17094 0.0062 20389 0.0060 18734 0.0058 15342 0.0052 14obj 50.9%	16480 0.0105 16084 0.0105 11055 0.0105 16311 0.0101 1440 0.0087 8755 0.0079 5853 0.0077 12231 0.0075 7418 0.0066 7942 0.0062 17094 0.0062 20389 0.0060 18734 0.0058 15342 0.0052 14obj 50.9%	11055 0.0152 16480 0.0116 16084 0.0112 16311 0.0107 12231 0.0092 8755 0.0085 7942 0.0076 4518 0.0072 7418 0.0072 1440 0.0068 5853 0.0065 20897 0.0064 12obj 50.8%	11055 0.0180 16480 0.0122 16084 0.0118 16311 0.0112 8755 0.0090 7418 0.0076 4518 0.0074 8386 0.0073 17094 0.0068 1440 0.0063 5853 0.0054 11obj 50.4%	22486 0.0182 11055 0.0180 16480 0.0129 16084 0.0122 16311 0.0116 8386 0.0115 8755 0.0094 7418 0.0083 17094 0.0072 12188 0.0068 4518 0.0067 11obj 50.5%
alt sum 460.0 0.2668	alt sum 460.0 0.2952	alt sum 460.0 0.2952	alt sum 460.0 0.2908	alt sum 460.0 0.2947	alt sum 460.0 0.3125
16480 0.0209 11055 0.0179 16311 0.0160 4175 0.0143 16084 0.0135 18845 0.0123 17094 0.0094 16878 0.0089 7418 0.0087 8755 0.0081 7942 0.0072 11obj 51.4%	16480 0.0209 11055 0.0179 4583 0.0179 16311 0.0166 12231 0.0122 16084 0.0107 16878 0.0103 17094 0.0100 7418 0.0088 7942 0.0081 18734 0.0074 4518 0.0065 8755 0.0065 13obj 52.1%	16480 0.0209 11055 0.0179 4583 0.0179 16311 0.0166 12231 0.0122 16084 0.0107 16878 0.0103 17094 0.0100 7418 0.0088 7942 0.0081 18734 0.0074 4518 0.0065 8755 0.0065 13obj 52.1%	16480 0.0209 16311 0.0195 11055 0.0179 4583 0.0179 16084 0.0125 16878 0.0109 17094 0.0103 12231 0.0092 8386 0.0087 4518 0.0082 7418 0.0082 8755 0.0068 12obj 52.0%	16480 0.0209 4583 0.0179 16311 0.0165 11055 0.0141 16084 0.0128 8386 0.0123 16878 0.0115 17094 0.0106 7418 0.0090 4518 0.0087 1963 0.0082 8755 0.0072 12obj 50.8%	8386 0.0207 16480 0.0192 4583 0.0179 16311 0.0159 1963 0.0140 16084 0.0133 22486 0.0123 16878 0.0118 17094 0.0108 11055 0.0100 7418 0.0076 9854 0.0071 12obj 51.4%

alt	sum										
470.0	0.3711	470.0	0.3660	470.0	0.3660	470.0	0.3468	470.0	0.3484	470.0	0.3443
15441	0.0211	16878	0.0209	16878	0.0209	16878	0.0209	16878	0.0209	16878	0.0170
16878	0.0201	4583	0.0179	4583	0.0179	4583	0.0179	4583	0.0179	19764	0.0169
4583	0.0179	19764	0.0117	19764	0.0117	19764	0.0154	19764	0.0169	4583	0.0164
4175	0.0165	12231	0.0109	12231	0.0109	1963	0.0140	1963	0.0140	1963	0.0140
11055	0.0156	16311	0.0108	16311	0.0108	8386	0.0115	8386	0.0133	20966	0.0127
16480	0.0124	16084	0.0104	16084	0.0104	20966	0.0104	20966	0.0111	7418	0.0096
16311	0.0122	16480	0.0104	16480	0.0104	16311	0.0102	7418	0.0103	1844	0.0095
16084	0.0118	1937	0.0101	1937	0.0101	1937	0.0099	16311	0.0097	16564	0.0095
19764	0.0100	8386	0.0099	8386	0.0099	16084	0.0097	16084	0.0092	16311	0.0093
1937	0.0086	20966	0.0095	20966	0.0095	8755	0.0094	1844	0.0091	7969	0.0092
2179	0.0084	4518	0.0087	4518	0.0087	16480	0.0093	8755	0.0090	8386	0.0092
17094	0.0081	1963	0.0080	1963	0.0080	4518	0.0093	7969	0.0090	1440	0.0089
20966	0.0075	7969	0.0080	7969	0.0080	1844	0.0086	16564	0.0090	16084	0.0087
7418	0.0073	1844	0.0079	1844	0.0079	7969	0.0085	16480	0.0088	8755	0.0085
7969	0.0070	16564	0.0077	16564	0.0077	7418	0.0081	20496	0.0079	20496	0.0083
8755	0.0069	20897	0.0075	20897	0.0075	17094	0.0081	15obj	50.5%	16085	0.0082
16obj	51.6%	11055	0.0075	11055	0.0075	16obj	52.3%			16obj	51.1%
		17094	0.0075	17094	0.0075						
		18obj	50.6%	18obj	50.6%						

Table F2. Objects making a large contribution to the statistical model flux calculation.
 Shown is the international identifier (intl id), USSPACECOM object number (obj), object description (description), country of origin (orig), launch date (date), and reentry date (reentry).

intl id	obj	description	orig	launch	reentry
1963-024A	604	TIROS 7	US	19 JUN 63	
1963-025B	614	HITCH HIKER 1	US	27 JUN 63	
1965-038B	1378	OPS 8386 R/B (ALTAIR)	US	20 MAY 65	
1965-051C	1440	TIROS 10 DEB	US	2 JUL 65	
1965-082BW	1715	OV 2 1/LCS 2 DEB	US	15 OCT 65	5 FEB 93
1965-082EB	1836	OV 2 1/LCS 2 DEB	US	15 OCT 65	17 APR 93
1965-082GY	1963	OV 2 1/LCS 2 DEB	US	15 OCT 65	
1965-082LS	3355	OV 2 1/LCS 2 DEB	US	15 OCT 65	3 NOV 92
1965-106B	1844	COSMOS 100 R/B	USSR	17 DEC 65	
1965-112Q	1937	COSMOS 103 DEB	USSR	28 DEC 65	
1966-026F	2179	OPS 0340 DEB	US	31 MAR 66	20 APR 93
1966-034B	2167	OPS 1527 DEB	US	22 APR 66	
1967-043B	2780	OPS 1967	US	9 MAY 67	14 MAR 93
1969-082AT	4175	OPS 7613 DEB	US	30 SEP 69	14 DEC 92
1969-082FV	4518	OPS 7613 DEB	US	30 SEP 69	5 JUN 93
1969-084B	4120	METEOR 1-2 R/B	USSR	6 OCT 69	
1970-011A	4330	OHSUMI (LAMBDA-4S 5)	JPN	11 FEB 70	
1970-085A	4583	METEOR 1-6	USSR	15 OCT 70	
1971-003C	18277	METEOR 1-7 DEB	USSR	20 JAN 71	
1971-015C	5009	COSMOS 397 DEB	USSR	25 FEB 71	11 APR 93
1971-015CT	15342	COSMOS 397 DEB	USSR	25 FEB 71	23 DEC 92
1972-011B	5853	COSMOS 476 R/B	USSR	1 MAR 72	
1972-058CH	7942	LANDSAT 1 DEB	US	23 JUL 72	16 APR 93
1972-058FC	8386	LANDSAT 1 DEB	US	23 JUL 72	8 DEC 93
1973-078C	6895	EXPLORER 50 R/B(1)	US	26 OCT 73	
1974-066B	7418	COSMOS 673 R/B	USSR	16 AUG 74	
1974-089G	8138	NOAA 4 DEB	US	15 NOV 74	14 NOV 92
1975-056B	7969	COSMOS 744 R/B	USSR	20 JUN 75	
1975-072B	8063	COS B R/B	US	9 AUG 75	
1976-024A	8754	COSMOS 808	USSR	16 MAR 76	20 NOV 93
1976-024B	8755	COSMOS 808 R/B	USSR	16 MAR 76	
1976-039D	14514	LAGEOS DEB	US	4 MAY 76	8 DEC 93
1976-126W	9725	COSMOS 886 DEB	USSR	27 DEC 76	21 DEC 92
1977-015B	9854	COSMOS 895 R/B	USSR	26 FEB 77	
1977-057A	10113	METEOR 1-28	USSR	29 JUN 77	28 AUG 93
1977-061A	10134	COSMOS 925	USSR	7 JUL 77	29 APR 93
1977-061B	10135	COSMOS 925 R/B	USSR	7 JUL 77	
1978-026AD	12188	LANDSAT 3 DEB	US	5 MAR 78	13 MAR 93
1978-026BR	12224	LANDSAT 3 DEB	US	5 MAR 78	31 DEC 92
1978-026BY	12231	LANDSAT 3 DEB	US	5 MAR 78	19 MAR 93
1978-094A	11055	COSMOS 1043	USSR	10 OCT 78	
1978-094C	22536	COSMOS 1043	USSR	10 OCT 78	11 MAR 93
1979-017AM	16084	SOLWIND DEB	US	24 FEB 79	
1979-017AN	16085	SOLWIND DEB	US	24 FEB 79	
1979-017BX	16308	SOLWIND DEB	US	24 FEB 79	
1979-017CA	16311	SOLWIND DEB	US	24 FEB 79	
1979-017FE	16480	SOLWIND DEB	US	24 FEB 79	
1979-017GJ	16551	SOLWIND DEB	US	24 FEB 79	
1979-017GX	16564	SOLWIND DEB	US	24 FEB 79	
1979-017JF	16878	SOLWIND DEB	US	24 FEB 79	
1979-017JH	17094	SOLWIND DEB	US	24 FEB 79	
1979-067A	11457	COSMOS 1116	USSR	20 JUL 79	11 MAR 93
1981-053JJ	14439	COSMOS 1275 DEB	USSR	4 JUN 81	14 JAN 93
1983-046A	14075	COSMOS 1463	USSR	19 MAY 83	24 JAN 93
1984-011F	14694	WESTAR 6 R/B (PAM)	US	3 FEB 84	
1984-106J	22141	COSMOS 1603 DEB	USSR	28 SEP 84	11 OCT 92
1984-106R	22148	COSMOS 1603 DEB	USSR	28 SEP 84	13 NOV 92
1984-106Y	22155	COSMOS 1603 DEB	USSR	28 SEP 84	22 OCT 92
1984-106Z	22156	COSMOS 1603 DEB	USSR	28 SEP 84	14 OCT 92
1984-123C	15441	NOAA 9 DEB	US	12 DEC 84	11 NOV 92
1986-017A	16609	MIR	USSR	19 FEB 86	

1986-017FU	21882	MIR DEB	USSR	19	FEB	86	21	JAN	93
1986-017FW	21884	MIR DEB	USSR	19	FEB	86	19	JAN	93
1986-017GE	22023	MIR DEB	USSR	19	FEB	86	12	DEC	92
1986-017GF	22024	MIR DEB	USSR	19	FEB	86	4	MAY	93
1986-017GG	22045	MIR DEB	USSR	19	FEB	86	4	MAY	93
1986-017GJ	22106	MIR DEB	USSR	19	FEB	86	26	FEB	93
1986-017GK	22107	MIR DEB	USSR	19	FEB	86	10	DEC	92
1986-017GM	22121	MIR DEB	USSR	19	FEB	86	28	OCT	93
1986-017GN	22122	MIR DEB	USSR	19	FEB	86	2	DEC	92
1986-017GP	22123	MIR DEB	USSR	19	FEB	86			
1986-017GQ	22124	MIR DEB	USSR	19	FEB	86	3	NOV	92
1986-017GR	22127	MIR DEB	USSR	19	FEB	86			
1986-017GR	22127	MIR DEB	USSR	19	FEB	86			
1986-017GS	22128	MIR DEB	USSR	19	FEB	86			
1986-017GT	22129	MIR DEB	USSR	19	FEB	86	17	NOV	92
1986-017GV	22131	MIR DEB	USSR	19	FEB	86	12	NOV	92
1986-017GW	22209	MIR DEB	USSR	19	FEB	86	9	APR	93
1986-017GX	22225	MAK 2	USSR	19	FEB	86	1	APR	93
1986-017GY	22228	MIR DEB	USSR	19	FEB	86	8	DEC	92
1986-071H	16985	COSMOS 1778-1780 DEB	USSR	16	SEP	86	26	NOV	92
1987-012K	18927	ASTRO C DEB	JPN	5	FEB	87	13	APR	93
1987-020M	18734	COSMOS 1823 DEB	USSR	20	FEB	87	21	NOV	92
1988-113H	19764	COSMOS 1985 DEB	USSR	23	DEC	88			
1989-100A	20389	COSMOS 2053	USSR	27	DEC	89			
1990-015A	20496	USA 51	US	14	FEB	90			
1990-028A	20546	PEGSAT	US	5	APR	90			
1990-081BH	20897	FENGYUN 1-2 DEB	PRC	3	SEP	90	21	JAN	93
1990-104A	20966	COSMOS 2106	USSR	28	NOV	90			
1990-104AG	22486	COSMOS 2106 DEB	USSR	28	NOV	90	5	APR	93
1991-005A	21065	COSMOS 2122	USSR	18	JAN	91	28	MAR	93
1991-005D	22299	COSMOS 2122 DEB	USSR	18	JAN	91	2	JAN	93
1991-021A	21190	COSMOS 2137	USSR	19	MAR	91			
1991-024A	21213	ALMAZ 1	USSR	31	MAR	91	17	OCT	92
1991-072A	21743	COSMOS 2164	USSR	10	OCT	91	12	DEC	92
1992-007B	21868	JERS R/B	JPN	11	FEB	92			
1992-046A	22054	SOYUZ TM-15	USSR	27	JUL	92	1	FEB	93
1992-055A	22090	PROGRESS M-14	USSR	15	AUG	92	21	OCT	92
1992-062A	22133	COSMOS 2210	USSR	22	SEP	92	20	NOV	92
1992-065A	22173	FOTON 5	USSR	8	OCT	92	24	OCT	92
1992-065C	22199	FOTON 5 DEB	USSR	8	OCT	92	20	NOV	92
1992-065E	22201	FOTON 5 DEB	USSR	8	OCT	92	30	OCT	92
1992-065F	22202	FOTON 5 DEB	USSR	8	OCT	92	3	NOV	92
1992-070A	22194	STS 52	US	22	OCT	92	1	NOV	92
1992-071A	22203	PROGRESS M-15	USSR	27	OCT	92	7	FEB	93
1992-075A	22217	RESURS 500	USSR	15	NOV	92	22	NOV	92
1992-077A	22226	COSMOS 2220	USSR	20	NOV	92	18	JAN	93
1992-078A	22229	MSTI	US	21	NOV	92	18	JUL	93
1992-078B	22230	SCOUT G-1 R/B	US	21	NOV	92	9	FEB	93
1992-086A	22259	STS-53	US	2	DEC	92	9	DEC	92
1992-087A	22260	COSMOS 2223	USSR	9	DEC	92	16	DEC	93
1992-091A	22280	COSMOS 2225	USSR	22	DEC	92	18	FEB	93
1992-091C	22520	COSMOS 2225 DEB	USSR	22	DEC	92	23	FEB	93
1992-091D	22525	COSMOS 2225 DEB	USSR	22	DEC	92	25	FEB	93
1992-091E	22526	COSMOS 2225 DEB	USSR	22	DEC	92	22	FEB	93
1992-091F	22527	COSMOS 2225 DEB	USSR	22	DEC	92	27	FEB	93
1992-091G	22529	COSMOS 2225 DEB.	USSR	22	DEC	92	24	FEB	93
1992-093FY	22483	COSMOS 2227 DEB	USSR	25	DEC	92	22	FEB	93
1992-095B	22301	COSMOS 2229 R/B	USSR	29	DEC	92	16	JAN	93
1993-002B	22310	MOLNIYA 1-85 R/B(1)	USSR	13	JAN	93	4	MAR	93
1993-002C	22311	MOLNIYA 1-85 PLAT	USSR	13	JAN	93	5	FEB	93
1993-003A	22313	STS 54	US	13	JAN	93	19	JAN	93
1993-004A	22317	COSMOS 2231	USSR	19	JAN	93	25	MAR	93
1993-006B	22322	COSMOS 2232 R/B(1)	USSR	26	JAN	93	9	MAR	93
1993-012A	22530	PROGRESS M-16	USSR	21	FEB	93	27	MAR	93

Appendix G: Derivation and Implementation of the Statistical Model

In this appendix, we expand upon the derivation in Kessler^[3] and present our implementation. In the kinetic theory of gases, the flux within a volume, F , the number of impacts upon a surface per unit area per unit time, is given by $F = S v$, where S is the spatial density of objects within the volume and v is the relative velocity between the objects and the surface area. On a cross-sectional area σ , in time t , the number of collisions would be $N = f \sigma t$. The spatial density, S , for a single object, which over time T , spends time Δt within a volume ΔU , is $S = \Delta t/T\Delta U$.

Assume, for an orbiting object, the spatial density may be written as a product of latitude-dependent and radially dependent terms: $S(R, \beta) = f(\beta) s(R)$.

Radial Dependence

The volume, ΔU , of a thin spherical shell at radius R , of thickness ΔR , between perigee, q , and apogee, q' , of some orbiting object is $\Delta U = 4 \pi R^2 \Delta R$. An object will traverse the shell twice per orbit, spending a time $\Delta t = 2 \Delta R/V_R$ in the shell, with V_R the radial velocity of the object when traversing the shell.

The energy of an orbiting object is $E = \mu m/R - mv^2/2 = \mu m/2a$, where $2a = (q + q')$ is the semimajor axis, and μ is the gravitational attraction constant, Gm_E of the Earth.

The period is

$$T = 2\pi \sqrt{\frac{a^3}{\mu}}$$

and the velocity is

$$v = \sqrt{\mu \left(\frac{2}{R} - \frac{1}{a} \right)}.$$

The radial velocity of the object is $V_R = V \sin \gamma$, where γ is the angle between a tangent to a radial sphere of radius R and the object velocity vector. Conservation of momentum requires $V \cos \gamma = qV_{perigee}$,

$$V_{perigee} = \sqrt{\mu \left(\frac{2}{q} - \frac{1}{a} \right)} = \sqrt{\mu \left(\frac{2}{q} - \frac{2}{(q+q')} \right)} = \sqrt{2\mu \left(\frac{2q+q'-q}{q(q+q')} \right)} = \sqrt{2\mu \left(\frac{q'}{q(q+q')} \right)},$$

and

$$V \cos \gamma R = \sqrt{\mu \left(\frac{2}{R} - \frac{1}{a} \right)} \cos \gamma R = \sqrt{\mu \left(\frac{2a-R}{Ra} \right)} \cos \gamma R = qV_{perigee} = q \sqrt{2\mu \left(\frac{q'}{q(q+q')} \right)}.$$

Squaring terms (3) and (5) of the multiple component equation above,

$$\left(\frac{2a-R}{Ra}\right)\cos^2\gamma R^2 = \frac{2qq'}{q+q'} = \frac{2qq'}{2a}$$

and

$$\cos^2\gamma = \frac{qq'}{R(2a-R)}.$$

Then

$$V_R = V \sin\gamma = \sqrt{\mu} \sqrt{\left(\frac{2}{R} - \frac{1}{a}\right)} \sqrt{1 - \frac{qq'}{R(2a-R)}}. \quad (1)$$

The radial spatial density becomes

$$\begin{aligned} s(R) &= \frac{\Delta t}{T\Delta U} = \frac{2\Delta R}{(V_R)(4\pi R^2\Delta R)2\pi\sqrt{a^3/\mu}} = \frac{\sqrt{\mu}}{4\pi^2 R^2 \sqrt{a^3\mu\left(\frac{2}{R} - \frac{1}{a}\right)\left(1 - \frac{qq'}{R(2a-R)}\right)}} = \\ &= \frac{\sqrt{\mu}}{4\pi^2 R^2 \sqrt{a^3\mu\left(\frac{2a-R}{Ra}\right)\left(\frac{R(2a-R)-qq'}{R(2a-R)}\right)}} = \frac{1}{4\pi^2 aR} \frac{1}{\sqrt{R(q+q'-R)-qq'}} = \\ &= \frac{1}{4\pi^2 aR} \frac{1}{\sqrt{Rq+Rq'-R^2-qq'}} = \frac{1}{4\pi^2 aR^2} \frac{1}{\sqrt{(R-q)(q'-R)}} \end{aligned} \quad (2)$$

Latitude Dependence

Above, we considered the time spent in radially traversing a thin spherical shell. Here, we assume orbital motion exclusively within a spherical shell and consider the time to traverse a band between latitudes β and β' within the shell. The spatial density, S , within a volume, ΔU , is again given by $S = \Delta t/T\Delta U$ where Δt is the time spent within the volume over a total time $T = 2\pi/\omega$, with ω the angular velocity of the orbiting object.

The spatial density is then

$$S = \frac{\Delta t}{T\Delta U} = \left(\frac{2\Delta\beta}{\omega \sin\alpha}\right)\left(\frac{\omega}{2\pi}\right)\left(\frac{1}{2\pi R^2 \cos\beta\Delta\beta\Delta R}\right) = \frac{1}{2\pi^2 R^2 \sin\alpha \cos\beta\Delta R}$$

and

Flux

The number of collisions between objects 1 and 2 in time, t , is

$$N = \int_{\text{all space}} S_1 S_2 V_{rel} t \sigma dU ,$$

where S_1 and S_2 are the spatial densities of the two objects, σ is the collision cross section, and V_{rel} is the relative velocity between the two objects. The volume differential, after integrating over longitude, is $dU = 2\pi R^2 \cos\beta dR d\beta$. The integral can be evaluated over all space, but it need only be evaluated over that volume for which the spatial density of both objects is nonzero. The flux, as seen by one of the objects due to the other object, is

$$F = \frac{N}{\sigma t} = \int_{\text{all space}} S_1 S_2 V_{rel} dU . \quad (7)$$

Relative Velocity

To evaluate the above expression, it is necessary to calculate the relative velocity V_{rel} , which is defined as $\vec{V}_{rel} = \vec{V}_1 - \vec{V}_2$. Then,

$$V_{rel}^2 = \vec{V}_{rel} \cdot \vec{V}_{rel} = V_1^2 + V_2^2 - 2V_1 V_2 \cos\phi . \quad (8)$$

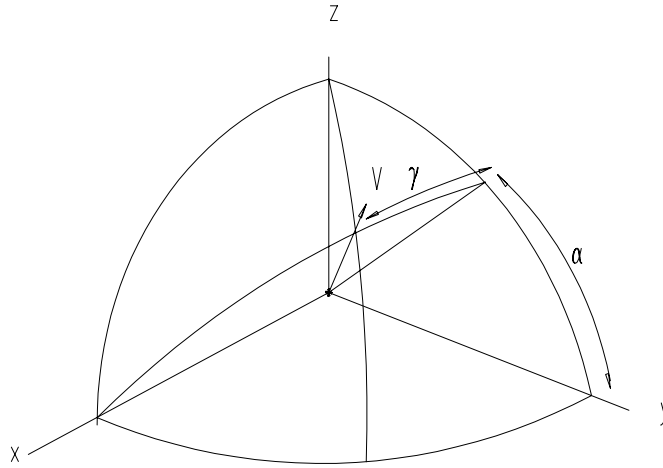


Figure G2. Velocity vector relationships.

Figure G2, above, shows the relationship between the components of the velocity vector \vec{V} and the angles γ and α defined above. In the figure, the x axis comes from the center of the Earth, the y axis is tangent to a line of constant latitude, and the z axis, which is tangent to an Earth-centered sphere, completes a Cartesian coordinate system. The velocity vector \vec{V} is given by

$$\vec{V} = V (\sin \gamma \hat{x} + \cos \gamma \cos \alpha \hat{y} + \cos \gamma \sin \alpha \hat{z}),$$

where $\hat{x}, \hat{y}, \hat{z}$ are unit vectors along the axes. The magnitude of the relative velocity between the two

velocity vectors, \vec{V}_1 and \vec{V}_2 , is then given by

$$V_{rel}^2 = \vec{V}_1 \cdot \vec{V}_2 = V_1 V_2 (\sin \gamma_1 \sin \gamma_2 + \cos \gamma_1 \cos \gamma_2 \cos \alpha_1 \cos \alpha_2 + \cos \gamma_1 \cos \gamma_2 \sin \alpha_1 \sin \alpha_2)$$

and

$$V_{rel}^2 = V_1 V_2 \left[\sin \gamma_1 \sin \gamma_2 + \cos \gamma_1 \cos \gamma_2 \cos(\alpha_1 - \alpha_2) \right]. \quad (9)$$

Equations (1) and (4) give γ in terms of R , q , and q' and α in terms of β and i . For a given R and β , there will be four equally probable values of V_{rel} over which we may average in the evaluation of flux. In the determination of relative angular distribution, each is considered individually.

Implementation

The flux experienced by object 0, due to a population of orbiting objects, is

$$F = \sum_j \iint_{R, \beta \in S_0, S_1 \neq 0} S_0(R, \beta) S_j(R, \beta) V_{0,jrel} 2\pi R^2 \cos(\beta) dR d\beta. \quad (10)$$

Using equation (6) to evaluate S_0 and S_1 and using equation (9) for V_{rel} , we have all of the information necessary to numerically integrate equation (10). We are trying to calculate flux as a function of altitude; this can be accomplished by putting object 0 in a circular orbit. In the simplest implementation of equation (10),

$$S_j = \left(\frac{1}{4\pi^2 a R \sqrt{(R-q)(q'-R)}} \right) \left(\frac{2}{\pi \sqrt{\sin^2 i_j - \sin^2 \beta}} \right),$$

$$S_0 = \left(\frac{1}{4\pi^2 \alpha \Delta R} \right) \left(\frac{2}{\pi \sqrt{\sin^2 i_0 - \sin^2 \beta}} \right),$$

and

$$F(R) = \sum_{jk} S_0(R, \beta_k, i_0) S_j(R, \beta_k, i_j, q_j, q_j') \bar{V}(R, \beta_k, i_0, i_j, q_j, q_j') 2\pi R^2 \cos(\beta_k) \Delta R \Delta \beta,$$

with all $\Delta \beta_k = 0.5^\circ$ and $\Delta R = 10$ km. The form of S_0 assumes a circular orbit for the target object. The form of S_j was used as a test implementation, but not to generate results. For a target object in circular orbit, γ_0 is zero; then, in equation (9), there are only two values of V at each integration point, and \bar{V} is the average of those two values given by

$$\bar{V}_o \cdot \bar{V}_j = V_o V_j \left[\cos \gamma_0 \cos \gamma_1 (\cos \alpha_0 \cos \alpha_j \pm \sin \alpha_0 \sin \alpha_j) \right]$$

and

$$\left(\bar{V}_o \cdot \bar{V}_j \right)_{ave} = \sqrt{V_o V_j \left[\cos \gamma_0 \cos \gamma_1 \cos \alpha_0 \cos \alpha_j \right]}.$$

Singularities in R and β can be eliminated by calculating average values $\bar{s}(R, q, q')$ and $\bar{f}(\beta)$ over intervals of R and β , $\Delta R = R' - R$ and $\Delta\beta = \beta' - \beta$. Assuming that R is constant over the integration interval, we evaluate

$$\begin{aligned}\bar{s}(R, R') &= \frac{4\pi \int_R^{R'} s(R) R^2 dR}{4\pi \int_R^{R'} R^2 dR} = \frac{\int_R^{R'} \frac{1}{2\pi^2 Ra} \frac{1}{\sqrt{(R-q)(q'-R)}} R^2 dR}{\int_R^{R'} R^2 dR} = \\ &= \frac{R \int_R^{R'} \frac{-1}{(q-R)(q'-R)} dR}{4\pi^2 a R \Delta R} = \frac{1}{4\pi^2 a R \Delta R} \sin^{-1} \left(\frac{2R-q-q'}{q'-q} \right) \Bigg|_R^{R'}\end{aligned}$$

and

$$\bar{s}(R, q, q') = \frac{1}{4\pi^2 a R \Delta R} (F_1(R, q, q') - F_2(R, q, q'))$$

where

$$F_1 = \sin^{-1} \left(\frac{2R' - 2a}{q' - q} \right) \text{ if } q < R' < q', \quad F_1 = \frac{\pi}{2} \text{ if } R' > q', \quad F_1 = -\frac{\pi}{2} \text{ if } R' < q$$

$$F_2 = \sin^{-1} \left(\frac{2R - 2a}{q' - q} \right) \text{ if } q < R < q', \quad F_2 = -\frac{\pi}{2} \text{ if } R < q, \quad F_2 = \frac{\pi}{2} \text{ if } R > q'.$$

$$\bar{f}(\beta, \beta') = \frac{\int_{\beta}^{\beta'} f(\beta) \cos \beta d\beta}{\int_{\beta}^{\beta'} \cos \beta d\beta} = \frac{\int_{\beta}^{\beta'} \frac{d \sin \beta}{\sqrt{\sin^2 i - \sin^2 \beta}}}{\int_{\beta}^{\beta'} d \sin \beta} = \frac{2}{\pi} \sin^{-1} \left(\frac{\sin \beta}{\sin i} \right) \Bigg|_{\beta}^{\beta'} = \frac{2}{\pi} \frac{G_1(\beta') - G_2(\beta)}{\sin \beta' - \sin \beta}$$

$$G_1 = \sin^{-1} \left(\frac{\sin \beta'}{\sin i} \right) \text{ if } \beta < i, \quad G_1 = \frac{\pi}{2} \text{ if } \beta' \geq i,$$

$$G_2 = \sin^{-1} \left(\frac{\sin \beta}{\sin i} \right) \text{ if } \beta < i, \quad G_2 = \frac{\pi}{2} \text{ if } \beta' \geq i.$$

Then,

$$F(R) = \sum_{jk} \frac{1}{4\pi \bar{R}_k^2 \Delta R} \bar{s}_j(\bar{R}, q, q') \bar{f}(\bar{\beta}_k, i_0) \bar{f}(\bar{\beta}_k, i_j) \bar{V}(\bar{R}, \bar{\beta}, i_j, i_0) 2\pi R^2 \cos(\bar{\beta}_k) \Delta R \Delta \beta.$$

Relative Angular Distribution

There are two values of relative velocity for the target object in a circular orbit:

$$V_{rel1} = \sqrt{V_0^2 + V_j^2 - 2V_0V_j \cos \gamma_0 \cos \gamma_j \cos(\alpha_j - \alpha_0)},$$

and

$$V_{rel2} = \sqrt{V_0^2 + V_j^2 - 2V_0V_j \cos \gamma_0 \cos \gamma_j \cos(\alpha_j - \alpha_0)}.$$

Equation (8) can be solved for the relative angle ϕ as

$$\phi_{rel_{jk}} = \cos^{-1} \left(\frac{V_j^2 + V_0^2 - V_{relk}^2}{2V_0V_j} \right).$$

The angular distribution is given by

$$D(\phi_i) = \frac{d(\phi_i)}{\sum d(\phi_i)},$$

where

$$\text{if } (\phi_i - 7.5^\circ) \leq \phi < (\phi_i + 7.5^\circ) \quad d(\phi) = d(\phi_i) + S_0 S_j V_{rel} \cos \beta.$$

The $d(\phi_i)$ are summed over all velocity components for all objects over all latitudes. Table G1, below, shows the $d(\phi_i)$ for December 1992 for objects entering the 250- to 500-km altitude band, with 15° intervals. Conjunctions occurring at altitudes between 300 and 450 km are considered. The coefficients are comparable to those generated in section 4.3.

Table G1. Normalized angular coefficients generated from catalog data.

Rel. ang.	0°	15°	30°	45°	60°	75°	90°	105°	120°	135°	150°	165°
$d(\phi_i)$	0.003	0.004	0.176	0.318	0.294	0.148	0.028	0.014	0.006	0.004	0.004	0.001

Appendix H: Precession of Arguments of Perigee and Ascending Node

The Lagrange Planetary Equations for argument of perigee, ω , and argument of ascending node, Ω , are

$$3 \frac{d\omega}{dt} = \frac{\sqrt{1-e^2}}{na^2e} \frac{\partial H}{\partial e} - \frac{1}{na^2\sqrt{1-e^2}} \frac{\cos i}{\sin i} \frac{\partial H}{\partial i}$$

and

$$\frac{d\Omega}{dt} = \frac{1}{na^2\sqrt{1-e^2} \sin i} \frac{\partial H}{\partial i}$$

where t is time in seconds, n is the mean motion, a is the semimajor axis, i is the orbital inclination, 28.45° , e is the eccentricity ≈ 0.00 for GRO, and H is the perturbing potential. The precession of ω and Ω , for an orbiting object, is due to the Earth's oblateness with a potential at radius, r , and latitude, L , given by

$$H = \frac{\mu}{r} \frac{J_2}{2} \left(\frac{r_{eq}}{r} \right)^2 P_2(\sin L) = \frac{\mu}{r} \frac{J_2}{2} \left(\frac{r_{eq}}{r} \right)^2 \left(3 \sin^2 i \sin^2(\omega + f) - 1 \right).$$

Here μ is the Earth's gravitational constant, $3.986012 \times 10^5 \text{ km}^3/\text{sec}^2$, r_{eq} is the Earth's equatorial radius 6378.145 km, and f is the true anomaly of the orbiting object at time t . Since we are concerned with the long-term secular perturbations, we average H over a revolution of our orbiting object by calculating

$$\bar{H} = \int_0^{2\pi} H df = \mu J_2 \left(\frac{r_{eq}^2}{(a\sqrt{1-e^2})^3} \right) \left(1 - \frac{3}{2} \sin^2 i \right).$$

In the evaluation of the integral, $r = \frac{a\sqrt{1-e^2}}{1-e\cos(f)}$ is employed. Then,

$$\Delta\omega = \left(\overline{\frac{d\omega}{dt}} \right) 2\pi n = 3\pi J_2 \left(\frac{r_{eq}}{a\sqrt{1-e^2}} \right)^2 \left(2 - \frac{5}{2} \sin^2(i) \right) \text{ rad/rev}$$

and

$$\Delta\Omega = \left(\overline{\frac{d\Omega}{dt}} \right) 2\pi n = -3\pi J_2 \left(\frac{r_{eq}}{a\sqrt{1-e^2}} \right)^2 \cos(i) \text{ rad/sec}.$$

From figure 2, section 5.1.4, the average semimajor axis is about $a_{average} = 6750 \text{ km}$. Then the period, P , is given by

$$P = 2\pi \sqrt{\frac{a^3}{\mu}} = 2\pi n = 5519.08 \text{ sec},$$

and there, are on average, 15.6548 rev/day over the simulation. We obtain

$$\Delta\omega = 0.013044 \text{ rad/rev} = 0.7473^\circ/\text{day} \text{ or } 30.77 \text{ days for 1 cycle in } \omega.$$

$$\Delta\Omega = 0.008005 \text{ rad/rev} = 0.4587^\circ/\text{rev} \text{ or } 50.14 \text{ days for 1 cycle in } \Omega.$$

Appendix I: State Vector Uncertainty Analysis

Time-Overlapped Data Analysis

Conjunctions for which there are two predictions, one on the day of conjunction and one on the previous day, allow an estimate of the 24-hour dispersion in state vector position. One must realize that, with a 1.14-day state vector update period, there will be 24-hour periods over which a state vector is only propagated with no update and other periods in which two updates occur, representing in fact two days of dispersion. Still a statistical analysis is of considerable interest because the long-term behavior of GP-processed data should be very close to that of SP-processed data.

Let \bar{r}_1 be the position component of the state vector determined on the day of conjunction at time t_1 and let \bar{r}_2 be the state vector position determined on the previous day at time t_2 . Let \bar{r}_2' be the vector \bar{r}_2 propagated to time t_1 , given by

$$\bar{r}_2' = \bar{R}_2 + \bar{V}_2 t - \frac{1}{2} g t^2 \frac{\bar{r}_2}{|\bar{r}_2|}$$

where

$$g = 0.0098 \frac{R_0^2}{|\bar{r}_2|^2} \text{ km/sec}^2 \text{ and } t = t_1 - t_2,$$

with R_0 being the radius of the Earth. Then the components ΔU , ΔV , ΔW —the position differences along the radial, downtrack, and cross track directions—are given by

$$R_{XYZ}^{UVW} \left(\bar{r}_1 - \bar{r}_2' \right) = \begin{bmatrix} \frac{\bar{r}_1}{|\bar{r}_1|} \cdot \\ \frac{\bar{r}_1 \times \bar{h}_1}{|\bar{r}_1 \times \bar{h}_1|} \cdot \\ \frac{\bar{r}_1 \times \bar{v}_1}{|\bar{r}_1 \times \bar{v}_1|} \cdot \end{bmatrix} \left(\bar{r}_1 - \bar{r}_2' \right) = \begin{bmatrix} \Delta U \\ \Delta V \\ \Delta W \end{bmatrix}.$$

State Vector Uncertainty at Epoch

In section 5.1.4, the observation of an average daily decrease in semimajor axis of 156 m/day with a standard deviation, σ_a , of 53 m was documented. This information allows an estimate of USSPACECOM semimajor axis uncertainty at epoch, σ_{epoch} , for GP processing and normal tasking. Assume 15 percent of the 156 m/day decrease (23 m) in the GRO semimajor axis as the uncertainty buildup over a day due to atmospheric variation. Then,

$$\sigma_a^2 = 2\sigma_{epoch}^2 + \sigma_{atm}^2 = 0.053^2 + 0.023^2,$$

and

$$\sigma_{epoch} = \sqrt{\frac{0.053^2 - 0.023^2}{2}} = 34 \text{ m}.$$

REPORT DOCUMENTATION PAGE			Form Approved OMB No. 0704-0188	
Public reporting burden for this collection of information is estimated to average 1 hour per response, including the time for reviewing instructions, searching existing data sources, gathering and maintaining the data needed, and completing and reviewing the collection of information. Send comments regarding this burden estimate or any other aspect of this collection of information, including suggestions for reducing this burden, to Washington Headquarters Services, Directorate for Information Operations and Reports, 1215 Jefferson Davis Highway, Suite 1204, Arlington, VA 22202-4302, and to the Office of Management and Budget, Paperwork Reduction Project (0704-0188), Washington, DC 20503.				
1. AGENCY USE ONLY (Leave Blank)	2. REPORT DATE May 2006	3. REPORT TYPE AND DATES COVERED NASA Technical Memorandum		
4. TITLE AND SUBTITLE A 160-Day Simulation of Space Station Debris Avoidance Operations with the United States Space Command (USSPACECOM)			5. FUNDING NUMBERS	
6. AUTHOR(S) Alfred Lunde,* James Lee Foster, Jr.**				
7. PERFORMING ORGANIZATION NAME(S) AND ADDRESS(ES) *Johnson Space Center, **Barrios Technology, Inc.			8. PERFORMING ORGANIZATION REPORT NUMBERS S-977	
9. SPONSORING/MONITORING AGENCY NAME(S) AND ADDRESS(ES) National Aeronautics and Space Administration Washington, DC 20546-0001			10. SPONSORING/MONITORING AGENCY REPORT NUMBER TM-2006-213720	
11. SUPPLEMENTARY NOTES				
12a. DISTRIBUTION/AVAILABILITY STATEMENT Unclassified/Unlimited Available from the NASA Center for AeroSpace Information (CASI) 7121 Standard Hanover, MD 21076-1320 Category: 12			12b. DISTRIBUTION CODE	
13. ABSTRACT (Maximum 200 words) A joint simulation was performed by the NASA Johnson Space Center (JSC) and United States Space Command (USSPACECOM) to obtain information concerning the current space debris population for debris avoidance operations. Simulation results, which are extrapolated within this document, are intended for use in future space station operations. The simulation, performed from September 1992 to March 1993, used the Gamma Ray Observatory (GRO)—orbiting at a 28.5-deg orbital inclination, and substituting for a space station orbital inclination—as a target vehicle. As the simulation was carried out, USSPACECOM used the database maintained by its tracking network to search for conjunctions between the GRO and the tracked debris, and then transmitted results of the simulation to JSC for analysis. Over the entire altitude band studied, the debris flux and frequency of penetration of Space Shuttle orbiter "alert" and "maneuver" boxes were found to be much lower than the predictions of current models. However, if a maneuver box similar to that used for the Space Shuttle is used for a future space station, the number of maneuvers to avoid orbital debris will be prohibitive. Results of this study showed a very dynamic debris environment over the time period and altitudes covered.				
14. SUBJECT TERMS space debris; Gamma Ray Observatory; environment effects; penetration; flux; maneuvers; aerospace environments			15. NUMBER OF PAGES 74	16. PRICE CODE
17. SECURITY CLASSIFICATION OF REPORT Unclassified	18. SECURITY CLASSIFICATION OF THIS PAGE Unclassified	19. SECURITY CLASSIFICATION OF ABSTRACT Unlimited	20. LIMITATION OF ABSTRACT Unlimited	
